ANALYTIC TECHNIQUES FOR THE TIME-DOMAIN SIMULATION OF UNIFORM LOSSY TRANSMISSION LINES IN NONLINEAR CIRCUITS

by

Jaijeet Shankar Roychowdhury

Memorandum No. UCB/ERL M92/137

9 December 1992

ANALYTIC TECHNIQUES FOR THE TIME-DOMAIN SIMULATION OF UNIFORM LOSSY TRANSMISSION LINES IN NONLINEAR CIRCUITS

by

Jaijeet Shankar Roychowdhury

Memorandum No. UCB/ERL M92/137

9 December 1992

ELECTRONICS RESEARCH LABORATORY

College of Engineering
University of California, Berkeley
94720

Analytic Techniques for the Time-Domain Simulation of Uniform Lossy Transmission Lines in Nonlinear Circuits

Jaijeet S. Roychowdhury

University of California
Berkeley, California

Department of Electrical Engineering
and Computer Sciences

Abstract

The problem of time-domain simulation of uniform lossy transmission lines within nonlinear circuits is addressed in this dissertation. The existing convolution method is improved upon by identifying a formulation in which analytic expressions exist for the impulse responses of a simple lossy line. These expressions are convolved (using accurate numerical formulae) with the port variables of the lossy line for simulation. Experimental results demonstrate significant advantage in accuracy and speed over the lumped RLC method for real circuits involving a few cycles.

Convolution is inherently slow for simulations with many time points because of its quadratic complexity. Previous attempts to address this problem have concentrated on approximating responses by expansions. A new linear time technique (the state-based method) that derives from an analytic solution of the Telegrapher Equations is presented. Convolution over all previous time is replaced by a space integral, over a maximum interval of the length of the line. Samples of the voltages and currents within the line, from which the space integral is computed, can be dynamically changed dynamically during the simulation. The number of such samples can be much smaller than the number of lumps required in the lumped RLC method because their locations can be changed to track waveforms, leading to the automatic exploitation of circuit latency. Experimental results demonstrate significant advantage over other techniques.

Extension of the state-based method to lossy lines with high frequency nonidealities, such as skin effect, is also described.

Prof. A. Richard Newton
Thesis Committee Chairman

Acknowledgements

The five and a half years that I have spent at the University of California at Berkeley have been a very stimulating stage of my life. Many individuals have contributed to the work presented here.

My research advisor Richard Newton is responsible to a great extent for my being in CAD in the first place, and has been a source of inspiration and support over the last five years. His knowledge and vision have had a great influence on this work. The freedom that he accords his students and the flexibility of his outlook were particularly valuable for the progress of my doctoral work. But for him I would leave Berkeley much poorer.

Without the benefit of the decades of research experience and the valuable guidance of my co-advisor Donald Pederson, the work described in this dissertation would have taken much longer to complete. From interactions with him I have learned how to structure, organize and conduct research, to write about technical material, to describe equations in words, and to present work effectively.

The CAD group in Berkeley is undoubtedly one of the leading research centers in the world, and much of the credit for its eminent position goes to Robert Brayton and Alberto Sangiovanni-Vincentelli and their dynamic research groups. The courses offered by Profs. Brayton and Sangiovanni-Vincentelli are among the most intellectually stimulating of all the CAD courses, and the atmosphere provided by their research groups has had a very positive influence on my own research.

Ernest Kuh provided valuable guidance during the later stages of this work. Interaction with members of his group, in particular Shen Lin and Charles Hough, has been of help. Discussions with many have contributed to this work; especially those with Eric Beyne, Leon Chua, Randy Geiger, Georges Gielen, Marwan Hassoun, Ken Kundert, Richard Matick, Heinz Mattes, A. J. Rainal, Zaki Rakib, Albert Ruehli, Andrei Vladimirescu, Jacob White and Yo-Chien Yuan. Special thanks to Cormac Conroy for helping with the GTL driver model of one of the examples.

From the inception of the research described in this dissertation, support was provided in part by Raytheon Co.. This support is gratefully acknowledged. In particular, Gerry Marino provided invaluable personal help and advice, providing examples and serving as a beta-test site for experimental software. The support provided in part by SRC and the California State Micro Program is acknowledged. Computing equipment was provided

by grants from Digital Equipment Corporation. Recent support for this work by AT&T is gratefully acknowledged. In particular, the personal help of Sally Liu and Peter Lloyd is greatly appreciated. The support of nCHIP, Inc., during the early stages of this work, is acknowledged. In particular, the personal help of Jim Kaschmitter, Bruce McWilliams, Dave Tuckerman and Dick Lang is greatly appreciated.

I would like to extend a special note of thanks to Shoshichi Kobayashi for being on my dissertation committee.

Many friends and colleagues made my stay in Berkeley what it was: in particular Pranav Ashar, Adnan Aziz, Wendell Baker, Barnali Banerjee, Julie Basu, Mark Beardslee, Pamela Chan, Madhavi Chandrachood, Henry Chang, Edoardo Charbon, Tanvi Chawla, Dev Chen, Preeti Chopra, Umakanta Choudhury, Randy Cieslak, Cormac Conroy, Kia Cooper, Dilip DaCunha, Chetan Damania, Pinaki Das, Abhijit Dasgupta, Shoma Dasgupta, Mladen Despić, Ta-Fang Fang, Eric Felt, David Gates, Abhijit Ghosh, Nita Goyal, Shubhrojit Guhathakurta, Ashish Hazra, Beorn Johnson, Asawaree Kalavade, Subbarao Kambhampati, Vikas Kapur, Naomi Karp, Navaz Katki, Takis Konstantopoulos, Neema Kudwa, Luciano Lavagno, Brian Lee, Chris Lennard, Enrico Malavasi, Sharad Malik, Karti Mayaram, Renu Mehra, Elise Mills, Linda Milor, Urbashi Mitra, Rajeev Murgai, Dipankar Nandi, Dr. Shyamal Nandi, Mrs. Pranati Nandi, Kathy Nix, Berenice Ong, Flora Oviedo, Eva Pantazidi, Marina Pantazidou, Canna Patel, Sanjit Roy, Alexander Saldanha, Jagesh Sanghavi, Kumud Sanwal, Sudeshna Sarkar, Sanjay Sarma, Hamid Savoj, Tamali Sengupta, Ellen Sentovich, Narendra Shenoy, KanwarJit Singh, Vigyan Singhal, Arvind Srinivasan, Mani Srivastava, Gitanjali Swamy, Niranjan Thatte, Umesh Vazirani, Amrita Verma and Dinesh Verma.

It would not have been possible for me to join the graduate program at Berkeley had I not been at the Indian Institute of Technology, Kanpur. Many of my professors there had a direct influence on my continuing my education through the graduate level; especially R. N. Biswas, P. R. K. Rao, V. P. Sinha, R. Raghuram, J. K. Bhattacharya, Kalyan Banerjee, C. Dasgupta, N. C. Mathur, K. R. Srivatsan and L. P. Singh. Many of my friends there added variety to my stay, notably Sudhanshu Bahadur, Goutom Banerjee, Sandip Bose, Jayaram Chengalur, Gautam Gauba, Amit Gupta, Viraf Hathiram, George Joy, Gurinder Kalra, Rishikesha Krishnan, Pallav Kulshreshtha, Alok Mathur, Harsh Mathur, Narayanan Menon, Manavendra Misra, Onuttom Narayan, Sanjiv Patel, Amrit Mohan Prasad, J. Radhakrishnan, Syed Sibte Haidar Rizvi, Prasenjit Saha, Dheeraj Sanghi, R. Saravanan, Di-

pankar Sarkar, Siddhartha Sen, Vinay Mohan Singh, Deepak Srinivasan, Prateek Srivastava, Siddarth Subramanian and Shabbir Yusuf.

Most of all, the presence of my parents and sister ensured that I undertook and completed this work.

Contents

List of Figures

List of Tables

Chapter 1

Introduction

During the past two decades, automated design tools have been used increasingly for the analysis and design of VLSI circuits [25]. Design tools have developed in two broad categories - verification tools and syndissertation tools. Verification tools are used to check whether a given circuit or design performs correctly according to specification. Syndissertation tools, on the other hand, are used to produce a circuit or design given a performance specification. Verification tools save the time and expense of physical circuit fabrication and often provide designers with insight into the operation of circuits. Syndissertation tools are used for creating reliable, efficient designs and reducing design time.

For analog circuits, the most widely accepted method of verification is circuit simulation. While existing circuit simulation tools [37, 17, 10] have proven adequate for the design of most IC-based systems, faster devices and new packaging technologies have emerged that require new and more sophisticated models and techniques. A new packaging technology called the *multi-chip module* (MCM) has been developed over the last decade and has recently become popular because of the advantages it offers over conventional packaging[1]. In a MCM, bare (i.e., without individual packaging) ICs are mechanically attached to a ceramic or semiconductor substrate, with thin metallic lines called *interconnect* running over the substrate to provide electrical connectivity between chips. However, the verification of MCMs is a challenge since existing simulators cannot model the interconnect, which must be represented as a collection of *lossy transmission lines*, adequately. Lossy transmission

[1]Two electrical advantages of MCMs are reduced parasitics due to shorter interconnect lengths and the absence of individual packaging, and smaller delays due to physical proximity. Among the packaging/system level advantages are increased packing density and simpler, more modular overall system design, with attendant reliability benefits. An excellent analysis of MCM benefits is presented in [14].

lines exhibit complex analog phenomena such as reflection[2], dispersion[3], crosstalk[4] and skin effect[5], making it necessary for analog simulation to be used for the verification of digital MCM interconnections. Simulating lossy transmission lines efficiently is a difficult problem, particularly when strong nonlinearities (e.g., in digital logic) are present in the circuit.

Interconnect structures are the "wires" on an IC, module or PWB[6], ideally meant to be parasitic-free elements that provide electrical connection. Before the advent of the MCM (or hybrid), there were two levels of packaging structures in general use up to the PWB level: the IC or single-chip module (Level 1, to use the terminology of [14]), and the PWB (Level 2). The interconnect associated with Level 1 structures are typically thin (small cross-sectional area) and short (line-delays much smaller than the wavelength). The small cross-sectional area results in high series resistance, but the small length makes the use of RC models adequate. On the other hand, PWB or Level 2 interconnect are typically wide and long. Thus their resistance is small and so lumped capacitors, or lossless transmission lines (where inductance cannot be neglected) are adequate models. The emergence of MCM (often called Level 1.5) interconnect, which are both thin[7] and long, has made it necessary to use *lossy transmission lines* as models for such interconnect.

Many different models have been proposed for lossy transmission lines, the simplest being the uniformly distributed, constant R,L,C,G line (the "simple lossy line"). Other models handle more sophisticated effects by allowing R,L,C and G to vary with frequency ("frequency varying models"). The most important frequency varying models are those that deal with *skin-effect* [53, 57, 2, 36, 54], a phenomenon due to which fast-varying currents tend to concentrate towards the surface of a conductor. Qualitatively speaking, this reduces the effective cross-sectional area of a conductor thereby increasing its series resistance. Many studies have been conducted about the relevance of skin-effect to interconnect in the different levels of packaging structures [56, 21, 26, 42, 16]; that by Deutsch et. al. [11] is particularly informative. These studies have demonstrated that it is "sufficient to use frequency-independent series loss[8] in modelling rise-time dispersion and coupled noise for

[2] A phenomenon in which waves travelling through a line are reflected back to the source

[3] A phenomenon caused by series resistance that smoothens waveshapes and increases rise and fall times

[4] Spurious signals caused by capacitive and inductive coupling among interconnect in close proximity with each other

[5] A phenomenon due to which fast-varying currents tend to concentrate towards the surface of a conductor

[6] Printed Wiring Board, also known as PCB

[7] For example, a typical case (copper interconnect, 4μm high by 8μm wide) has series resistance of about 5Ω/cm [16].

[8] i.e., the simple lossy line

a large group of interconnection types", and that "this simplification will probably remain valid for many years to come" (excerpts from [11]). Other effects that have frequency varying models (such as dielectric dispersion and the slow wave effect) are usually of relatively little importance.

The transient simulation of lossy transmission lines is more difficult than that of lossless lines, for which satisfactory techniques exist [34, 33, 39, 43, 35]. The difficulty arises because time-domain equations for lossy lines lack the computational simplicity of those for lossless lines. Lossless lines have the property that at any given time, the influence of past activity can be captured entirely from the values of the port variables (the currents and voltages at the two ends) at a single previous instant of time. In contrast, lossy lines require information about either the entire history of their port variables up to the present time (c.f. the convolution formulation), or the values of the voltages and currents within the line (leading to the state-based method, described in this dissertation).

Equations describing lossy lines in the frequency domain are however easily obtained. This fact has been used for transient simulation within entirely linear circuits [16, 7]. All time-domain inputs to the circuit are converted numerically to the frequency domain (typically by means of the FFT), the circuit is analysed at several frequency points, and frequency-domain information from the solved circuit is reconverted back to the time domain. Apart from being inapplicable to circuits with nonlinear elements, this technique relies on numerical transforms of waveforms which can be inaccurate at the sharp transitions typical in high-speed digital circuits. Direct use of frequency-domain equations is also made by the waveform relaxation (WR) approach by Chang [3, 4, 5] and Wang et al [50]. This technique is applicable to lossy lines embedded in arbitrary nonlinear circuits. The WR methodology [30, 55] of holding all waveforms but one fixed at assumed values makes it possible to convert waveforms between the time and frequency domains; when a lossy line's equations are encountered, all computation is performed in the frequency domain, whereas the equations of other devices in the circuit are handled in the time domain. As in the previous method, the reliance of this technique on numerical transformation makes it susceptible to inaccuracies near sharp transitions.

Several techniques are based on representing the lossy line by a combination of circuit elements that are easier to simulate. In the lumped-RLC method [9], the oldest and best-known such technique, the lossy line is modelled as segments connected in series with each segment consisting of lumped R, L, C and G elements. Conceptual simplicity

combined with the convenience of being able to use existing simulators without modification have made this the most popular simulation technique in use today. Unfortunately, In high-speed simulations, many segments may be needed for accurate representation of the line; an inadequate number of segments may lead to spurious responses (Fig. 1.1). These responses are reminiscent of Gibbs' phenomenon [28, page 498] because the error near sharp edges reduces slowly with increase in the number of segments used. Using a large number of segments increases the size of the simulator circuit matrix, often to the extent that lossy line elements dominate the circuit computation time; in addition, a widely-separated time-constant problem is introduced because the time-constant of each segment needs to be much smaller than circuit rise times and the line's delay for accuracy. These factors can lead to large computation times for simulation. A variant of the lumped-RLC method that requires fewer segments for a prescribed accuracy is the pseudo-lumped method [22, 23], in which each segment is represented by a lossless line and lumped R and G elements. The delay of the transmission line in each segment is still constrained to be much smaller than circuit rise times, and high computation times are encountered in cases where time-steps are limited to values smaller than this delay. A third method [4] in this category relies on a more sophisticated choice of lumps in order to use fewer segments. The irrational transfer-functions of the lossy line are approximated by rational functions with a finite number of poles and zeros, i.e., a reduced-order model is obtained. A lumped network may be used to describe the reduced-order model. A related approach [31] uses Padé approximants to match the moments of the irrational transfer-functions up to some degree. The moments are calculated at infinite frequency, leading to better characterization of high frequency behaviour. The approximating rational function is equivalent to a lumped network (although the state variables are simulated without explicit representation as a lumped network in [31]). Yet another technique in this category is a variation proposed by Semlyen et al [46] in which approximations are made to time-domain responses instead of to the frequency-domain transfer-functions. The responses are approximated by the sum of a finite number of exponentials of different time-constants.

Another broad approach to lossy line simulation is based on using time-domain equations that capture the overall behaviour of the line, in the sense that the only circuit unknowns in the formulation are the port variables. Such techniques increase the size of the simulator matrix by only two equations independent of the parameters of the lossy line. Liu et al [32] were apparently first to use convolution to simulate similar devices, i.e.

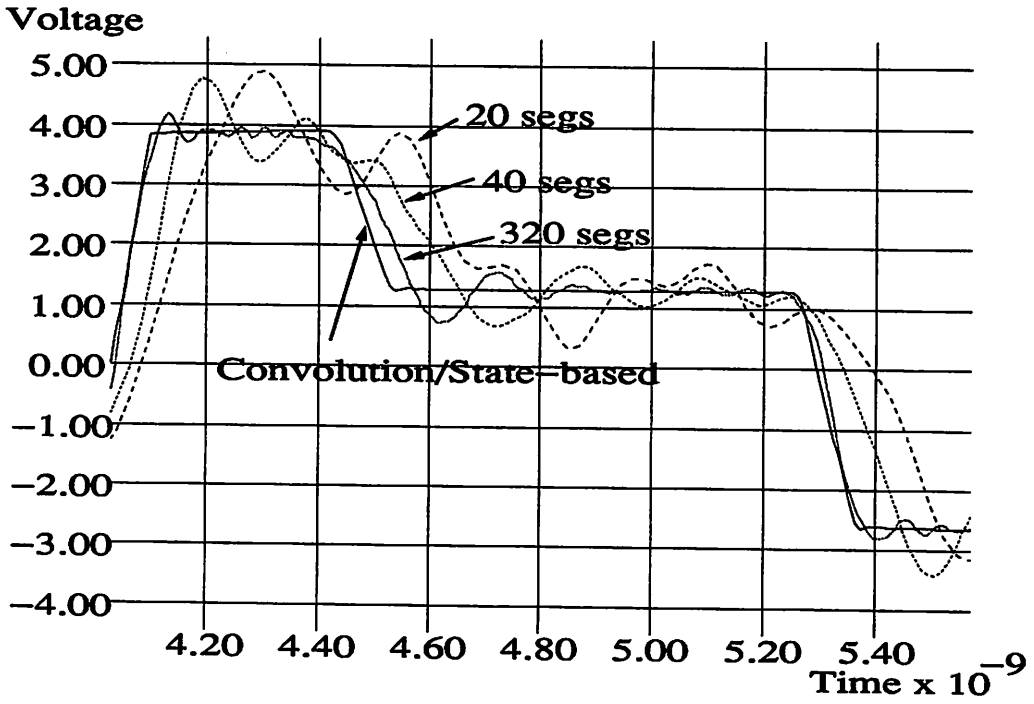

Figure 1.1: Lumped-RLC method, varying number of segments

antennas, in conjunction with nonlinear loads. Djordjević et al [12] applied the technique to simulate lossy lines. That the lossy line is a linear two-port was exploited by expressing the "outputs" of the two-port as a convolution of the "inputs" with impulse responses (or Green's functions) characteristic of the line. In a comparison of techniques for lossy line simulation [13], the convolution approach was found slow and only slightly more accurate than the lumped-RLC approach. In the early formulation, the length and nature of the impulse responses was a limitation: for lossless lines, the impulse responses were infinite in duration and consisted of periodic sharp spikes; those of lossy lines diminished gradually while being otherwise similar. Impulse-responses that fall to negligible levels after a short time result in efficient computation. If the responses remain significant for a period greater than the total simulation time, convolution from time $t_0 = 0$ to $t = t_n$ is necessary at every timepoint t_n. This operation requires computation proportional to n, resulting in total computation proportional to N^2 (quadratic time-complexity) in a simulation with N time-points. Augmenting the line with a quasi-matched load was attempted in [12] to shorten the responses. Schutt-Aine et al [44, 45] reformulated the convolution equations

using a scattering parameter approach that led to "well-behaved" impulse responses[9]. Even though these responses decreased monotonically, their effective duration could be greater than the total simulation time, depending on the values of R, L, G, and C of the line. The quadratic complexity problem of impulse response based methods remained.

The existing literature about the convolution approach has dealt mainly with equation formulation for well-behaved impulse responses. Obtaining the impulse responses and performing the convolution numerically have received less attention. The main advantage of convolution is that if the impulse responses are known exactly, no approximation needs to be made to the line's mechanism, leading to maximal accuracy. In existing work, however, exact expressions have not been used[10]; instead, numerical techniques have been applied to invert frequency-domain expressions. The FFT[11] has been employed in the work mentioned above. Other techniques for numerical inversion, for example using Padé approximations (Singhal [47, 48], Vlach [49]), do not appear to have been used to obtain impulse responses, having been applied to inverting waveforms at circuit nodes instead. Convolution appears to have been implemented using simple sample-and-sum approximation. The state-based approach described in this dissertation is very similar mathematically to the convolution method; in particular, the only circuit unknowns are the port variables.

Multiconductor, or coupled, transmission lines are important because coupling causes crosstalk, leading to possible false switching in digital circuits. In the lossless case, multiconductor lines can be decomposed numerically into uncoupled lossless lines and linear memoryless transformation networks; moreover, the special case of identical, locally-coupled lines is amenable to analytical decomposition (Romeo[39]). However, general lossy multiconductor lines cannot be decomposed into uncoupled simple lossy lines and transformation networks; the decomposition procedure (Schutt-Aine et al [45]) involves solving a frequency-dependent eigenvalue problem and results in frequency-varying lines (see next paragraph) and transformation networks with memory. Gao et al [19] have extended Romeo's work to show that identical, locally coupled simple lossy multiconductor lines can also be decomposed analytically into uncoupled simple lossy lines and linear memoryless terminal

[9]The "well-behaved" impulse response for a lossless line is a single Dirac delta function at the line delay; for lossy lines, the impulse responses decrease asymptotically and monotonically to zero.

[10]Analytic expressions for output waveforms for some specific circuit configurations (e.g., perfectly terminated, open, infinite line) of lossy lines are known [15, 27, 51, 8]; these are not applicable to the general case of arbitrary nonlinear termination.

[11]Fast Fourier Transform.

networks[12]. The state-based method as well as convolution using analytic forms are applicable to this special multiconductor case.

Models more complex than the simple lossy line are needed to account for second-order phenomena such as skin effect and dielectric dispersion [11, 16]. Such models ("frequency-varying models") have electrical parameters R, L, G and C varying with frequency. The frequency-domain techniques mentioned above are capable of simulating frequency-varying models; variations of the lumped-RLC method [57] have been proposed that use lumped networks to approximate the line's frequency variation. The rational-function and exponential techniques mentioned previously can also be applied to frequency-varying lines. The convolution technique is applicable to frequency-varying lines; however, the analytic forms for impulse responses developed in Chapter 2 of this dissertation are valid only for simple lossy lines. (Note that the numerical formulae of Chapter 3 are applicable to frequency-varying lines.) The state-based method has been extended to the frequency varying case. The techniques in this dissertation, though mainly limited to simple lossy lines, are of practical utility. Deutsch [8] has shown, for example, that the simple lossy line is an adequate model for the majority of simulations today and in the near future.

After presenting the formulations of the analytic convolution and state-based techniques in Chapter 2, a new technique for numerical convolution is presented in Chapter 3. Experimental results obtained by applying the new techniques to test circuits are presented in Chapter 4, followed by concluding remarks in Chapter 5.

[12]Unfortunately, part of our work in [40] was a duplication of this result.

Chapter 2

Analytic Convolution and State Based Formulations

In this chapter, an analytic formulation for uniform lossy transmission lines suitable for implementation into time-stepping circuit simulators (e.g. SPICE3 [37], ADVICE[17], ASTAP[52]) is developed. The time-domain Telegrapher Equations [44] are augmented with additive terms. Laplace transforms are taken to obtain ODEs in the s domain without ignoring possible non-zero initial conditions. The ODEs are decoupled using a scattering parameter formulation [44] and integrated to obtain a s-domain solution. Laplace inversion yields time-domain constitutive relations suitable for implementation using the numerical methods of Chapter 3.

The time-domain equations thus obtained may be used in three ways. Setting the augmenting terms to zero leads to two different methods for simulating the Simple Lossy Line – the Convolution and State Based methods. Both methods yield identical results in the theoretical limit of perfect numerical implementation; however, the Convolution method is quadratic time computationally while the State Based method is linear time. An important difference between these and previous methods (Chapter 1) is that the impulse responses and other functions needed in these methods need not be determined by numerical inversion but are available in analytic closed form.

In addition, setting the augmenting terms to suitable non-zero values results in the incorporation of high frequency nonidealities (see Chapter 1) into the simulation. Using a heuristic that is most effective for the small cross-sectional dimensions typical of multi-chip

modules preserves the linear time property of the State Based method for lines with high frequency nonidealities.

2.1 Analytic Formulation

Let $w_1(x,t)$ and $w_2(x,t)$ be two arbitrary functions defined on $[0,l] \times [0,\infty)$. Consider the following (the familiar Telegrapher Equations [45] with "inputs" w_1 and w_2, l being the length of the transmission line):

$$\frac{\partial v}{\partial x} = -\left(L_{dc}\frac{\partial i}{\partial t} + R_{dc}\, i\right) + w_1 \tag{2.1}$$

$$\frac{\partial i}{\partial x} = -\left(C_{dc}\frac{\partial v}{\partial t} + G_{dc}\, v\right) + w_2 \tag{2.2}$$

The above equations hold for x varying between 0 and l. $v(x,t)$ and $i(x,t)$ are the voltage and current at the point x in the line at time t, respectively. It is assumed that the simulation starts from time 0.

The inputs to the transmission line are the port variables $v_1(t) = v(0,t)$, $i_1(t) = i(0,t)$, $v_2(t) = v(l,t)$ and $i_2(t) = -i(l,t)$. These four port variables specify the *boundary conditions* of Equations 2.1 and 2.2.

In addition to the boundary conditions, w_1 and w_2, which represent the external inputs to the line, the internal state of the transmission line also determines the future behaviour of the line. This internal state is stored in the energy-storing distributed inductance and capacitance and is specified by the voltages and currents in the line's interior at time 0, $v_0(x) = v(x,0)$ and $i_0(x) = i(x,0)$. $v_0(x)$ and $i_0(x)$ are the *initial conditions* for Equations 2.1 and 2.2. The combination of the Telegrapher Equations, the boundary and initial conditions and the "inputs" w_1 and w_2 specify the future behaviour of the line uniquely.

Time-domain Laplace transforms are taken of Equations 2.1 and 2.2 to arrive at ordinary differential equations in x and the Laplace variable s:

$$\frac{\partial V}{\partial x} = -\left(sL_{dc} + R_{dc}\right) I + L_{dc}\, i_0(x) + W_1(x,s) \tag{2.3}$$

$$\frac{\partial I}{\partial x} = -\left(sC_{dc} + G_{dc}\right) V + C_{dc}\, v_0(x) + W_2(x,s) \tag{2.4}$$

Here V, I refer to $V(x,s)$ and $I(x,s)$, the Laplace-transformed variables. $W_1(x,s)$ and $W_2(x,s)$ are the Laplace transforms of $w_1(x,t)$ and $w_2(x,t)$.

To uncouple the above equations, a basis change is performed from the variables V and I to new ("scattering parameter") variables p and q, defined as follows:

$$p(x,s) = \frac{V(x,s) + Z^{dc}(s)\, I(x,s)}{2} \tag{2.5}$$

$$q(x,s) = \frac{V(x,s) - Z^{dc}(s)\, I(x,s)}{2} \tag{2.6}$$

$Z^{dc}(s)$ is the frequency-domain characteristic impedance of the line:

$$Z^{dc}(s) = \sqrt{\frac{sL_{dc} + R_{dc}}{sC_{dc} + G_{dc}}} \tag{2.7}$$

Equations 2.5 and 2.6 are rewritten to express V and I in terms of p and q. Using these equations, Equations 2.3 and 2.4 are rewritten in terms of p and q. Two decoupled linear first-order ODEs in x are obtained by adding and subtracting Equations 2.3 and 2.4:

$$\begin{aligned} \frac{\partial p}{\partial x} + \lambda^{dc}(s)\, p &= \frac{L_{dc}\, i_0(x) + Z^{dc}(s)\, C_{dc}\, v_0(x)}{2} \\ &\quad + \frac{W_1(x,s) + Z^{dc}(s)\, W_2(x,s)}{2} \end{aligned} \tag{2.8}$$

$$\begin{aligned} \frac{\partial q}{\partial x} - \lambda^{dc}(s)\, q &= \frac{L_{dc}\, i_0(x) - Z^{dc}(s)\, C_{dc}\, v_0(x)}{2} \\ &\quad + \frac{W_1(x,s) - Z^{dc}(s)\, W_2(x,s)}{2} \end{aligned} \tag{2.9}$$

$\lambda^{dc}(s)$ is the frequency-domain propagation constant of the line:

$$\lambda^{dc}(s) = \sqrt{(sC_{dc} + G_{dc})(sL_{dc} + R_{dc})} \tag{2.10}$$

The general solution of any first-order ordinary differential equation of the type

$$\frac{\partial y}{\partial x} + P(x)\, y = Q(x) \tag{2.11}$$

is

$$y = e^{-\int P(x)\, dx} \left(C_1 + \int Q(x)\, e^{\int P(y)\, dy}\, dx \right) \tag{2.12}$$

Equation 2.12 is then applied to Equations 2.8 and 2.9 to obtain the solutions for p and q:

$$\begin{aligned} p(x,s) = e^{-\lambda^{dc} x} \Bigg(A + \frac{1}{2} \int_0^x e^{\lambda^{dc} y} \left[L_{dc}\, i_0(y) + Z^{dc}(s)\, C_{dc}\, v_0(y) \right] dy \\ + \frac{1}{2} \int_0^x e^{\lambda^{dc} y} \left[W_1(y,s) + Z^{dc}(s)\, W_2(y,s) \right] dy \Bigg) \end{aligned} \tag{2.13}$$

$$q(x,s) = e^{\lambda^{dc}x}\left(B + \frac{1}{2}\int_0^x e^{-\lambda^{dc}y}\left[L_{dc}\, i_0(y) - Z^{dc}(s)\, C_{dc}\, v_0(y)\right] dy \right.$$
$$\left. + \frac{1}{2}\int_0^x e^{-\lambda^{dc}y}\left[W_1(y,s) - Z^{dc}(s)\, W_2(y,s)\right] dy\right) \quad (2.14)$$

The boundary condition at $x = 0$ is applied to Equation 2.13, and that at $x = l$ to Equation 2.14, to determine the constants A and B which are substituted for to obtain:

$$p(x,s) - e^{-\lambda^{dc}x}p(0,s) = \int_0^x \frac{e^{-\lambda^{dc}(x-y)}}{2}\left[L_{dc}\, i_0(y) + Z^{dc}(s)\, C_{dc}\, v_0(y)\right] dy$$
$$+ \int_0^x \frac{e^{-\lambda^{dc}(x-y)}}{2}\left[W_1(y,s) + Z^{dc}(s)\, W_2(y,s)\right] dy \quad (2.15)$$
$$q(l,s)e^{-\lambda^{dc}(l-x)} - q(x,s) = \int_x^l \frac{e^{-\lambda^{dc}(y-x)}}{2}\left[L_{dc}\, i_0(y) - Z^{dc}(s)\, C_{dc}\, v_0(y)\right] dy$$
$$+ \int_x^l \frac{e^{-\lambda^{dc}(y-x)}}{2}\left[W_1(y,s) - Z^{dc}(s)\, W_2(y,s)\right] dy \quad (2.16)$$

Now p and q are substituted for in terms of V and I (using Equations 2.5 and 2.7, and the resulting equations divided by $Z^{dc}(s)$[1] to obtain:

$$\left[V(x,s)Y^{dc}(s) + I(x,s)\right] - e^{-\lambda^{dc}x}\left[V(0,s)Y^{dc}(s) + I(0,s)\right]$$
$$= \int_0^x e^{-\lambda^{dc}(x-y)}\left[L_{dc}\, i_0(y)\, Y^{dc}(s) + C_{dc}\, v_0(y)\right] dy$$
$$+ \int_0^x e^{-\lambda^{dc}(x-y)}\left[W_1(y,s)\, Y^{dc}(s) + W_2(y,s)\right] dy \quad (2.17)$$
$$\left[V(l,s)Y^{dc}(s) - I(l,s)\right] e^{-\lambda^{dc}(l-x)} - \left[V(x,s)Y^{dc}(s) - I(x,s)\right]$$
$$= \int_x^l e^{-\lambda^{dc}(y-x)}\left[L_{dc}\, i_0(y)\, Y^{dc}(s) - C_{dc}\, v_0(y)\right] dy$$
$$+ \int_x^l e^{-\lambda^{dc}(y-x)}\left[W_1(y,s)\, Y^{dc}(s) - W_2(y,s)\right] dy \quad (2.18)$$

where

$$Y^{dc}(s) = \frac{1}{Z^{dc}(s)} = \sqrt{\frac{sC_{dc} + G_{dc}}{sL_{dc} + R_{dc}}} \quad (2.19)$$

The first integral in x on the RHS of Equations 2.17 and 2.18 is evaluated next[2]. The interval $[0, l]$ is divided into a number of segments between the points $x_0, x_1, \ldots, x_{n_l}$,

[1] Without loss of generality, we assume $\frac{R_{dc}}{L_{dc}} > \frac{G_{dc}}{C_{dc}}$ in the following. If $\frac{R_{dc}}{L_{dc}} < \frac{G_{dc}}{C_{dc}}$, this division by $Z^{dc}(s)$ is not carried out, but the rest of the derivation is repeated verbatim. This change is key in obtaining well-behaved impulse responses.

[2] It is tempting to apply the inverse Laplace transform at this point to Equations 2.17 and 2.18, transmitting the inversion operator through the spatial integrals. Such a course leads to erroneous results because the integrands involved are not uniformly continuous.

with $x_0 = 0$ and $x_{n_l} = l$. (It is at these sample points that information about the line state is used in the algorithm.) Let k be the index of the sample point located at x, i.e., $x_k = x$. Over each interval $I_j = [x_{j-1}, x_j]$, it is assumed that the initial states $v_0(x)$ and $i_0(x)$ can be represented by *piecewise linear* segments v_{0j} and i_{0j}. The first integral on the RHS of Equations 2.17 and 2.18 is split into a sum of integrals, each over I_j; over each I_j, the integrand is simply an exponential which is easily integrated. The evaluation of the second space integral on the RHS is deferred until later.

$$
\begin{aligned}
&[Y_0\,V(x,s)\,H_Y^{dc}(s) + I(x,s)] - [Y_0\,V(0,s)\,H_{\gamma Y}^{dc}(x,s) + I(0,s)\,H_\gamma^{dc}(x,s)] \\
&\quad = i_{0k} H_{S\gamma Y}(x - x_k, s) - i_{00} H_{S\gamma Y}(x - x_0, s) \\
&\qquad + Y_0 \left[v_{0k} H_{S\gamma}(x - x_k, s) - v_{00} H_{S\gamma}(x - x_0, s) \right] \\
&\qquad - \frac{1}{\gamma_0} \left[\begin{array}{c} -\left(\frac{i_{01} - i_{00}}{x_1 - x_0}\right) H_{S^2\gamma Y}(x - x_0, s) + \left(\frac{i_{0k} - i_{0,k-1}}{x_k - x_{k-1}}\right) H_{S^2\gamma Y}(x - x_k, s) \\ + Y_0 \left[-\left(\frac{v_{01} - v_{00}}{x_1 - x_0}\right) H_{S^2\gamma}(x - x_0, s) + \left(\frac{v_{0k} - v_{0,k-1}}{x_k - x_{k-1}}\right) H_{S^2\gamma}(x - x_k, s) \right] \\ + \sum_{j=1}^{k-1} \left[\begin{array}{c} H_{S^2\gamma Y}(x - x_j, s) \left[-\left(\frac{i_{0,j+1} - i_{0j}}{x_{j+1} - x_j}\right) + \left(\frac{i_{0j} - i_{0,j-1}}{x_j - x_{j-1}}\right) \right] \\ + Y_0 H_{S^2\gamma}(x - x_j, s) \left[-\left(\frac{v_{0,j+1} - v_{0j}}{x_{j+1} - x_j}\right) + \left(\frac{v_{0j} - v_{0,j-1}}{x_j - x_{j-1}}\right) \right] \end{array} \right] \end{array} \right] \\
&\qquad + \int_0^x e^{-\lambda^{dc}(x-y)} \left[W_1(y,s)\,Y^{dc}(s) + W_2(y,s) \right] dy
\end{aligned}
\tag{2.20}
$$

$$
\begin{aligned}
&[Y_0\,V(l,s)\,H_{\gamma Y}^{dc}(l\text{–}x,s) - I(l,s)\,H_\gamma^{dc}(l\text{–}x,s)] - [Y_0\,V(x,s)\,H_Y^{dc}(s) - I(x,s)] \\
&\quad = i_{0k} H_{S\gamma Y}(x_k - x, s) - i_{0,n_l} H_{S\gamma Y}(x_{n_l} - x, s) \\
&\qquad - Y_0 \left[v_{0k} H_{S\gamma}(x_k - x, s) - v_{0,n_l} H_{S\gamma}(x_{n_l} - x, s) \right] \\
&\qquad - \frac{1}{\gamma_0} \left[\begin{array}{c} -\left(\frac{i_{0,k+1} - i_{0k}}{x_{k+1} - x_k}\right) H_{S^2\gamma Y}(x_k - x, s) + \left(\frac{i_{0,n_l} - i_{0,n_l-1}}{x_{n_l} - x_{n_l-1}}\right) H_{S^2\gamma Y}(x_{n_l} - x, s) \\ - Y_0 \left[-\left(\frac{v_{0,k+1} - v_{0k}}{x_{k+1} - x_k}\right) H_{S^2\gamma}(x_k - x, s) + \left(\frac{v_{0,n_l} - v_{0,n_l-1}}{x_{n_l} - x_{n_l-1}}\right) H_{S^2\gamma}(x_{n_l} - x, s) \right] \\ + \sum_{j=k+1}^{n_l-1} \left[\begin{array}{c} H_{S^2\gamma Y}(x_j - x, s) \left[-\left(\frac{i_{0,j+1} - i_{0j}}{x_{j+1} - x_j}\right) + \left(\frac{i_{0j} - i_{0,j-1}}{x_j - x_{j-1}}\right) \right] \\ - Y_0 H_{S^2\gamma}(x_j - x, s) \left[-\left(\frac{v_{0,j+1} - v_{0j}}{x_{j+1} - x_j}\right) + \left(\frac{v_{0j} - v_{0,j-1}}{x_j - x_{j-1}}\right) \right] \end{array} \right] \end{array} \right] \\
&\qquad + \int_x^l e^{-\lambda^{dc}(y-x)} \left[W_1(y,s)\,Y^{dc}(s) - W_2(y,s) \right] dy
\end{aligned}
\tag{2.21}
$$

where

$$Y_0 = \sqrt{\frac{C_{dc}}{L_{dc}}} \tag{2.22}$$

$$H_{S\gamma Y}(x,s) = L_{dc}\,Y^{dc}(s)\,\frac{e^{-\lambda^{dc}(s)\,x}}{\lambda^{dc}(s)} \tag{2.23}$$

$$H_{S\gamma}(x,s) = \sqrt{L_{dc} C_{dc}}\,\frac{e^{-\lambda^{dc}(s)\,x}}{\lambda^{dc}(s)} \tag{2.24}$$

$$H_{S^2\gamma Y}(x,s) = L_{dc}^{\frac{3}{2}}\sqrt{C_{dc}}\,Y^{dc}(s)\,\frac{e^{-\lambda^{dc}(s)\,x}}{\lambda^{dc}(s)^2} \tag{2.25}$$

$$H_{S\gamma}(x,s) = L_{dc}C_{dc}\,\frac{e^{-\lambda^{dc}(s)\,x}}{\lambda^{dc}(s)^2} \tag{2.26}$$

Let $h_{S\gamma Y}$, $h_{S\gamma}$, $h_{S^2\gamma Y}$ and $h_{S^2\gamma}$ denote the inverse Laplace transforms of $H_{S\gamma Y}$, $H_{S\gamma}$, $H_{S^2\gamma Y}$ and $H_{S^2\gamma}$ respectively. Expressions for these, as well as h_Y^{dc}, $h_{\gamma Y}^{dc}$, h_γ^{dc}, defined earlier, are derived next. Define

$$\gamma_0 = \sqrt{L_{dc}C_{dc}},\quad \beta = \frac{1}{2}\left(\frac{R_{dc}}{L_{dc}} + \frac{G_{dc}}{C_{dc}}\right),\quad \alpha = \frac{1}{2}\left(\frac{R_{dc}}{L_{dc}} - \frac{G_{dc}}{C_{dc}}\right) \tag{2.27}$$

and note that

$$H_Y^{dc}(s) = \frac{1}{Y_0}\sqrt{\frac{sC_{dc}+G_{dc}}{sL_{dc}+R_{dc}}} = \sqrt{\frac{(s+\beta)-\alpha}{(s+\beta)+\alpha}} \tag{2.28}$$

$$H_\gamma^{dc}(x,s) = e^{-x\sqrt{sC_{dc}(sL_{dc}+R_{dc})}} = e^{-\gamma_0\,x\sqrt{(s+\beta)^2-\alpha^2}} \tag{2.29}$$

$$H_{\gamma Y}^{dc}(x,s) = H_Y^{dc}(x,s)\,H_\gamma^{dc}(x,s) \tag{2.30}$$

$$H_{S\gamma}(x,s) = \frac{e^{-\gamma_0 x\sqrt{(s+\beta)^2-\alpha^2}}}{\sqrt{(s+\beta)^2-\alpha^2}} \tag{2.31}$$

$$H_{S\gamma Y}(x,s) = \frac{e^{-\gamma_0 x\sqrt{(s+\beta)^2-\alpha^2}}}{(s+\beta)+\alpha} \tag{2.32}$$

$$H_{S^2\gamma}(x,s) = \frac{e^{-\gamma_0 x\sqrt{(s+\beta)^2-\alpha^2}}}{(s+\beta)^2-\alpha^2} \tag{2.33}$$

$$H_{S^2\gamma Y}(x,s) = \frac{e^{-\gamma_0 x\sqrt{(s+\beta)^2-\alpha^2}}}{\{(s+\beta)+\alpha\}\left\{\sqrt{(s+\beta)^2-\alpha^2}\right\}} \tag{2.34}$$

From Table 2.1, the relation[3] $I_0' = I_1$ [1] and elementary properties of the Laplace transform, the following expressions are obtained for $h_Y^{dc}(t)$, $h_\gamma^{dc}(x,t)$, $h_{\gamma Y}^{dc}(x,t)$, $h_{S\gamma}(x,t)$, $h_{S\gamma Y}(x,t)$, $h_{S^2\gamma}(x,t)$ and $h_{S^2\gamma Y}(x,t)$:

$$h_Y(t) = [\delta(t) + \alpha\,\{I_1(\alpha t) - I_0(\alpha t)\}]\,e^{-\beta t} \tag{2.35}$$

$$h_\gamma(x,t) = \left[\delta(t-\gamma_0 x) + u(t-\gamma_0 x)\frac{\alpha\gamma_0 x\,I_1\left(\alpha\sqrt{t^2-(\gamma_0 x)^2}\right)}{\sqrt{t^2-(\gamma_0 x)^2}}\right]e^{-\beta t} \tag{2.36}$$

[3] I_k is the *modified Bessel function* of k^{th} order

No.	$F(s)$	$f(t)$
1	$\frac{1}{\sqrt{s^2-\alpha^2}}e^{-T\sqrt{s^2-\alpha^2}}$	$1(t-T)I_0\left(\alpha\sqrt{t^2-T^2}\right)$
2	$e^{-T\sqrt{s^2-\alpha^2}}-e^{-sT}$	$1(t-T)\frac{\alpha T}{\sqrt{t^2-T^2}}I_1\left(\alpha\sqrt{t^2-T^2}\right)$
3	$\frac{1}{\sqrt{s^2-\alpha^2}}$	$I_0(\alpha t)$
4	$\frac{\sqrt{s+\alpha}}{\sqrt{s-\alpha}}-1$	$\alpha\left[I_0(\alpha t)+I_1(\alpha t)\right]$
5	$\sqrt{s+\alpha}-\sqrt{s+\beta}$	$\frac{1}{2\sqrt{\pi t^3}}\left[e^{-\beta t}-e^{-\alpha t}\right]$
6	$\frac{1}{s^{\frac{3}{2}}}$	$\frac{2}{\sqrt{\pi}}\sqrt{t}$
7	$\frac{1}{s^{\frac{3}{2}}}e^{-\sqrt{sT}}$	$2\sqrt{\frac{t}{\pi}}e^{-\frac{T}{4t}}-\sqrt{T}\,erfc\left(\frac{\sqrt{T}}{2\sqrt{t}}\right)$
8	$\frac{1}{s^2}e^{-\sqrt{sT}}$	$\left(\frac{T}{2}+t\right)erfc\left(\frac{\sqrt{T}}{2\sqrt{t}}\right)-\sqrt{\frac{Tt}{\pi}}e^{-\frac{T}{4t}}$

Table 2.1: Laplace Transform Pairs (Fodor[18])

$$h_{\gamma Y}(x,t)=\Bigg[\delta(t-\gamma_0 x)+u(t-\gamma_0 x)\,\alpha\times \left\{\frac{tI_1\left(\alpha\sqrt{t^2-(\gamma_0 x)^2}\right)}{\sqrt{t^2-(\gamma_0 x)^2}}-I_0\left(\alpha\sqrt{t^2-(\gamma_0 x)^2}\right)\right\}\Bigg]e^{-\beta t} \tag{2.37}$$

$$h_{S\gamma}(x,t)=u(t-\gamma_0 x)\,I_0\left(\alpha\sqrt{t^2-(\gamma_0 x)^2}\right)\,e^{-\beta t} \tag{2.38}$$

$$h_{S\gamma Y}(x,t)=u(t-\gamma_0 x)\Bigg[e^{-\alpha(t-\gamma_0 x)} +\alpha\gamma_0 x\int_{\gamma_0 x}^{t}e^{-\alpha(t-\tau)}\frac{I_1\left(\alpha\sqrt{\tau^2-(\gamma_0 x)^2}\right)}{\sqrt{\tau^2-(\gamma_0 x)^2}}\,d\tau\Bigg]e^{-\beta t} \tag{2.39}$$

$$h_{S^2\gamma}(x,t)=u(t-\gamma_0 x)\,e^{-\beta t}\int_{\gamma_0 x}^{t}I_0\left(\alpha\sqrt{t^2-\tau^2}\right)\,d\tau \tag{2.40}$$

$$h_{S^2\gamma Y}(x,t)=u(t-\gamma_0 x)\,e^{-\beta t}\int_{\gamma_0 x}^{t}e^{-\alpha(t-\tau)}I_0\left(\alpha\sqrt{\tau^2-(\gamma_0 x)^2}\right)\,d\tau \tag{2.41}$$

In the above $u(t)$ and $\delta(t)$ represent the unit step and delta functions respectively.

Equations 2.20 and 2.21 can now be Laplace inverted to yield the time-domain constitutive relations of the lossy transmission line at any x.

$$
\begin{aligned}
&[Y_0\, v(x,t) * h_Y^{dc}(t) + i(x,t)] - [Y_0\, v(0,t) * h_{\gamma Y}^{dc}(x,t) + i(0,t) * h_\gamma^{dc}(x,t)] \\
&\quad = i_{0k} h_{S\gamma Y}(x - x_k, t) - i_{00} h_{S\gamma Y}(x - x_0, t) \\
&\qquad + Y_0 \left[v_{0k} h_{S\gamma}(x - x_k, t) - v_{00} h_{S\gamma}(x - x_0, t) \right] \\
&\qquad - \frac{1}{\gamma_0} \left[\begin{array}{l}
- \left(\frac{i_{01} - i_{00}}{x_1 - x_0} \right) h_{S^2\gamma Y}(x - x_0, t) + \left(\frac{i_{0k} - i_{0,k-1}}{x_k - x_{k-1}} \right) h_{S^2\gamma Y}(x - x_k, t) \\
+ Y_0 \left[- \left(\frac{v_{01} - v_{00}}{x_1 - x_0} \right) h_{S^2\gamma}(x - x_0, t) + \left(\frac{v_{0k} - v_{0,k-1}}{x_k - x_{k-1}} \right) h_{S^2\gamma}(x - x_k, t) \right] \\
\displaystyle + \sum_{j=1}^{k-1} \left[\begin{array}{l}
h_{S^2\gamma Y}(x - x_j, t) \left[- \left(\frac{i_{0,j+1} - i_{0j}}{x_{j+1} - x_j} \right) + \left(\frac{i_{0j} - i_{0,j-1}}{x_j - x_{j-1}} \right) \right] \\
+ Y_0 h_{S^2\gamma}(x - x_j, t) \left[- \left(\frac{v_{0,j+1} - v_{0j}}{x_{j+1} - x_j} \right) + \left(\frac{v_{0j} - v_{0,j-1}}{x_j - x_{j-1}} \right) \right]
\end{array} \right]
\end{array} \right] \\
&\qquad + \mathcal{L}^{-1} \left\{ \int_0^x e^{-\lambda^{dc}(x-y)} \left[W_1(y,s)\, Y^{dc}(s) + W_2(y,s) \right] dy \right\}
\end{aligned}
\tag{2.42}
$$

$$
\begin{aligned}
&[Y_0\, v(l,t) * h_{\gamma Y}^{dc}(l - x, t) - i(l,t) * h_\gamma^{dc}(l - x, t)] - [Y_0\, v(x,t) * h_Y^{dc}(t) - i(x,t)] \\
&\quad = i_{0k} h_{S\gamma Y}(x_k - x, t) - i_{0,n_l} h_{S\gamma Y}(x_{n_l} - x, t) \\
&\qquad - Y_0 \left[v_{0k} h_{S\gamma}(x_k - x, t) - v_{0,n_l} h_{S\gamma}(x_{n_l} - x, t) \right] \\
&\qquad - \frac{1}{\gamma_0} \left[\begin{array}{l}
- \left(\frac{i_{0,k+1} - i_{0k}}{x_{k+1} - x_k} \right) h_{S^2\gamma Y}(x_k - x, t) + \left(\frac{i_{0,n_l} - i_{0,n_l-1}}{x_{n_l} - x_{n_l-1}} \right) h_{S^2\gamma Y}(x_{n_l} - x, t) \\
- Y_0 \left[- \left(\frac{v_{0,k+1} - v_{0k}}{x_{k+1} - x_k} \right) h_{S^2\gamma}(x_k - x, t) + \left(\frac{v_{0,n_l} - v_{0,n_l-1}}{x_{n_l} - x_{n_l-1}} \right) h_{S^2\gamma}(x_{n_l} - x, t) \right] \\
\displaystyle + \sum_{j=k+1}^{n_l-1} \left[\begin{array}{l}
h_{S^2\gamma Y}(x_j - x, t) \left[- \left(\frac{i_{0,j+1} - i_{0j}}{x_{j+1} - x_j} \right) + \left(\frac{i_{0j} - i_{0,j-1}}{x_j - x_{j-1}} \right) \right] \\
- Y_0 h_{S^2\gamma}(x_j - x, t) \left[- \left(\frac{v_{0,j+1} - v_{0j}}{x_{j+1} - x_j} \right) + \left(\frac{v_{0j} - v_{0,j-1}}{x_j - x_{j-1}} \right) \right]
\end{array} \right]
\end{array} \right] \\
&\qquad + \mathcal{L}^{-1} \left\{ \int_x^l e^{-\lambda^{dc}(y-x)} \left[W_1(y,s)\, Y^{dc}(s) - W_2(y,s) \right] dy \right\}
\end{aligned}
\tag{2.43}
$$

In the above equations, $*$ denotes the convolution operator, defined in Chapter 3. The evaluation of the terms involving W_1 and W_2 is deferred until Sections 2.2 and 2.5.

The equations obtained by substituting $x = l$ in Equation 2.42 and $x = 0$ in Equation 2.43 are of special interest:

$$
\begin{aligned}
&[Y_0\, v_2(t) * h_Y^{dc}(t) - i_2(t)] - [Y_0\, v_1(t) * h_{\gamma Y}^{dc}(l,t) + i_1(t) * h_\gamma^{dc}(l,t)] \\
&\quad = i_{0,n_l} h_{S\gamma Y}(0,t) - i_{00} h_{S\gamma Y}(l,t) \\
&\qquad + Y_0 \left[v_{0,n_l} h_{S\gamma}(0,t) - v_{00} h_{S\gamma}(l,t) \right] \\
&\qquad - \frac{1}{\gamma_0} \left[\begin{array}{l}
- \left(\frac{i_{01} - i_{00}}{x_1 - x_0} \right) h_{S^2\gamma Y}(l,t) + \left(\frac{i_{0,n_l} - i_{0,n_l-1}}{l - x_{n_l-1}} \right) h_{S^2\gamma Y}(0,t) \\
+ Y_0 \left[- \left(\frac{v_{01} - v_{00}}{x_1 - x_0} \right) h_{S^2\gamma}(l,t) + \left(\frac{v_{0,n_l} - v_{0,n_l-1}}{l - x_{n_l-1}} \right) h_{S^2\gamma}(0,t) \right] \\
\displaystyle + \sum_{j=1}^{n_l-1} \left[\begin{array}{l}
h_{S^2\gamma Y}(l - x_j, t) \left[- \left(\frac{i_{0,j+1} - i_{0j}}{x_{j+1} - x_j} \right) + \left(\frac{i_{0j} - i_{0,j-1}}{x_j - x_{j-1}} \right) \right] \\
+ Y_0 h_{S^2\gamma}(l - x_j, t) \left[- \left(\frac{v_{0,j+1} - v_{0j}}{x_{j+1} - x_j} \right) + \left(\frac{v_{0j} - v_{0,j-1}}{x_j - x_{j-1}} \right) \right]
\end{array} \right]
\end{array} \right]
\end{aligned}
$$

$$+\mathcal{L}^{-1}\left\{\int_0^l e^{-\lambda^{dc}(l-y)}\left[W_1(y,s)\,Y^{dc}(s)+W_2(y,s)\right]dy\right\} \tag{2.44}$$

$$\begin{aligned}
&[Y_0\,v_2(t)*h^{dc}_{\gamma Y}(l,t)+i_2(t)*h^{dc}_{\gamma}(l,t)]-[Y_0\,v_1(t)*h^{dc}_{Y}(t)-i_1(t)]\\
&\quad=i_{00}h_{S\gamma Y}(0,t)-i_{0,n_l}h_{S\gamma Y}(l,t)\\
&\qquad-Y_0\left[v_{00}h_{S\gamma}(0,t)-v_{0,n_l}h_{S\gamma}(l,t)\right]\\
&\qquad-\frac{1}{\gamma_0}\left[\begin{array}{l}
-\left(\frac{i_{01}-i_{00}}{x_1-x_0}\right)h_{S^2\gamma Y}(0,t)+\left(\frac{i_{0,n_l}-i_{0,n_l-1}}{l-x_{n_l-1}}\right)h_{S^2\gamma Y}(l,t)\\
-Y_0\left[-\left(\frac{v_{01}-v_{00}}{x_1-x_0}\right)h_{S^2\gamma}(0,t)+\left(\frac{v_{0,n_l}-v_{0,n_l-1}}{l-x_{n_l-1}}\right)h_{S^2\gamma}(l,t)\right]\\
+\sum_{j=1}^{n_l-1}\left[\begin{array}{l}
h_{S^2\gamma Y}(x_j,t)\left[-\left(\frac{i_{0,j+1}-i_{0j}}{x_{j+1}-x_j}\right)+\left(\frac{i_{0j}-i_{0,j-1}}{x_j-x_{j-1}}\right)\right]\\
-Y_0h_{S^2\gamma}(x_j,t)\left[-\left(\frac{v_{0,j+1}-v_{0j}}{x_{j+1}-x_j}\right)+\left(\frac{v_{0j}-v_{0,j-1}}{x_j-x_{j-1}}\right)\right]
\end{array}\right]
\end{array}\right]\\
&\qquad+\mathcal{L}^{-1}\left\{\int_0^l e^{-\lambda^{dc}(y)}\left[W_1(y,s)\,Y^{dc}(s)-W_2(y,s)\right]dy\right\}
\end{aligned} \tag{2.45}$$

2.2 Simple Lossy Lines

Setting w_1 and w_2 to zero in Equations 2.1 and 2.2 leads to the analytic formulation for transmission lines with constant, or frequency-independent, R, L, G and C. Such lines are referred to here as Simple Lossy Lines (SLLs). All terms with W_1 and W_2 drop out in the above equations, in particular in Equations 2.44 and 2.45, reproduced below.

$$\begin{aligned}
&[Y_0\,v_2(t)*h^{dc}_{Y}(t)-i_2(t)]-[Y_0\,v_1(t)*h^{dc}_{\gamma Y}(l,t)+i_1(t)*h^{dc}_{\gamma}(l,t)]\\
&\quad=i_{0,n_l}h_{S\gamma Y}(0,t)-i_{00}h_{S\gamma Y}(l,t)\\
&\qquad+Y_0\left[v_{0,n_l}h_{S\gamma}(0,t)-v_{00}h_{S\gamma}(l,t)\right]\\
&\qquad-\frac{1}{\gamma_0}\left[\begin{array}{l}
-\left(\frac{i_{01}-i_{00}}{x_1-x_0}\right)h_{S^2\gamma Y}(l,t)+\left(\frac{i_{0,n_l}-i_{0,n_l-1}}{l-x_{n_l-1}}\right)h_{S^2\gamma Y}(0,t)\\
+Y_0\left[-\left(\frac{v_{01}-v_{00}}{x_1-x_0}\right)h_{S^2\gamma}(l,t)+\left(\frac{v_{0,n_l}-v_{0,n_l-1}}{l-x_{n_l-1}}\right)h_{S^2\gamma}(0,t)\right]\\
+\sum_{j=1}^{n_l-1}\left[\begin{array}{l}
h_{S^2\gamma Y}(l-x_j,t)\left[-\left(\frac{i_{0,j+1}-i_{0j}}{x_{j+1}-x_j}\right)+\left(\frac{i_{0j}-i_{0,j-1}}{x_j-x_{j-1}}\right)\right]\\
+Y_0h_{S^2\gamma}(l-x_j,t)\left[-\left(\frac{v_{0,j+1}-v_{0j}}{x_{j+1}-x_j}\right)+\left(\frac{v_{0j}-v_{0,j-1}}{x_j-x_{j-1}}\right)\right]
\end{array}\right]
\end{array}\right]
\end{aligned} \tag{2.46}$$

$$[Y_0\,v_2(t)*h^{dc}_{\gamma Y}(l,t)+i_2(t)*h^{dc}_{\gamma}(l,t)]-[Y_0\,v_1(t)*h^{dc}_{Y}(t)-i_1(t)]$$

$$
\begin{aligned}
&= i_{00}h_{S\gamma Y}(0,t) - i_{0,n_l}h_{S\gamma Y}(l,t) \\
&\quad -Y_0\left[v_{00}h_{S\gamma}(0,t) - v_{0,n_l}h_{S\gamma}(l,t)\right] \\
&\quad -\frac{1}{\gamma_0}\left[\begin{array}{c}
-\left(\frac{i_{01}-i_{00}}{x_1-x_0}\right)h_{S^2\gamma Y}(0,t) + \left(\frac{i_{0,n_l}-i_{0,n_l-1}}{l-x_{n_l-1}}\right)h_{S^2\gamma Y}(l,t) \\
-Y_0\left[-\left(\frac{v_{01}-v_{00}}{x_1-x_0}\right)h_{S^2\gamma}(0,t) + \left(\frac{v_{0,n_l}-v_{0,n_l-1}}{l-x_{n_l-1}}\right)h_{S^2\gamma}(l,t)\right] \\
+\sum_{j=1}^{n_l-1}\left[\begin{array}{c}
h_{S^2\gamma Y}(x_j,t)\left[-\left(\frac{i_{0,j+1}-i_{0j}}{x_{j+1}-x_j}\right) + \left(\frac{i_{0j}-i_{0,j-1}}{x_j-x_{j-1}}\right)\right] \\
-Y_0 h_{S^2\gamma}(x_j,t)\left[-\left(\frac{v_{0,j+1}-v_{0j}}{x_{j+1}-x_j}\right) + \left(\frac{v_{0j}-v_{0,j-1}}{x_j-x_{j-1}}\right)\right]
\end{array}\right]
\end{array}\right]
\end{aligned}
\tag{2.47}
$$

Equations 2.46 and 2.47 are the constitutive equations of the Simple Lossy Line with the initial state $(v_0(x), i_0(x))$ at time $t_0 = 0$. The contribution of the initial state is represented by the terms on the RHS of the equations, whereas all the terms involving convolution are on the LHS. These equations can be used in two different ways for simulation: one leads to the quadratic time convolution technique while the other leads to the linear-time state-based technique.

2.3 Analytic Convolution Technique

If the time origin is kept fixed at $t_0 = 0$ in Equations 2.46 and 2.47, the implementation of the equations leads to the analytic convolution method. At any time point t_i in the simulation, each convolution is carried out from the time origin to the current time, i.e., values of v_1, v_2, i_1 and i_2 over the interval $[t_0, t_i]$ need to be used. The initial state $(v_0(x), i_0(x))$ used for the RHS of the equations is always the initial state at the time origin $t_0 = 0$. (Usually, this initial state is assumed zero, in which case the RHS of the equations vanish. If the line is at a non-zero DC initial state, a simple reformulation exploiting the linearity of the line yields a system with zero initial state.) The use of Equations 2.46 and 2.47 for the convolution formulation is illustrated in 2.1.

Because the interval of the convolution integral increases during the progress of the simulation, the computation needed for this integral at any time point t_i is proportional to i. For a total of n time points in the simulation, the total computation time for the convolutions is proportional to the sum of the computation at each $t_j, 0 < j \leq n$, which rises as n^2, a quadratic relationship between computation time and total simulation length for this method.

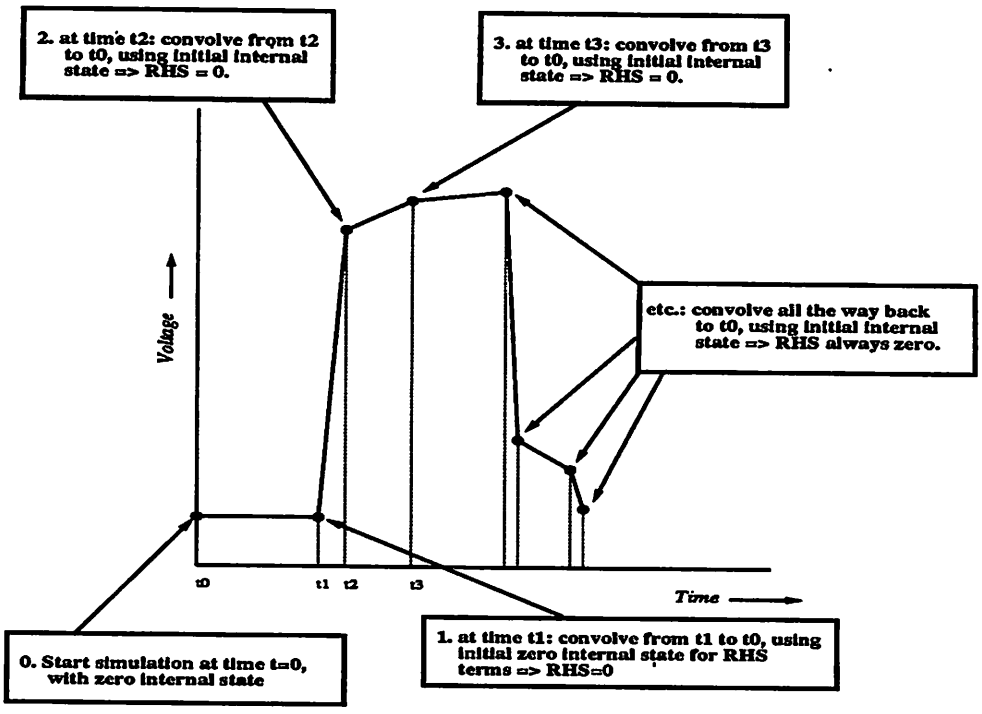

Figure 2.1: Equations 2.46 and 2.47 by analytic convolution

2.4 State Based Method

The fact that Equations 2.46 and 2.47 are derived from a system of PDEs makes it possible to solve them in another way: at time t_1 (the first time point after the origin $t_0 = 0$), the procedure is identical to the convolution method, with convolution over the interval $[t_0, t_1]$, and initial state zero. The new state of the line at time t_1 is calculated next, using Equations 2.42 and 2.43 for each x chosen to sample the internal state. At the next time-point t_2, the newly calculated, nonzero internal state at t_1 is used as $v_0(x)$ and $i_0(x)$, instead of the zero internal state at time t_0, in Equations 2.42, 2.43, 2.44 and 2.45. In other words, the time-invariance property of the Telegrapher Equations is used, redoing the derivation with initial time t_1. Thus the convolution operation at time t_2 starts from the previous time-point t_1, i.e., the time at which the internal state is used in the above equations, instead of from t_0 as in the convolution method. The internal state at t_2 is then calculated, and this internal state is used as the initial state at time t_3, and so on. This procedure (illustrated in Fig. 2.2) is the basis of the recursive computation; information from the port variables' history, which keeps increasing in size as the simulation progresses,

is condensed into the state, which is of constant size. The key feature leading to linear complexity in this technique is that the computation at time t_i is independent of i, since convolution is always performed over only one interval, $[t_{i-1}, t_i]$.

Equations 2.35 and 2.36 are valid at any location x within the line. During simulation, the primary computational load is the calculation of the internal line state, i.e., evaluation of Equations 2.35 and 2.36 at several different values of x. Note that the evaluation of the equations at a particular point x is independent of the current line state at any other point y, $y \neq x$[4]. This immediately suggests that the main computation of the algorithm is particularly suited to parallel implementation, with the new state at all internal points being computed simultaneously. Other methods, such as the lumped-RLC method, lack this feature as they do not utilise the innate decoupling in the lossy transmission line's mechanism.

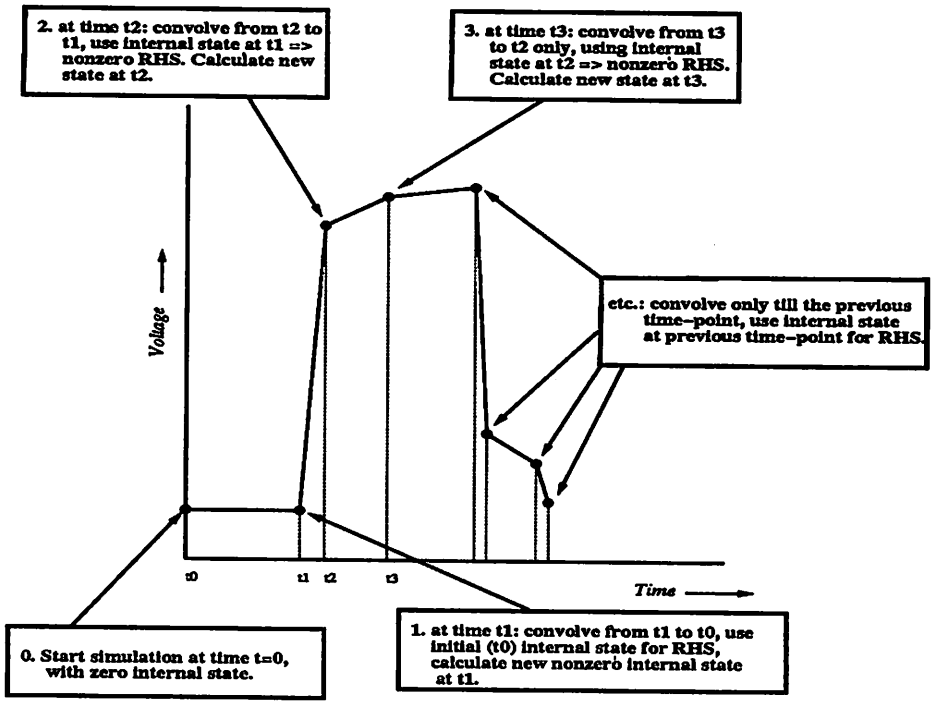

Figure 2.2: Equations 2.46 and 2.47 by the state based method

[4]This is a consequence of the fact that there exists a maximum velocity with which waves propagate within the line.

2.5 Frequency Varying Lines

For a frequency-varying transmission line with parameters $R(s)$, $L(s)$ $C(s)$ and $G(s)$, time-domain partial-differential equations similar to Equations 2.1 and 2.2 are not easily available. The established technique for incorporating the frequency variation of the electrical parameters of the line is to introduce them directly into the Laplace-domain Telegrapher Equations (Equations 2.3 and 2.4 with $W_1 = W_2 \equiv 0$), replacing the constant quantities R_{dc}, L_{dc}, G_{dc} and C_{dc}, and ignoring the initial state terms:

$$\frac{\partial V}{\partial x} = -(sL(s) + R(s))\, I \tag{2.48}$$

$$\frac{\partial I}{\partial x} = -(sC(s) + G(s))\, V \tag{2.49}$$

The solution procedure of Section 2.1 is followed, usingEquations 2.48 and 2.49 as a starting point, to arrive at the following Laplace-domain equations:

$$[Y_0\, V_2(s)\, H_Y(s) - I_2(s)] - [Y_0\, V_1(s)\, H_{\gamma Y}(s) + I_1(s)\, H_\gamma(s)] = 0 \tag{2.50}$$

$$[Y_0\, V_2(s)\, H_{\gamma Y}(s) + I_2(s)\, H_\gamma(s)] - [Y_0\, V_1(s)\, H_Y(s) - I_1(s)] = 0 \tag{2.51}$$

where $V_1(s)$, $V_2(s)$, $I_1(s)$ and $I_2(s)$ are the Laplace transforms of the voltages and currents at the two ends of the line, which is of length l, and

$$Y_0 = \sqrt{\frac{C_{dc}}{L_{dc}}}, \quad H_Y(s) = \frac{Y(s)}{Y_0}, \quad H_\gamma(s) = e^{-\lambda(s)\, l} \tag{2.52}$$

$$H_{\gamma Y}(s) = H_Y(s)\, H_\gamma(s), \quad Y(s) = \sqrt{\frac{sC(s) + G(s)}{sL(s) + R(s)}} \tag{2.53}$$

$$\lambda(s) = \sqrt{(sC(s) + G(s))(sL(s) + R(s))}, \tag{2.54}$$

$$R_{dc} = R(0), \quad L_{dc} = L(0) \tag{2.55}$$

$$C_{dc} = C(0), \quad G_{dc} = G(0) \tag{2.56}$$

Taking inverse Laplace transforms yields the time-domain constitutive equations for the frequency varying line:

$$[Y_0\, v_2(t) * h_Y(t) - i_2(t)] - [Y_0\, v_1(t) * h_{\gamma Y}(t) + i_1(t) * h_\gamma(t)] = 0 \tag{2.57}$$

$$[Y_0\, v_2(t) * h_{\gamma Y}(t) + i_2(t) * h_\gamma(t)] - [Y_0\, v_1(t) * h_Y(t) - i_1(t)] = 0 \tag{2.58}$$

where $v_1(t)$, $v_2(t)$, $i_1(t)$, $i_2(t)$ are the port variables of the line, and $h_Y(t)$, $h_\gamma(t)$ and $h_{\gamma Y}(t)$ are the inverse Laplace transforms of $H_Y(s)$, $H_\gamma(s)$ and $H_{\gamma Y}(s)$ respectively. As expected, Equations 2.57 and 2.58 are similar in form to Equations 2.46 and 2.47, with RHS (initial state terms) zero.

The above convolution formulation can be used directly to simulate the frequency-varying line. However, it is convenient to rewrite Equations 2.50 and 2.51 in the following equivalent form for the purposes of the decomposition mentioned earlier:

$$[Y_0\, V_2(s)\, H_Y^{dc}(s) - I_2(s)] - [Y_0\, V_1(s)\, H_{\gamma Y}^{dc}(l,s) + I_1(s)\, H_\gamma^{dc}(l,s)] + U_1(s) = 0 \tag{2.59}$$

$$[Y_0\, V_2(s)\, H_{\gamma Y}^{dc}(l,s) + I_2(s)\, H_\gamma^{dc}(l,s)] - [Y_0\, V_1(s)\, H_Y^{dc}(s) - I_1(s)] + U_2(s) = 0 \tag{2.60}$$

where

$$H_Y^{dc}(s) = \frac{Y^{dc}(s)}{Y_0}, \quad H_\gamma^{dc}(x,s) = e^{-\lambda^{dc}(s)\,x} \tag{2.61}$$

$$H_{\gamma Y}^{dc}(x,s) = H_Y^{dc}(s)\, H_\gamma^{dc}(x,s), \quad Y^{dc}(s) = \sqrt{\frac{sC_{dc} + G_{dc}}{sL_{dc} + R_{dc}}} \tag{2.62}$$

$$\lambda^{dc}(s) = \sqrt{(sC_{dc} + G_{dc})(sL_{dc} + R_{dc})} \tag{2.63}$$

Equations 2.59 and 2.60 represent a linear decomposition of the frequency varying line into two parts: a Simple Lossy part and a purely nonideal part, given by the terms $U_1(s)$ and $U_2(s)$, given as follows:

$$U_1(s) = Y_0\, V_2(s)\, \triangle H_Y(s) - [Y_0\, V_1(s)\, \triangle H_{\gamma Y}(s) + I_1(s)\, \triangle H_\gamma(s)] \tag{2.64}$$

$$U_2(s) = [Y_0\, V_2(s)\, \triangle H_{\gamma Y}(s) + I_2(s)\, \triangle H_\gamma(s)] - Y_0\, V_1(s)\, \triangle H_Y(s) \tag{2.65}$$

where

$$\triangle H_Y(s) = H_Y(s) - H_Y^{dc}(s), \quad \triangle H_\gamma(s) = H_\gamma(s) - H_\gamma^{dc}(l,s) \tag{2.66}$$

$$\triangle H_{\gamma Y}(s) = H_{\gamma Y}(s) - H_{\gamma Y}^{dc}(l,s) \tag{2.67}$$

Laplace inversion of Equations 2.59 and 2.60 yields the time-domain formulation:

$$[Y_0\, v_2(t) * h_Y^{dc}(t) - i_2(t)] - [Y_0\, v_1(t) * h_{\gamma Y}^{dc}(l,t) + i_1(t) * h_\gamma^{dc}(l,t)] + u_1(t) = 0 \tag{2.68}$$

$$[Y_0\, v_2(t) * h_{\gamma Y}^{dc}(l,t) + i_2(t) * h_{\gamma}^{dc}(l,t)] - [Y_0\, v_1(t) * h_Y^{dc}(t) - i_1(t)] + u_2(t) = 0 \qquad (2.69)$$

where $h_Y^{dc}(t)$, $h_\gamma^{dc}(x,t)$ and $h_{\gamma Y}^{dc}(x,t)$[5] are the inverse Laplace transforms of $H_Y^{dc}(s)$, $H_\gamma^{dc}(x,s)$ and $H_{\gamma Y}^{dc}(x,s)$ respectively. $u_1(t)$ and $u_2(t)$, the inverse transforms of $U_1(s)$ and $U_2(s)$, are given by:

$$u_1(t) = Y_0\, v_2(t) * \Delta h_Y(t) - [Y_0\, v_1(t) * \Delta h_{\gamma Y}(t) + i_1(t) * \Delta h_\gamma(t)] \qquad (2.70)$$

$$u_2(t) = [Y_0\, v_2(t) * \Delta h_{\gamma Y}(t) + i_2(t) * \Delta h_\gamma(t)] - Y_0\, v_1(t) * \Delta h_Y(t) \qquad (2.71)$$

where

$$\Delta h_Y(t) = h_Y(t) - h_Y^{dc}(t), \quad \Delta h_\gamma(t) = h_\gamma(t) - h_\gamma^{dc}(l,t) \qquad (2.72)$$

$$\Delta h_{\gamma Y}(t) = h_{\gamma Y}(t) - h_{\gamma Y}^{dc}(l,t) \qquad (2.73)$$

Equations 2.68 and 2.69 are equivalent to Equations 2.57 and 2.58. By rewriting them in the form of Equations 2.68 and 2.69, all terms except u_1 and u_2 can be computed recursively, as shown in Section 2.4. Calculating $u_1(t)$ and $u_2(t)$ (according to Equations 2.70 and 2.71) requires convolution; if, however, the responses Δh_Y, Δh_γ and $\Delta h_{\gamma Y}$ can be truncated with insignificant loss of accuracy, the convolution can be computed as an integral with fixed limits.

Define:

$$W_1(x,s) = -\frac{U_2(s)\,\delta(x) + U_1(s)\,\delta(x-l)}{2Y^{dc}(s)} \qquad (2.74)$$

$$W_2(x,s) = \frac{U_2(s)\,\delta(x) - U_1(s)\,\delta(x-l)}{2} \qquad (2.75)$$

Substituting these specific choices for W_1 and W_2 into the RHS of Equations 2.20 and 2.21 leads to the following:

$$\begin{aligned}
&[Y_0\, V(x,s)\, H_Y^{dc}(s) + I(x,s)] - [Y_0\, V(0,s)\, H_{\gamma Y}^{dc}(x,s) + I(0,s)\, H_\gamma^{dc}(x,s)] + U_1(s)\chi(x-l) \\
&\quad = i_{0k} H_{S\gamma Y}(x - x_k, s) - i_{00} H_{S\gamma Y}(x - x_0, s) \\
&\qquad + Y_0 [v_{0k} H_{S\gamma}(x - x_k, s) - v_{00} H_{S\gamma}(x - x_0, s)] \\
&\qquad - \frac{1}{\gamma_0} \left[\begin{array}{l} -\left(\frac{i_{01}-i_{00}}{x_1-x_0}\right) H_{S^2\gamma Y}(x - x_0, s) + \left(\frac{i_{0k}-i_{0,k-1}}{x_k-x_{k-1}}\right) H_{S^2\gamma Y}(x - x_k, s) \\ +Y_0 \left[-\left(\frac{v_{01}-v_{00}}{x_1-x_0}\right) H_{S^2\gamma}(x - x_0, s) + \left(\frac{v_{0k}-v_{0,k-1}}{x_k-x_{k-1}}\right) H_{S^2\gamma}(x - x_k, s) \right] \\ + \sum_{j=1}^{k-1} \left[\begin{array}{l} H_{S^2\gamma Y}(x - x_j, s) \left[-\left(\frac{i_{0,j+1}-i_{0j}}{x_{j+1}-x_j}\right) + \left(\frac{i_{0j}-i_{0,j-1}}{x_j-x_{j-1}}\right) \right] \\ +Y_0 H_{S^2\gamma}(x - x_j, s) \left[-\left(\frac{v_{0,j+1}-v_{0j}}{x_{j+1}-x_j}\right) + \left(\frac{v_{0j}-v_{0,j-1}}{x_j-x_{j-1}}\right) \right] \end{array} \right] \end{array} \right]
\end{aligned} \qquad (2.76)$$

[5] analytical expressions for these are given in Section 2.1.

$$
\begin{aligned}
&[Y_0\,V(l,s)\,H^{dc}_{\gamma Y}(l{-}x,s) - I(l,s)\,H^{dc}_{\gamma}(l{-}x,s)] - [Y_0\,V(x,s)\,H^{dc}_{Y}(s) - I(x,s)] + U_2(s)\chi(x) \\
&\quad = i_{0k}H_{S\gamma Y}(x_k - x,s) - i_{0,n_l}H_{S\gamma Y}(x_{n_l} - x,s) \\
&\qquad -Y_0\,[v_{0k}H_{S\gamma}(x_k - x,s) - v_{0,n_l}H_{S\gamma}(x_{n_l} - x,s)] \\
&\qquad -\frac{1}{\gamma_0}\left[\begin{array}{l}
-\left(\frac{i_{0,k+1}-i_{0k}}{x_{k+1}-x_k}\right)H_{S^2\gamma Y}(x_k - x,s) + \left(\frac{i_{0,n_l}-i_{0,n_l-1}}{x_{n_l}-x_{n_l-1}}\right)H_{S^2\gamma Y}(x_{n_l} - x,s) \\
-Y_0\left[-\left(\frac{v_{0,k+1}-v_{0k}}{x_{k+1}-x_k}\right)H_{S^2\gamma}(x_k - x,s) + \left(\frac{v_{0,n_l}-v_{0,n_l-1}}{x_{n_l}-x_{n_l-1}}\right)H_{S^2\gamma}(x_{n_l} - x,s)\right] \\
\quad + \sum_{j=k+1}^{n_l-1}\left[\begin{array}{l}
H_{S^2\gamma Y}(x_j - x,s)\left[-\left(\frac{i_{0,j+1}-i_{0j}}{x_{j+1}-x_j}\right) + \left(\frac{i_{0j}-i_{0,j-1}}{x_j-x_{j-1}}\right)\right] \\
-Y_0 H_{S^2\gamma}(x_j - x,s)\left[-\left(\frac{v_{0,j+1}-v_{0j}}{x_{j+1}-x_j}\right) + \left(\frac{v_{0j}-v_{0,j-1}}{x_j-x_{j-1}}\right)\right]
\end{array}\right]
\end{array}\right]
\end{aligned}
\tag{2.77}
$$

where:

$$
\chi(x) = \begin{cases} 1 & \text{if } x = 0 \\ 0 & \text{otherwise} \end{cases} \tag{2.78}
$$

Taking inverse Laplace transforms of the above equations results in:

$$
\begin{aligned}
&[Y_0\,v(x,t) * h^{dc}_{Y}(t) + i(x,t)] - [Y_0\,v(0,t) * h^{dc}_{\gamma Y}(x,t) + i(0,t) * h^{dc}_{\gamma}(x,t)] + u_1(t)\chi(x-l) \\
&\quad = i_{0k}h_{S\gamma Y}(x - x_k,t) - i_{00}h_{S\gamma Y}(x - x_0,t) \\
&\qquad +Y_0\,[v_{0k}h_{S\gamma}(x - x_k,t) - v_{00}h_{S\gamma}(x - x_0,t)] \\
&\qquad -\frac{1}{\gamma_0}\left[\begin{array}{l}
-\left(\frac{i_{01}-i_{00}}{x_1-x_0}\right)h_{S^2\gamma Y}(x - x_0,t) + \left(\frac{i_{0k}-i_{0,k-1}}{x_k-x_{k-1}}\right)h_{S^2\gamma Y}(x - x_k,t) \\
+Y_0\left[-\left(\frac{v_{01}-v_{00}}{x_1-x_0}\right)h_{S^2\gamma}(x - x_0,t) + \left(\frac{v_{0k}-v_{0,k-1}}{x_k-x_{k-1}}\right)h_{S^2\gamma}(x - x_k,t)\right] \\
\quad + \sum_{j=1}^{k-1}\left[\begin{array}{l}
h_{S^2\gamma Y}(x - x_j,t)\left[-\left(\frac{i_{0,j+1}-i_{0j}}{x_{j+1}-x_j}\right) + \left(\frac{i_{0j}-i_{0,j-1}}{x_j-x_{j-1}}\right)\right] \\
+Y_0 h_{S^2\gamma}(x - x_j,t)\left[-\left(\frac{v_{0,j+1}-v_{0j}}{x_{j+1}-x_j}\right) + \left(\frac{v_{0j}-v_{0,j-1}}{x_j-x_{j-1}}\right)\right]
\end{array}\right]
\end{array}\right]
\end{aligned}
\tag{2.79}
$$

$$
\begin{aligned}
&[Y_0\,v(l,t) * h^{dc}_{\gamma Y}(l-x,t) - i(l,t) * h^{dc}_{\gamma}(l-x,t)] - [Y_0\,v(x,t) * h^{dc}_{Y}(t) - i(x,t)] + u_2(t)\chi(x) \\
&\quad = i_{0k}h_{S\gamma Y}(x_k - x,t) - i_{0,n_l}h_{S\gamma Y}(x_{n_l} - x,t) \\
&\qquad -Y_0\,[v_{0k}h_{S\gamma}(x_k - x,t) - v_{0,n_l}h_{S\gamma}(x_{n_l} - x,t)] \\
&\qquad -\frac{1}{\gamma_0}\left[\begin{array}{l}
-\left(\frac{i_{0,k+1}-i_{0k}}{x_{k+1}-x_k}\right)h_{S^2\gamma Y}(x_k - x,t) + \left(\frac{i_{0,n_l}-i_{0,n_l-1}}{x_{n_l}-x_{n_l-1}}\right)h_{S^2\gamma Y}(x_{n_l} - x,t) \\
-Y_0\left[-\left(\frac{v_{0,k+1}-v_{0k}}{x_{k+1}-x_k}\right)h_{S^2\gamma}(x_k - x,t) + \left(\frac{v_{0,n_l}-v_{0,n_l-1}}{x_{n_l}-x_{n_l-1}}\right)h_{S^2\gamma}(x_{n_l} - x,t)\right] \\
\quad + \sum_{j=k+1}^{n_l-1}\left[\begin{array}{l}
h_{S^2\gamma Y}(x_j - x,t)\left[-\left(\frac{i_{0,j+1}-i_{0j}}{x_{j+1}-x_j}\right) + \left(\frac{i_{0j}-i_{0,j-1}}{x_j-x_{j-1}}\right)\right] \\
-Y_0 h_{S^2\gamma}(x_j - x,t)\left[-\left(\frac{v_{0,j+1}-v_{0j}}{x_{j+1}-x_j}\right) + \left(\frac{v_{0j}-v_{0,j-1}}{x_j-x_{j-1}}\right)\right]
\end{array}\right]
\end{array}\right]
\end{aligned}
\tag{2.80}
$$

By substituting $x = l$ in Equation 2.79 and $x = 0$ in Equation 2.80 and setting the initial conditions $v_0(x)$ and $i_0(x)$ to zero, the following equations relating the port variables are obtained:

$$[Y_0\, v_2(t) * h_Y^{dc}(t) - i_2(t)] - [Y_0\, v_1(t) * h_{\gamma Y}^{dc}(l,t) + i_1(t) * h_\gamma^{dc}(l,t)] + u_1(t) = 0 \tag{2.81}$$

$$[Y_0\, v_2(t) * h_{\gamma Y}^{dc}(l,t) + i_2(t) * h_\gamma^{dc}(l,t)] - [Y_0\, v_1(t) * h_Y^{dc}(t) - i_1(t)] + u_2(t) = 0 \tag{2.82}$$

Equations 2.81 and 2.82 are identical to the frequency varying line's equations (Equations 2.68 and 2.69), but were derived by an alternate route, starting from Equations 2.1 and 2.2 (with possible non-zero initial conditions) through Equations 2.79 and 2.80. From Section 2.4, they can be solved by using the State Based method, using Equations 2.79 and 2.80 and resetting the initial states at every new time point. The computation of u_1 and u_2 by Equations 2.70 and 2.71 at each time point requires convolution. As shown in Chapter 4, these convolutions may be truncated in short times in narrow MCM interconnect applications. This leads to an overall linear time algorithm for frequency varying lossy lines.

Chapter 3

Numerical Convolution

In Chapter 2, the state-based and convolution methods were derived. The computer implementation of both methods calls for the numerical computation of the convolution integral over a period of one or more time-steps. In this section, generalisations of the Backward Euler (BE) and Trapezoidal methods for ODEs suitable for convolution are formulated.

The convolution integral to be calculated is the following:

$$y(t) = \int_0^t x(\tau)\, h(t-\tau)\, d\tau \tag{3.1}$$

In Equation 3.1, $x(\tau)$ is the input to the linear system, $y(t)$ is the output and $h(\tau)$ is the impulse response or the *kernel* of the system. $h(\tau)$ is assumed to be a constant well-known causal function of time and may be finite or infinite in duration. At any given time t, $x(\tau)$ and $y(\tau)$ are assumed to be known over the half-open interval $[0,t)$[1]. Note that in a circuit context, $x(\tau)$ and $y(\tau)$ are usually also related by a relation other than Equation 3.1; one may be a function or a causal functional of the other.

The object of numerical convolution is to calculate $y(\cdot)$ in Equation 3.1 at some time $t_n > 0$, using values of $x(\tau)$ at only a discrete number of time-points. Denote these time-points as 0, t_1, t_2, ..., t_n, with $0 < t_i < t_{i+1}$, $i \in \{1,\ldots,n-1\}$. Also denote the values of $x(\tau)$ and $y(\tau)$ at these time-points as x_i and y_i respectively. In a circuit simulator, x_n and y_n would typically be circuit unknowns to be solved for at the time-point t_n, using the numerical formula to be developed in this section and also, information from the rest of the circuit. x_i, y_i for $0 \le i < n$ would be known values, previously calculated by the

[1] $x(\tau)$ and $y(\tau)$ can be assumed zero for $\tau < 0$ without loss of generality; see Appendix A.

simulator. Note that no restriction discretizing the impulse response $h(\tau)$ is required in this formulation.

Knowledge of the values of $x(t)$ at a discrete number of points is not sufficient to specify $y(t)$ uniquely by Equation 3.1; it is necessary to make assumptions about the overall nature of $x(t)$. In deriving linear multistep methods for differential equations [6, 20], the assumptions that $x(t)$ is *piecewise linear* and *piecewise constant* result in the well-known *trapezoidal* and *euler* methods, respectively. In this chapter, the same assumptions are made to arrive at new generalisations of these methods, suitable for numerical convolution.

3.1 Generalised Trapezoidal Method

The following assumption is made:

Assumption 3.1.1 *In each half-open interval* $[t_i, t_{i+1})$, $i = 0, \ldots, n-1$, $x(t)$ *is a polynomial of order* p, *i.e.,*

$$x(t) = c_0^i + c_1^i\, t + c_2^i\, t^2 + \cdots + c_p^i\, t^p, \quad t \in [t_i, t_{i+1}), \quad i = 0, \ldots, n-1 \tag{3.2}$$

where $c_0^i, \ldots, c_p^i$ *are constants for each* i.
Note that $x(t)$ *need not be continuous at the points* t_i, $i = 0, \ldots, n-1$.

It can be shown that the assumption that $p = 1$ in Equation 3.2 results in a generalization of the formula commonly known as the Extended Trapezoidal Rule for integration [1, page 855]. Similarly, for $p = 0$, a generalization of the Euler methods is obtained, and for other choices of p, other methods may be derived. For the purposes of the following, it is assumed that $p = 1$ in Equation 3.2, or that $x(t)$ *is piecewise-linear*, of the following form:

$$x(t) = c_0^i + c_1^i\, t, \quad t \in [t_i, t_{i+1}), \quad i = 0, \ldots, n-1 \tag{3.3}$$

where:

$$c_0^i = x_i - c_1^i\, t_i, \quad m_i \triangleq c_1^i = \frac{\tilde{x}_{i+1} - x_i}{t_{i+1} - t_i} \tag{3.4}$$

with:

$$x_i \triangleq x(t_i), \qquad \tilde{x}_i \triangleq \lim_{t \to t_{i-}} x(t) \tag{3.5}$$

implying that:

$$x(t) = x_i + m_i\,(t - t_i), \quad t \in [t_i, t_{i+1}), \quad i = 0, \ldots, n\text{–}1 \tag{3.6}$$

Equation 3.1 is rewritten for $t = t_n$:

$$y(t_n) \;=\; \int_0^{t_n} x(\tau)\, h(t_n - \tau)\, d\tau \tag{3.7}$$

Equation 3.7 is split up into a sum of integrals over the piecewise linear regions and expressed as:

$$y(t_n) \;=\; \sum_{i=0}^{n-1} \int_{t_i}^{t_{i+1}} x(\tau)\, h(t_n - \tau)\, d\tau \tag{3.8}$$

$$\Rightarrow \quad y(t_n) \;=\; \sum_{i=0}^{n-1} \int_{t_i}^{t_{i+1}} \left(x_i + m_i\,(\tau - t_i)\right) h(t_n - \tau)\, d\tau \tag{3.9}$$

by using Equation 3.6, and noting that a finite number of finite point discontinuities do not affect the value of a definite integral.

Equation 3.9 is evaluated by parts and manipulated algebraically to arrive at the following:

$$\begin{aligned} y_n \;=\; & \tilde{x}_n \frac{F(h, t_n - t_{n-1})}{t_n - t_{n-1}} \\ & + \sum_{i=1}^{n-1} x_i \left[\frac{F(h, t_n - t_{i-1}) - F(h, t_n - t_i)}{t_i - t_{i-1}} \right. \\ & \qquad \left. - \frac{F(h, t_n - t_i) - F(h, t_n - t_{i+1})}{t_{i+1} - t_i} \right] \\ & + \sum_{i=1}^{n-1} (x_i - \tilde{x}_i) \left[E(h, t_n - t_i) - \frac{F(h, t_n - t_{i-1}) - F(h, t_n - t_i)}{t_i - t_{i-1}} \right] \\ & + x_0 \left[E(h, t_n - 0) - \frac{F(h, t_n - 0) - F(h, t_n - t_1)}{t_1 - 0} \right] \end{aligned} \tag{3.10}$$

where:

$$E(h,t) \;\triangleq\; \int_0^t h(\tau)\, d\tau \tag{3.11}$$

$$F(h,t) \;\triangleq\; \int_0^t \int_0^\tau h(\tau')\, d\tau'\, d\tau \tag{3.12}$$

If $\tilde{x}_i = x_i$, as is the case when $x(t)$ is continuous and x_i are its samples, Equation 3.10 loses its second $\sum$ term. Moreover, if $x_0 = 0$, the last term in Equation 3.10 also drops out, and the equation becomes:

$$\begin{aligned} y_n &= x_n \frac{F(h, t_n - t_{n-1})}{t_n - t_{n-1}} \\ &\quad + \sum_{i=1}^{n-1} x_i \left[\frac{F(h, t_n - t_{i-1}) - F(h, t_n - t_i)}{t_i - t_{i-1}} \right. \\ &\quad \left. - \frac{F(h, t_n - t_i) - F(h, t_n - t_{i+1})}{t_{i+1} - t_i} \right] \end{aligned} \tag{3.13}$$

An operator form $\mathcal{A}^n$ of Equation 3.13, subject to the following assumption, is defined.

Assumption 3.1.2 *$x(t)$ is continuous, and $x_0 = 0$[2] in Equation 3.10.*

Definition 3.1.1 *$\mathcal{A}^n : \mathcal{R}^{2n-1} \mapsto \mathcal{R}$ is defined as:*

$$\begin{aligned} \mathcal{A}^n(\underline{x}) &\triangleq \tilde{x}_n \frac{F(h, t_n - t_{n-1})}{t_n - t_{n-1}} \\ &\quad + \sum_{i=1}^{n-1} x_i \left[\frac{F(h, t_n - t_{i-1}) - F(h, t_n - t_i)}{t_i - t_{i-1}} \right. \\ &\quad \left. - \frac{F(h, t_n - t_i) - F(h, t_n - t_{i+1})}{t_{i+1} - t_i} \right] \end{aligned}$$

where:

$$\underline{x} \triangleq [x_1, \ldots, x_{n-1}, \tilde{x}_1, \ldots, \tilde{x}_n]^\perp \in \mathcal{R}^{2n-1}$$

Note that $\mathcal{A}^n$ is linear, i.e.,

$$\mathcal{A}^n(\underline{x} + \underline{y}) = \mathcal{A}^n(\underline{x}) + \mathcal{A}^n(\underline{y})$$

The net result of the above construction is summarised as the following theorem:

Theorem 3.1.1 *Let $x(t)$ be a piecewise-linear function of t, with $x(0) = 0$. Let the break-points of $x(t)$ be $0, t_1, \ldots, t_n$, where $0, t_1, \ldots, t_n$ are an increasing sequence in $\mathcal{R}$, n being a natural number. Define:*

$$\begin{aligned} x_i &= x(t_i), \quad i \in \{1, \ldots, n-1\} \\ \tilde{x}_i' &= \lim_{t \to t_i^-} x(t), \quad i \in \{1, \ldots, n\} \\ \underline{x} &= [x_1, \ldots, x_{n-1}, \tilde{x}_1, \ldots, \tilde{x}_n]^\perp \end{aligned}$$

[2]This can be assumed without loss of generality; see Appendix A.

Then

$$\mathcal{A}^n(\underline{x}) = \int_0^{t_n} x(\tau)\, h(t_n - \tau)\, d\tau$$

where $\mathcal{A}^n$ is defined in Definition 3.1.1.

In view of Theorem 3.1.1, $\mathcal{A}^n$ is a numerical integration formula for Equation 3.1 that is *exact* when $x(t)$ is piecewise linear.

3.2 Generalised Euler Methods

Generalisations of the Backward and Forward Euler methods for numerical convolution can likewise be derived (the derivation is omitted, being similar to that for the Trapezoidal method).

Generalised Backward Euler:

$$\begin{aligned}\int_0^{t_n} x(\tau)\, h(t_n - \tau)\, d\tau \;\approx\; & x_n\, E(h, t_n - t_{n-1}) \\ & + \sum_{i=1}^{n-1} x_i\, [E(h, t_n - t_{i-1}) - E(h, t_n - t_i)]\end{aligned} \tag{3.14}$$

Generalised Forward Euler:

$$\int_0^{t_n} x(\tau)\, h(t_n - \tau)\, d\tau \;\approx\; \sum_{i=1}^{n-1} x_i\, [E(h, t_n - t_{i-1}) - E(h, t_n - t_i)] \tag{3.15}$$

where:

$$E(h,t) \triangleq \int_0^t h(\tau)\, d\tau \tag{3.16}$$

3.3 Analytic Expressions for $E(\cdot,\cdot)$ and $F(\cdot,\cdot)$

One of the advantages of using the above formulae is that analytic expressions for $E(\cdot,\cdot)$ and $F(\cdot,\cdot)$ have been identified for some of the lossy line's impulse responses. The following identities are valid for the special case $\alpha = \beta$ (refer Equations 2.35 – 2.37), which holds when either R or G equals zero[3]:

$$\int_0^t h_Y(u)\, du = e^{-\beta t} I_0(\beta t) \tag{3.17}$$

[3]The $G = 0$ case is useful in many practical applications.

$$\int_0^t \int_0^w h_Y(u)\,du\,dw = te^{-\beta t}\{I_0(\beta t) + I_1(\beta t)\} \tag{3.18}$$

$$\int_0^t h_{\gamma Y}(x,u)\,du = 1_{t-\gamma_0 x} e^{-\beta t} I_0\left(\beta\sqrt{t^2-(\gamma_0 x)^2}\right) \tag{3.19}$$

Unfortunately, analytic expressions have not been found so far for $\int_0^t \int_0^w h_{\gamma Y}(x,u)\,du\,dw$, $\int_0^t h_\gamma(x,u)\,du$, and $\int_0^t \int_0^w h_\gamma(x,u)\,du\,dw$. These are calculated numerically from the impulse responses – details are given in Appendix B.

3.4 Local Truncation Error

In this section, the error in using the numerical formula $\mathcal{A}^n$ when $x(t)$ is *not* piecewise-linear is estimated.

Consider $x(t)$ *piecewise-smooth*[4] over $[t_i, t_{i+1})$, $i \in \{0,\ldots,n-1\}$, with $x(0)=0$. Define x_i, $\tilde{x}_i$ and $\underline{x}$ as in Theorem 3.1.1. Consider:

$$\epsilon_n \triangleq \mathcal{A}^n(\underline{x}) - \int_0^{t_n} x(\tau)\,h(t_n-\tau)\,d\tau \tag{3.20}$$

To estimate an upper bound for ϵ_n, $x(t)$ is expanded in a Taylor series with an integral remainder over each interval $[t_i, t_{i+1})$. An analysis analogous to that for differential equations [6] is performed, resulting in the following expression:

$$\begin{aligned}\epsilon_n \;=\; & x''(\tau_n^*)\left\{\frac{F(h,t_n-t_{n-1})\,(t_n-t_{n-1})}{2} - G(h,t_n-t_{n-1})\right\} \\ & + \sum_{i=1}^{n-1} x''(\tau_i^*)\left[\frac{(t_i-t_{i-1})\,\{F(h,t_n-t_{i-1})+F(h,t_n-t_i)\}}{2}\right. \\ & \qquad \left. + G(h,t_n-t_i) - G(h,t_n-t_{i-1})\right]\end{aligned} \tag{3.21}$$

where

$$G(h,t) \triangleq \int_0^t \int_0^\tau \int_0^{\tau'} h(\tau'')\,d\tau''\,d\tau'\,d\tau, \tag{3.22}$$

$x''(\cdot)$ refers to the second derivative of $x(t)$, and $\tau_i^* \in [t_{i-1}, t_i]$, $i \in \{1,\ldots,n\}$.

It can be seen in Equation 3.21 that each interval $[t_i, t_{i+1}]$ contributes to the total error. When numerical integration is performed in a circuit context, the values of the circuit variables $x(t)$ and $y(t)$ in Equation 3.1 are computed forward in time, i.e., starting with x_0 and y_0, a value for t_1 is chosen, x_1 and y_1 found, t_2 is chosen, x_2 and y_2 found, and so on.

[4] *piecewise-smooth* implying that a Taylor-series expansion is possible over each region $[t_i, t_{i+1})$, $i \in \{0,\ldots,n-1\}$

As a result, $x_0, \ldots, x_{n-1}$, $y_0, \ldots, y_{n-1}$ and $0, \ldots, t_{n-1}$ are known before computing x_n and y_n. It is necessary to choose t_n as a first step for computing x_n and y_n.

Consider $\Delta\epsilon_n \triangleq \epsilon_n - \epsilon_{n-1}$, the extra error in $y(t)$ between timepoints t_n and t_{n-1}. This is zero if t_n is chosen equal to t_{n-1}, and its absolute value will increase from zero when $t_n > t_{n-1}$. $\Delta\epsilon_n$ is therefore the *local error* at time t_n. A criterion for choosing t_n, therefore, would be to ensure that the absolute value of the local error $\Delta\epsilon_n$ is less than some specified tolerance ϵ_{max}. Thus the following condition must be satisfied:

$$|\Delta\epsilon_n| = |\epsilon_n - \epsilon_{n-1}| < \epsilon_{max} \tag{3.23}$$

where ϵ_{max} is a specified constant. It is assumed that estimates are available for the $x''(\tau_i^*)$ (using, for instance, a divided-difference scheme [6]).

From the definition of ϵ_n,

$$\begin{aligned}
\Delta\epsilon_n \;=\; & x''(\tau_n^*)\left\{\frac{F(h, t_n - t_{n-1})\,(t_n - t_{n-1})}{2} - G(h, t_n - t_{n-1})\right\} \\
& + \sum_{i=1}^{n-1} x''(\tau_i^*)\left[\frac{(t_i - t_{i-1})}{2}\{F(h, t_n - t_{i-1}) + F(h, t_n - t_i)\right. \\
& \qquad -F(h, t_{n-1} - t_{i-1}) - F(h, t_{n-1} - t_i)\} \\
& \qquad +G(h, t_n - t_i) - G(h, t_n - t_{i-1}) \\
& \qquad \left. -G(h, t_{n-1} - t_i) + G(h, t_{n-1} - t_{i-1})\right]
\end{aligned} \tag{3.24}$$

If $h(\tau) \equiv 1$, then $F(t) = \frac{t^2}{2}$, $G(t) = \frac{t^3}{6}$. If these are substituted into Equation 3.24, it can be shown after algebraic manipulation that the coefficients of $x''(\tau_i^*)$ inside the $\sum$ become identically zero, and the expression reduces to the first term which simplifies to $x''(\tau_n^*)\frac{(t_n - t_{n-1})^3}{12}$, the local truncation error estimate for the trapezoidal method.

Chapter 4

Experimental Results

In this chapter, experimental results obtained by applying these new techniques to several industrial circuits are presented. In Section 4.1, the analytic convolution and state-based methods are compared to the lumped RLCG method in simulations of simple lossy lines. In Section 4.2, examples containing lines with skin effect are simulated by the convolution and state-based methods.

4.1 Simple Lossy Lines

Waveform and computation speed comparisons of the state-based, analytic convolution and the lumped-RLCG methods for four circuits are presented in this section. Execution times are summarised in Table 4.1.

The first circuit **raytheon1** is shown in Figure 4.1. It consists of a fast BJT inverter driver connected to a diode-resistor receiver through a 24 inch lossy transmission line. The parameters (per inch) of the transmission line are as follows: $R = 0.2\Omega$, $L = 9.13nH$, $C = 3.65pF$, $G = 0$. When modelling with lumped RLC segments, each inch of the line is split up into ten lumped segments; for the R-Lossless case, each line is split up into five segments. The characteristic impedance of the line is 50.012Ω and the delay per inch is $0.18255ns$. The nonlinear elements in the BJT driver comprise 12 transistors and 20 diodes. The nonlinear elements in the passive receiver circuit are 5 diodes.

Waveforms from the simulation of this circuit are shown in Figs. 4.3 (near-end voltage) and 4.2 (far-end voltage). The input voltage pulse to the inverter in the circuit had the following specifications: rise time = 1ns, fall time = 1ns, pulse width = 20ns, total

Circuit	Simulation Length	Execution Time[a]		
		lumped-RLC	Convolution	State-Based
raytheon1	60 ns	739 s	19.43 s	20 s
	120 ns	1550 s	62.31 s	41.3 s
	180 ns	2237 s	131.32 s	60 s
	240 ns	3002 s	220s	78s
raytheon2	60 ns	336.35 s	37 s	28.7 s
	120 ns	668.3 s	110 s	52 s
	180 ns	1027 s	239 s	78.7 s
	240 ns	1372 s	380 s	99.6 s
	1000 ns	5646 s	6301 s	428 s
raytheon3	60 ns	885 s	40 s	28 s
	120 ns	1791 s	141 s	57 s
	180 ns	2700 s	529.41 s	95.3 s
mosaic	10 ns	44.44 s	0.9 s	2 s
	20 ns	93.18 s	3.6 s	2 s
	40 ns	181.3 s	12.9 s	3.5 s
	80 ns	371 s	49.5 s	6 s

[a]CPU times on a DEC 5000/200 running Ultrix 4.1

Table 4.1: Simple Lossy Lines: Comparison of Execution Times

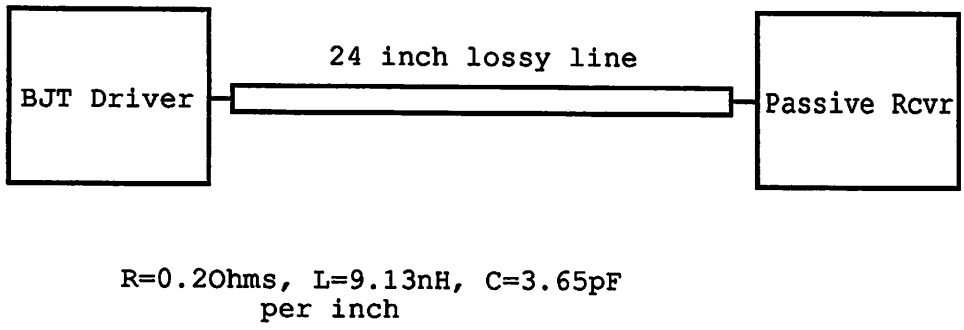

Figure 4.1: **raytheon1** circuit

simulation time: 60ns. It can be seen that the waveforms for all three methods agree well.

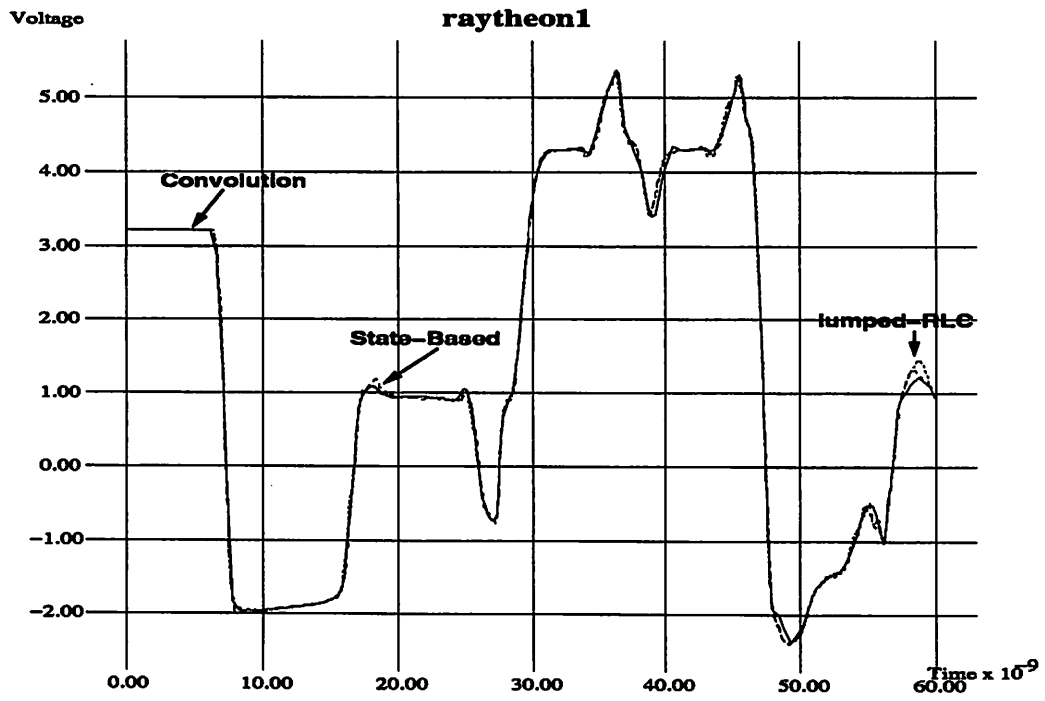

Figure 4.2: **raytheon1** receiver-end voltage

For this circuit, the convolution and state-based methods consume about the same computation for a simulation length of 60ns. As the simulation duration is increased to 240ns, the quadratic complexity of convolution becomes apparent from the disproportionate rise in execution time. The rise in execution time for the state-based and lumped-RLC methods is approximately linear. At 240ns, the state-based method is more than twice as fast as convolution, which in turn is more than a factor of 10 times faster than the lumped-RLC method. The accuracy of the convolution and state-based methods is seen to be similar. On account of the large number of segments used, the waveform for the lumped-RLC method is also accurate.

The second circuit **raytheon2** (Figure 4.4)) consists of a BJT driver driving three receiver circuits through several branched transmission lines. The parameters of the transmission line are the same as above; the driver and receiver circuits are also the same.

Waveforms from the simulation of this circuit are shown in Figs. 4.5 – 4.8, by increasing order of increasing distance from the BJT driver.

For **raytheon2**, the waveforms of the three methods are again very similar. The

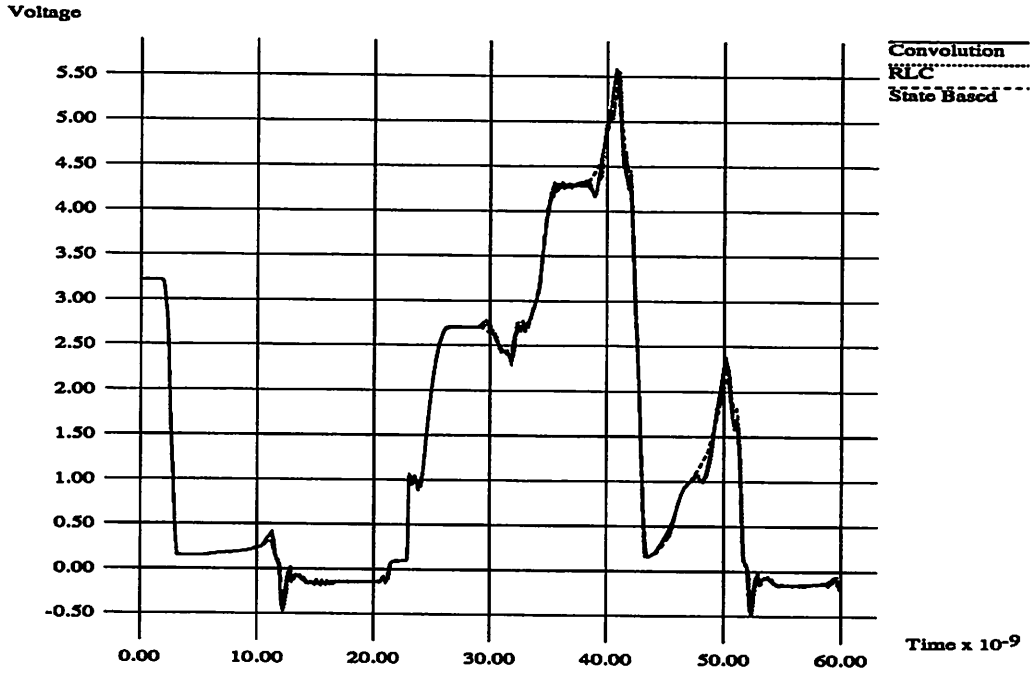

Figure 4.3: **raytheon1** near-end voltage

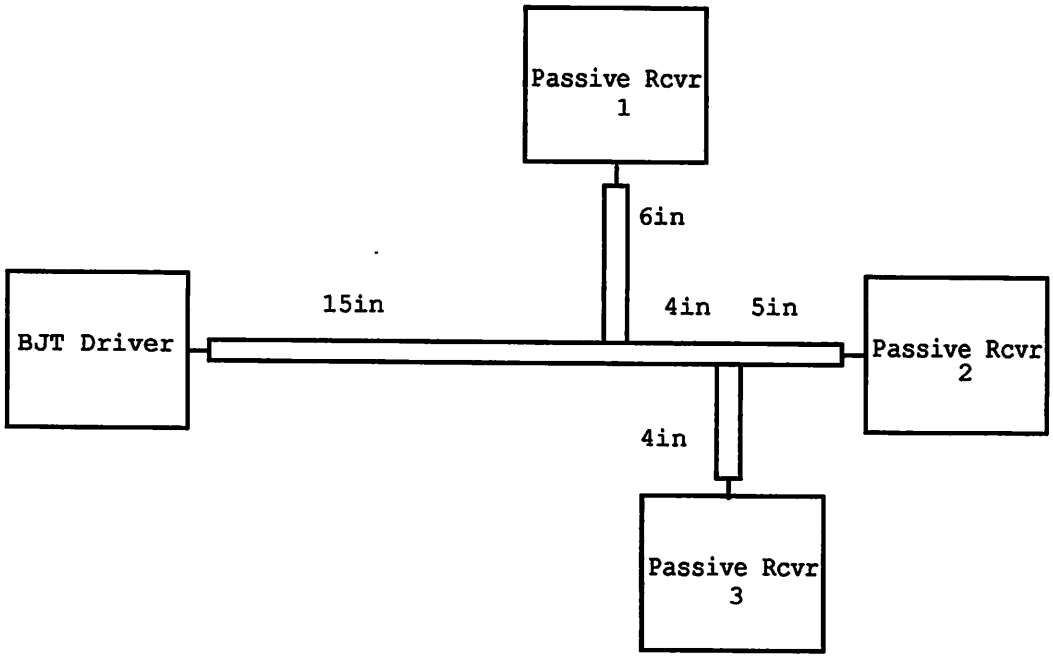

Figure 4.4: **raytheon2** circuit

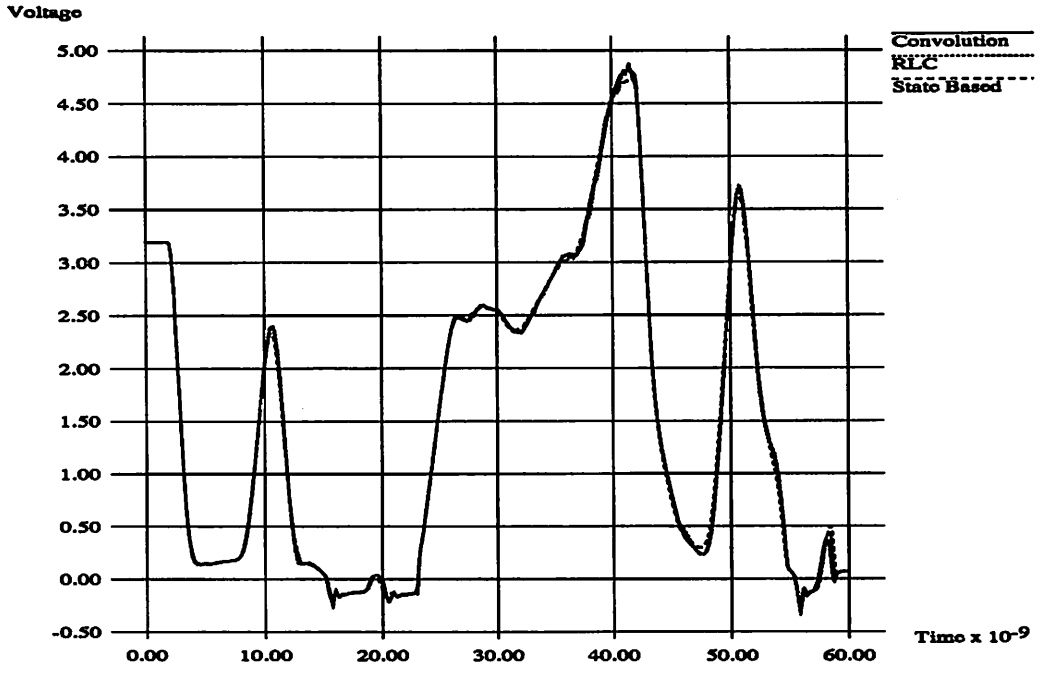

Figure 4.5: **raytheon2**, voltage at driver

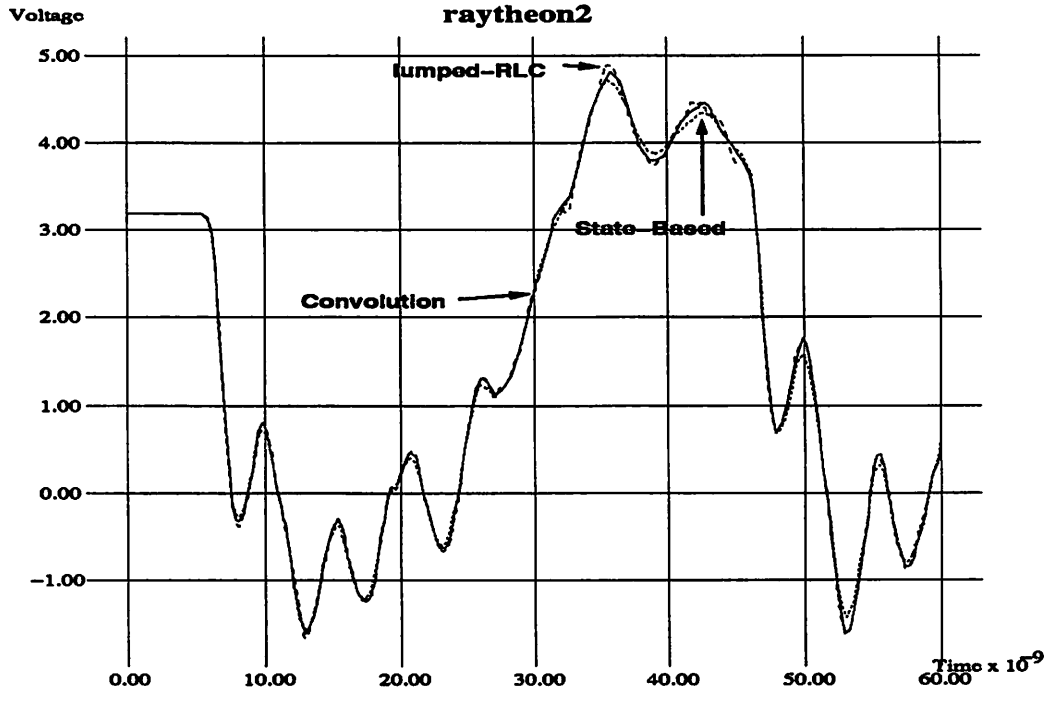

Figure 4.6: **raytheon2**, voltage at stub end 21 inches from driver

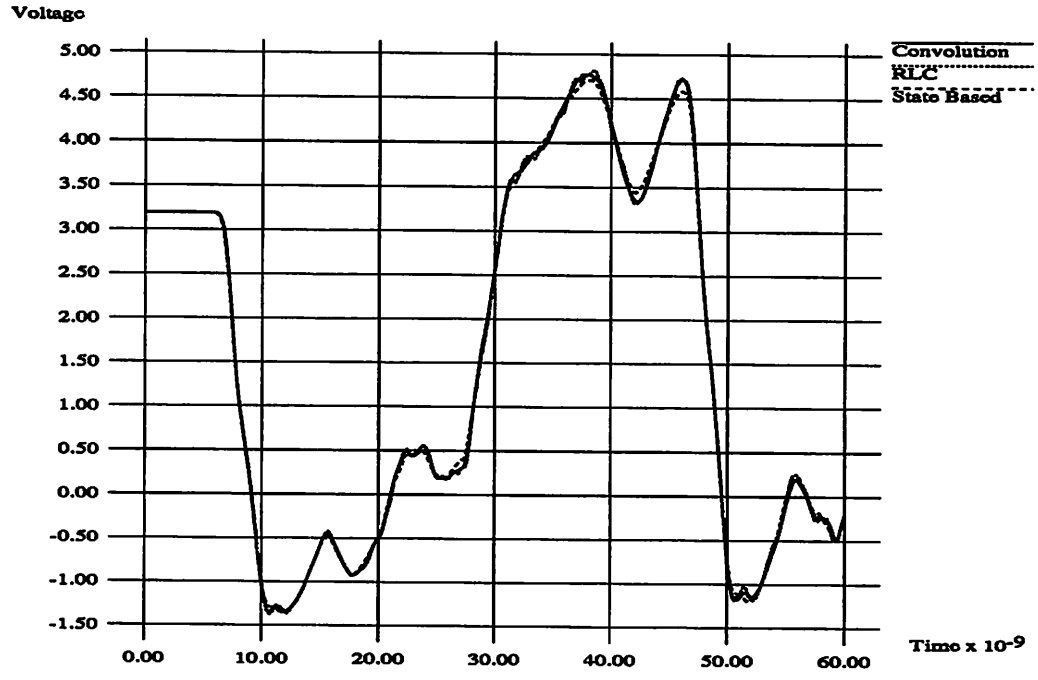

Figure 4.7: **raytheon2**, voltage at stub end 23 inches from driver

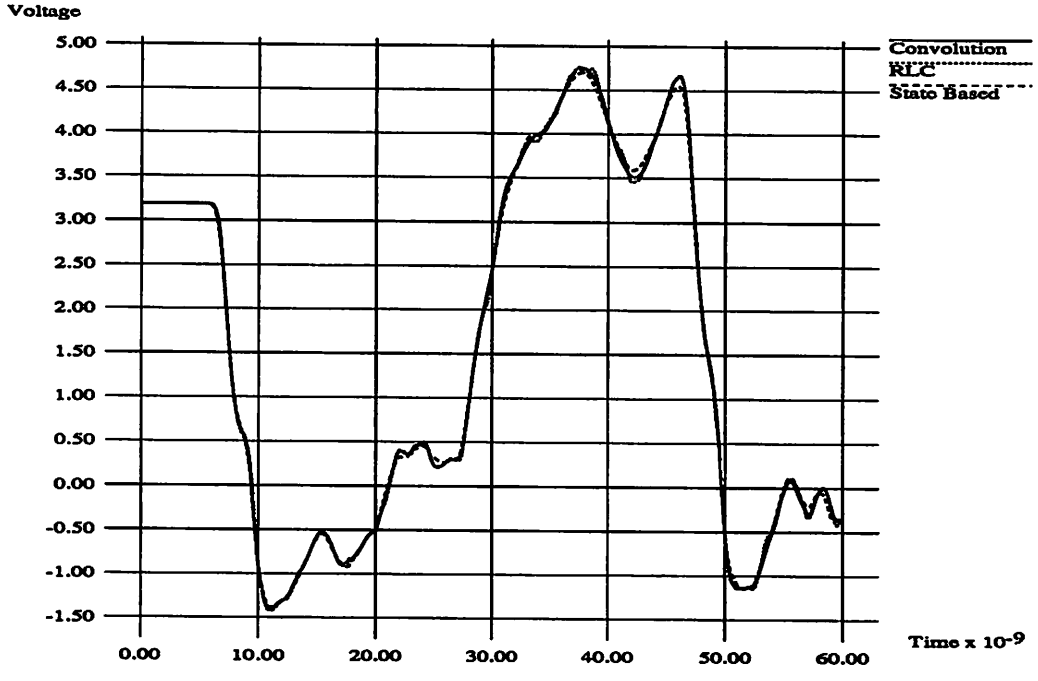

Figure 4.8: **raytheon2**, voltage at far-end of main line

state-based method is computationally advantageous over both lumped-RLC and convolution methods, for simulation lengths over 60ns. At 1000ns, the advantage in speed is more than a factor of 10 over the other methods. It is to be noted that the quadratic complexity of convolution makes it slower than the lumped-RLC method for this long simulation.

The third circuit **raytheon3**, shown in Figure 4.9, consists of a BJT driver connected to a receiver through two 2-inch single-conductor lossy lines and a 20-inch two-wire multiconductor line. The self-parameters of the coupled line are the same as in the previous circuits; the mutual capacitance and inductive coupling coefficient are $1.8pF$ per inch and 0.482, respectively. The sense wire of the multiconductor line is terminated at both ends by the nominal characteristic impedance of the line, 50Ω. The input pulse specifications are the same as in the previous circuits.

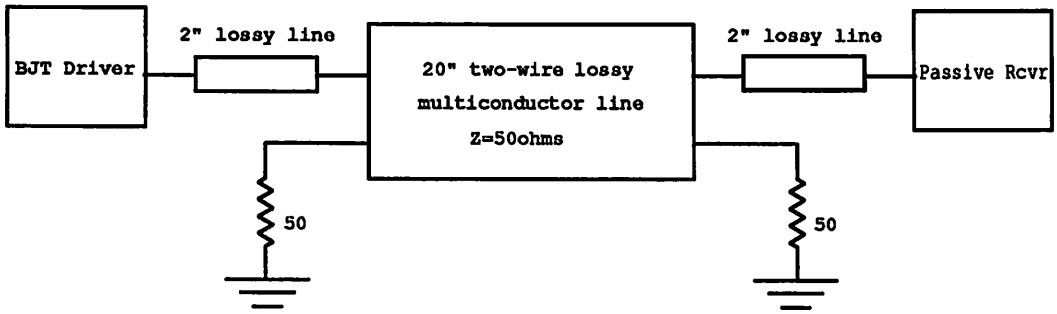

Figure 4.9: **raytheon3** circuit

The near end drive line voltage at the 2-wire coupled line is shown in Figure 4.10 and the near end sense line crosstalk is shown in Figure 4.11. The far end drive line voltage is shown in Figure 4.12 and the far end crosstalk is shown in Figure 4.13.

It is observed that all three methods again yield very similar results. For a simulation of 180ns, the state-based method is more than 5 times faster than the convolution approach and 20 times faster than the lumped-RLC method.

The fourth circuit **mosaic**, shown in Figure 4.14, consists of a voltage source connected through a series terminating resistor to one end of a transmission line. The other end of the transmission line is left open, save for two clamping diodes whose purpose is to limit the voltage swing to within about -0.7 to 5.7 volts. The interconnect parameters for this line are: C = 0.468pF, L = 8.792nH, R = 12.45Ω per cm, with the length being 16cm. The nominal characteristic impedance of the line is 137Ω, and the delay of the line is 1.024ns. The physical parameters of the line are: thickness=$2\mu m$, width=$11\mu m$, aluminium

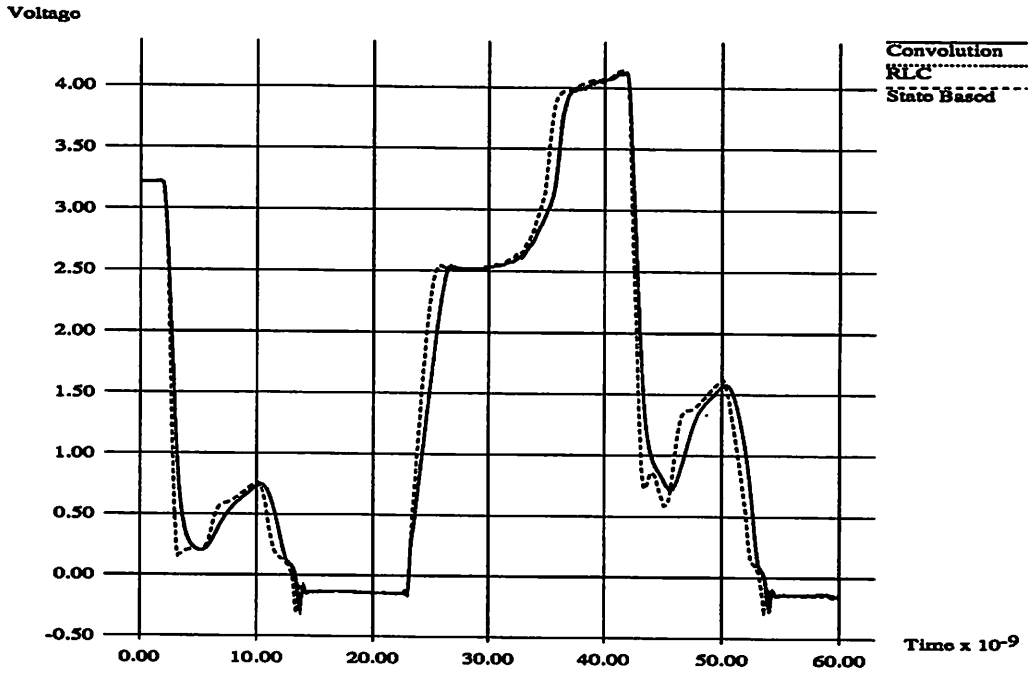

Figure 4.10: **raytheon3**, drive line near end voltage at coupled line

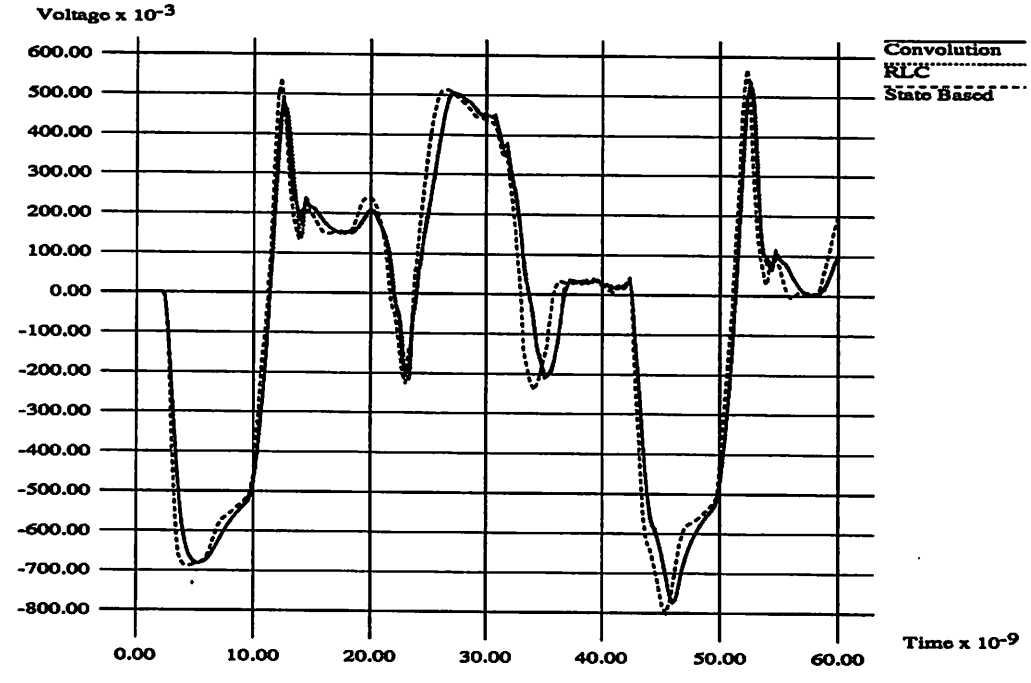

Figure 4.11: **raytheon3**, sense line near end voltage crosstalk

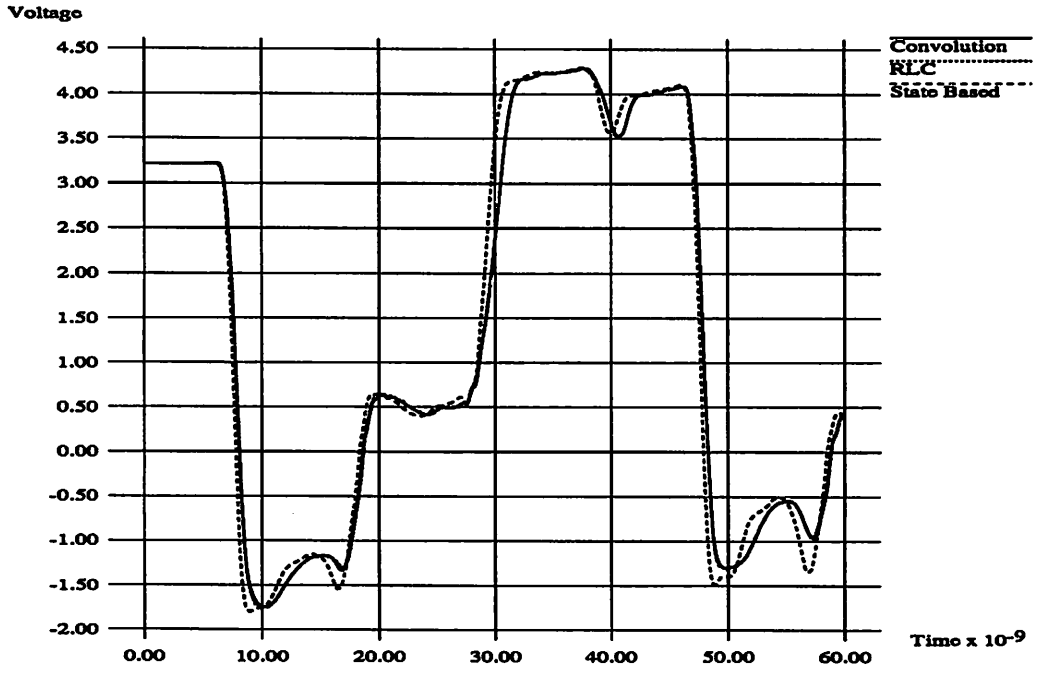

Figure 4.12: **raytheon3**, drive line far end voltage at coupled line

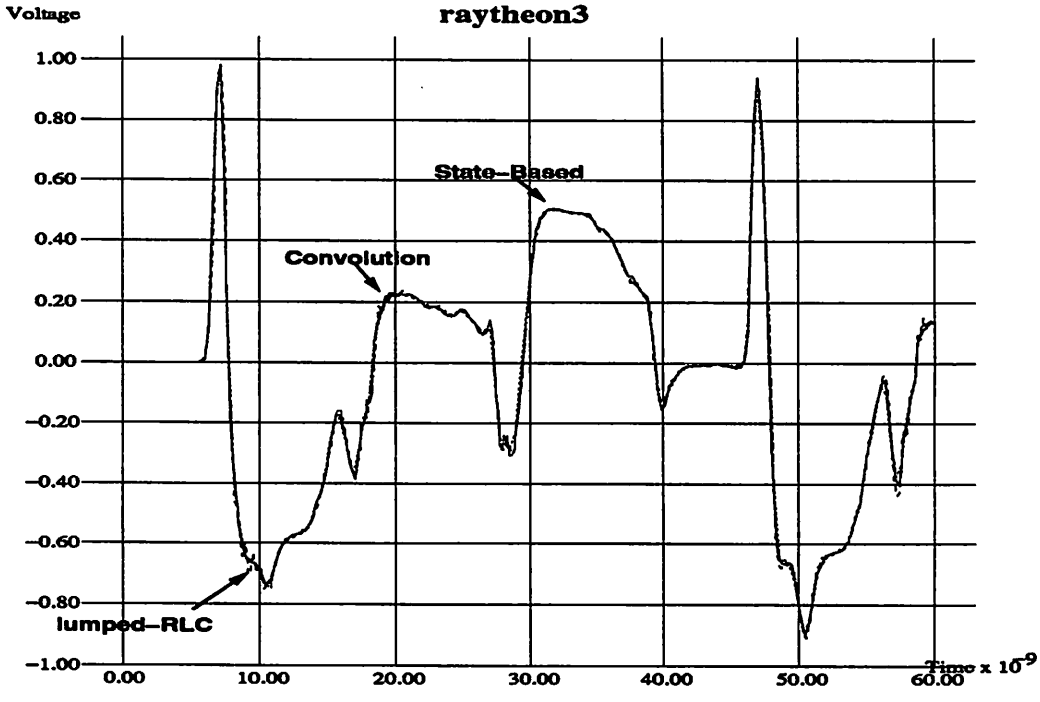

Figure 4.13: **raytheon3**, sense line far end crosstalk

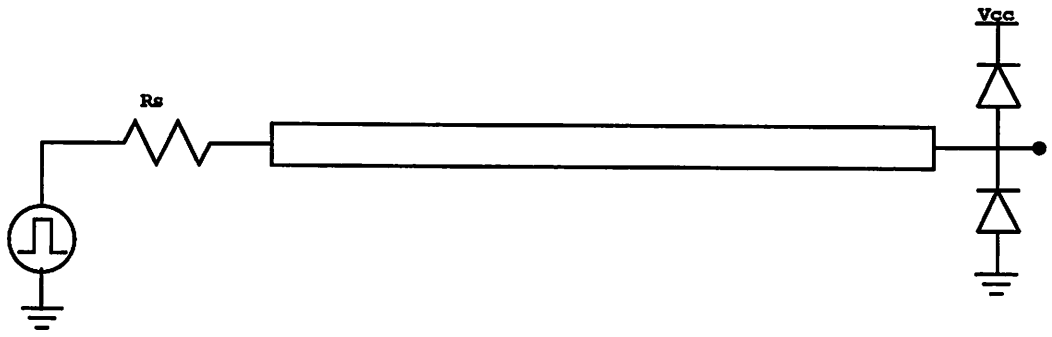

Figure 4.14: **mosaic** circuit

conductor, SiO_2 dielectric. The input pulse parameters are: rise and fall times of 100ps, pulse width 1ns, 0–5V swing. The series resistor R_s is 10Ω.

The voltages at the near and far ends of the transmission line are shown in Figs. 4.15 and 4.16. Using the lumped RLC method, which has 64 segments for the line, results in significant spurious oscillations in the far end waveform. In contrast, the state-based and convolution methods yield accurate waveforms. The speed advantage of the state-based method for an 80ns simulation is more than 8 and 60 over the convolution and lumped RLC methods, respectively.

The interconnect of the **mosaic** example is also used to illustrate the accuracy of the state-based and convolution methods compared to the Padé approximation method [31]. The linear driver in Figure 4.14 is replaced by a simple CMOS inverter and the receiving end of the interconnect is left open.[1]. Comparisons between the convolution/state-based, lumped-RLC and Padé approximation methods are shown for the voltage at the unterminated end of the line in Figure 4.17[2]. The close match between the lumped-RLC and the convolution/state-based methods can be seen, whereas the Padé approximation method's waveform is seen to have extraneous non-physical features. This is due to the inaccuracy of the model for significant R (in this case, 12.45Ω per cm). The inaccuracies increase with increase in R: setting $R = 50\Omega$ per cm results in the waveforms of Figure 4.18. Reducing the value of R for this line to 0.2Ω per cm improves the performance of

[1]This circuit is used in the suite of examples for testing SWEC and SPICE3-Padé, programs that implement the algorithms in [31].

[2]Comparisons performed using the SWEC implementation of Padé approximation, latest version as of Nov. 1, 1992. The SPICE3 implementation of Padé approximation was not stable and produced erroneous results in most examples, hence comparisons against the SPICE3 implementation are not shown.

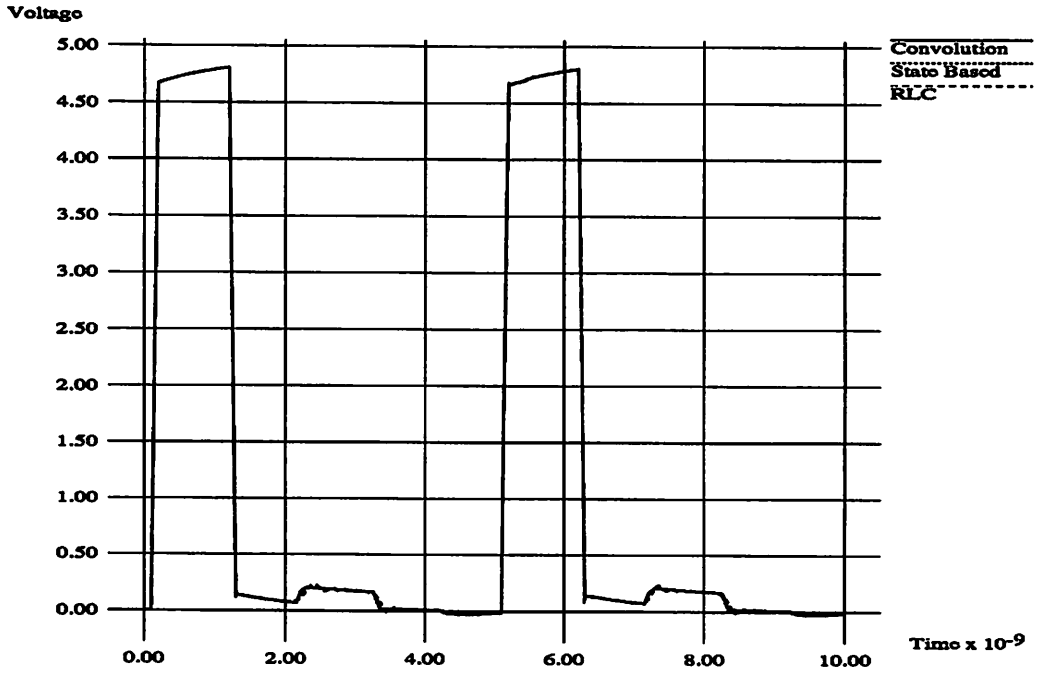

Figure 4.15: **mosaic** near end voltage

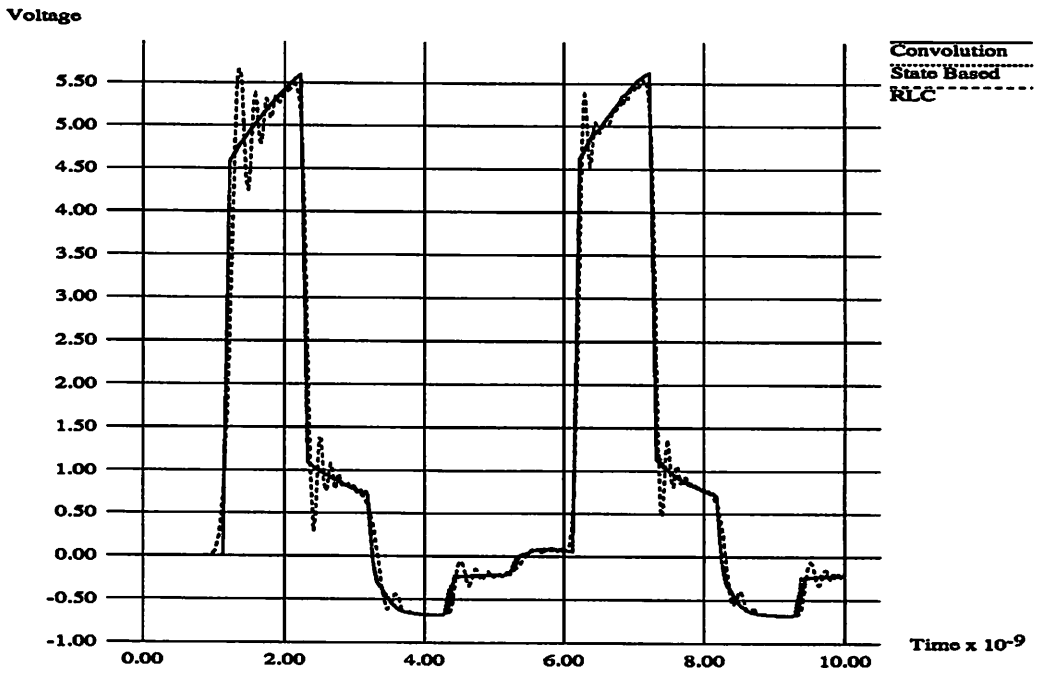

Figure 4.16: **mosaic** far end voltage

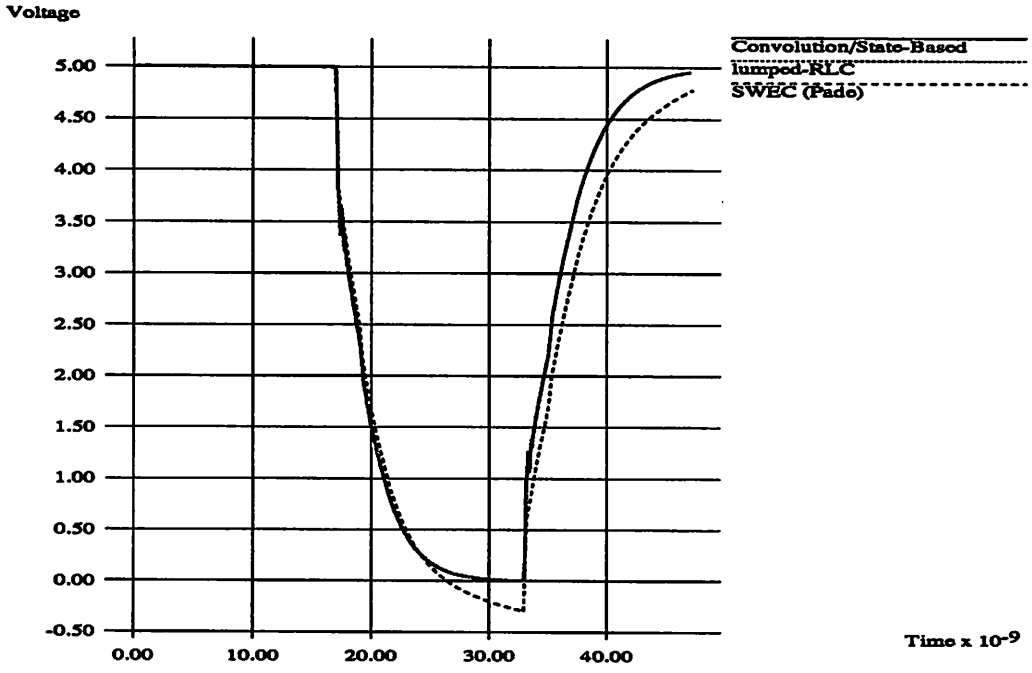

Figure 4.17: modified **mosaic**, far end voltage (Padé approx. method)

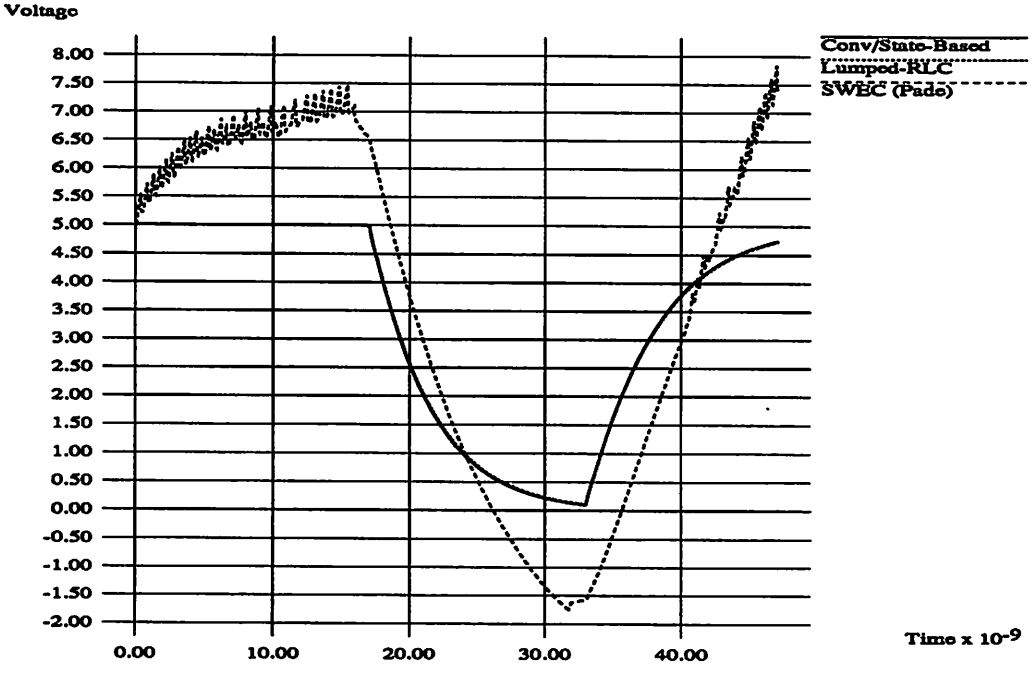

Figure 4.18: modified **mosaic**, $R = 50\Omega$ cm^{-1}, far end voltage (Padé approx. method)

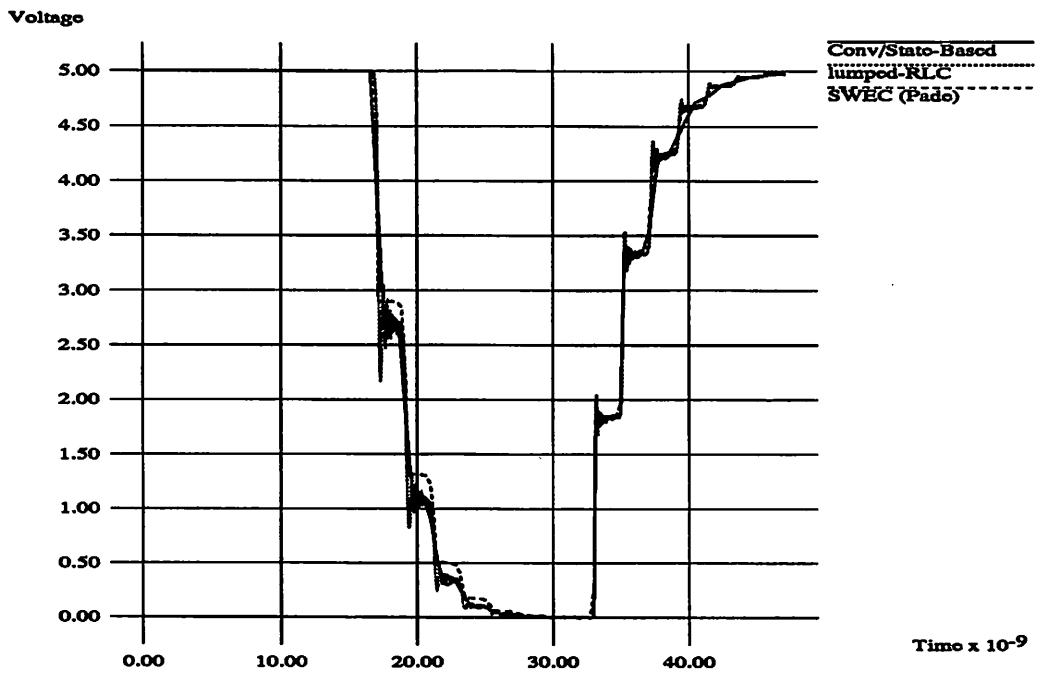

Figure 4.19: modified **mosaic**, $R = 0.2\Omega$ cm^{-1}, far end voltage (Padé approx. method)

the Padé approximation method, as seen in Figure 4.19. For the $R = 12.45\Omega$ per cm case, execution times for the lumped-RLC, convolution/state-based and Padé methods were 98s, 11s and 1.24s, respectively; for the $R = 50\Omega$ per cm case, the times were 43.7s, 31.2s and 1.24s, respectively; and for the $R = 0.2\Omega$ per cm case, they were 286s, 2s and 1.13s, respectively[3]. This demonstrates that the techniques of [31], while significantly faster than the convolution, state-based and lumped-RLC methods, can lead to large inaccuracies for thin MCM interconnect with high series resistance.

The fifth circuit **xerox-sun-lsi** is shown in Figure 4.20. The circuit consists of a high-speed bus, modelled as an 8-wire coupled transmission line, connecting three chips with CMOS Gunning Transceiver Logic (GTL) drivers [24]. The chips are clocked at 400Mhz (2.5ns cycle), with rise and fall times of 0.25ns. The bus is 1 foot long and is terminated at both ends by 50Ω resistors, the nominal characteristic impedance of the lines. The parameters of the coupled line (per inch) are: $R = 0.2\Omega$, $L = 9.13nH$, $C = 3.65pF$, $G = 0$, k (coeff. of inductive coupling) $= 0.482$ and C_m (coupling capacitance) $= 1.8pF$. Note that very thin interconnect, as in the **mosaic** example, cannot be used in GTL technology,

[3]DECstation 5000/125 running Ultrix V4.2A.

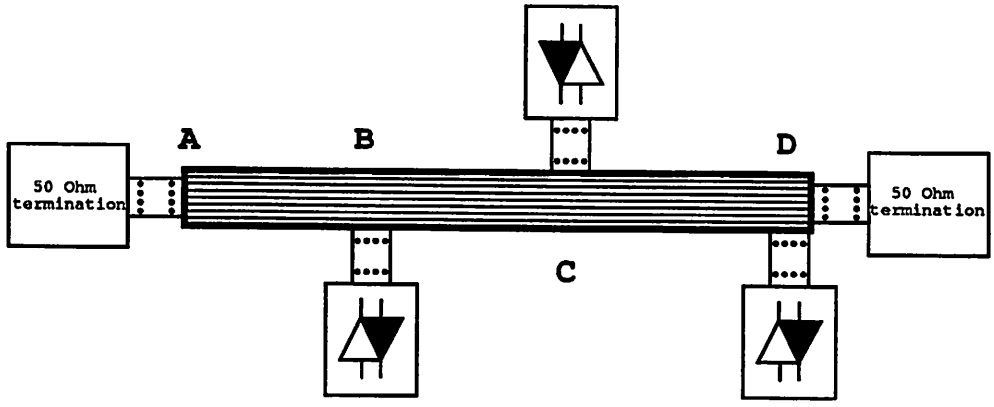

Figure 4.20: **xerox-sun-lsi** coupled line circuit

because the high series R of the line will dominate the parallel termination resistance.

In the simulation, the chip at B (Figure4.20) drives the bus with the other two chips acting as receivers. Each chip connection has a pad capacitance of $2.5pF$. The bus wires are inactive when at the high voltage level (V_t) of 1.2V, and active at the low voltage level of 0.2V. In order to estimate the worst-case crosstalk, all wires of the bus except the fourth from one end were switched simultaneously.

Execution times (for a 5ns simulation) were 24s for the convolution/state-based waveforms and 178s for a partial simulation using the lumped-RLC method[4] on a DECstation 5000/240 with 128MB of memory. The CMOS transistors caused convergence problems in SPICE3, hence RELTOL was increased to a value of 0.1, but without noticeable degradation of results. The circuit was also simulated using linear drivers approximating the GTL technology and the default RELTOL of 0.01. For the linear simulation, the execution times were 17.8ns for the convolution/state-based waveeforms and 121s for the lumped-RLC method. Figures 4.21, 4.22, 4.23 and 4.24 depict the progress of the waveform on Line 1 at points A, B, C and D of Figure 4.20, respectively. (Note that the circuit is being driven at B). The delays caused by the transmission line are clearly seen. Figures 4.25, 4.26, 4.27 and 4.28 depict the crosstalk on Line 4. As expected, the crosstalk centers around V_t, the DC level of the quiescent bus. Figures 4.29, 4.30, 4.31 and 4.32 depict the progress of the waveform on Line 5, and Figures 4.33, 4.34, 4.35 and 4.36 do the same for Line 7.

It is seen from Figures 4.21 – 4.36 that using linear approximations to GTL technology leads to significant degradation of results, hence nonlinear models must be used.

[4]The lumped-RLC simulation did not complete.

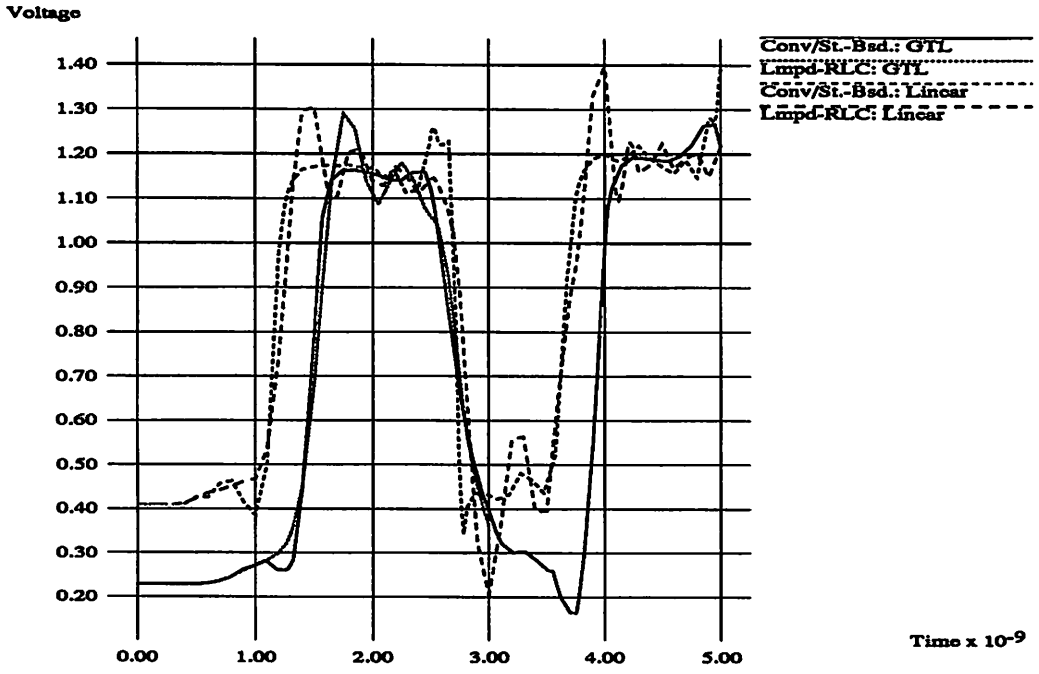

Figure 4.21: **xerox-sun-lsi** voltage at A, Line 1

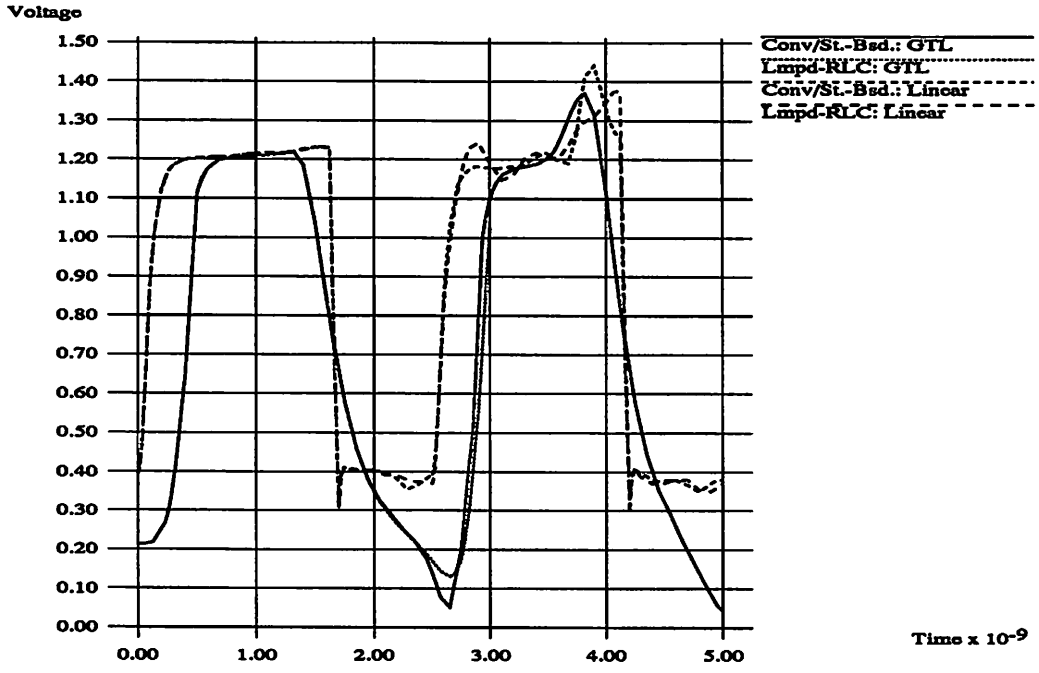

Figure 4.22: **xerox-sun-lsi** voltage at B, Line 1

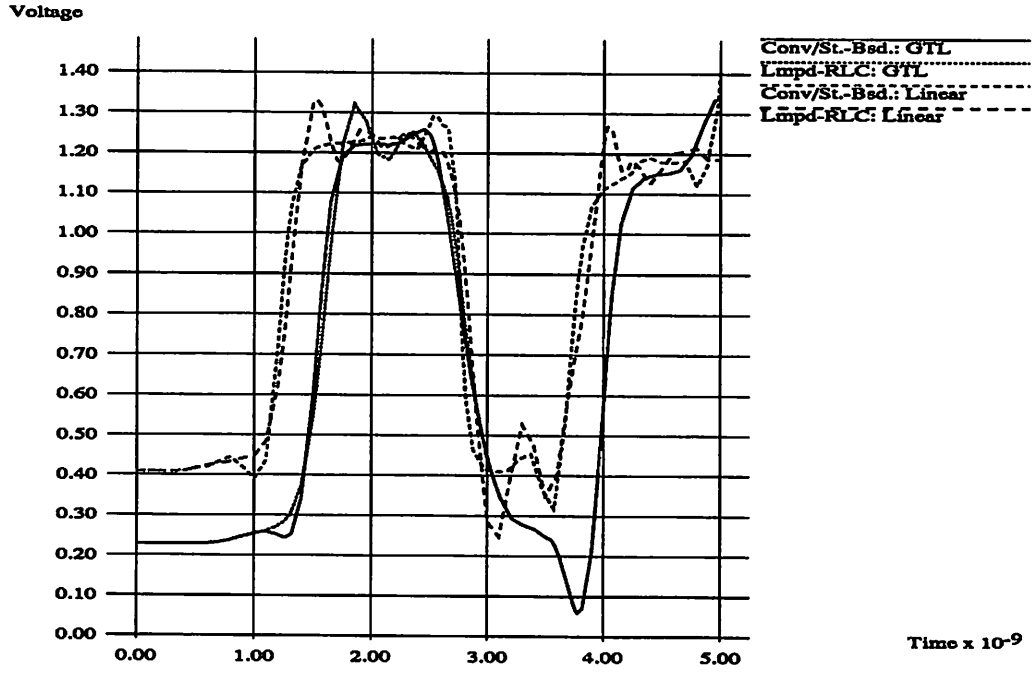

Figure 4.23: **xerox-sun-lsi** voltage at C, Line 1

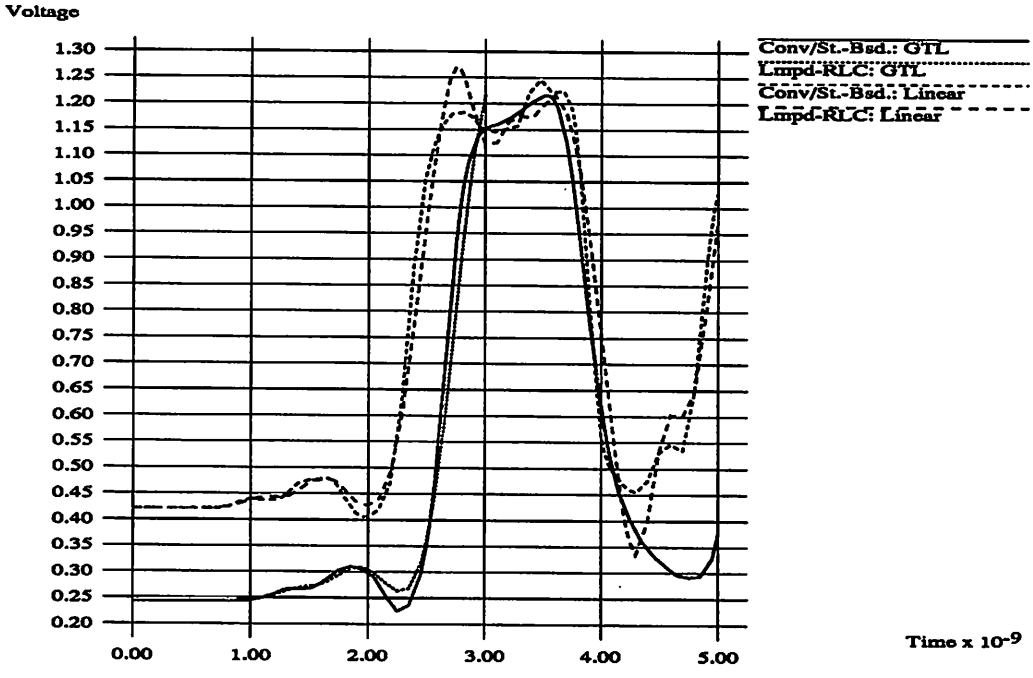

Figure 4.24: **xerox-sun-lsi** voltage at D, Line 1

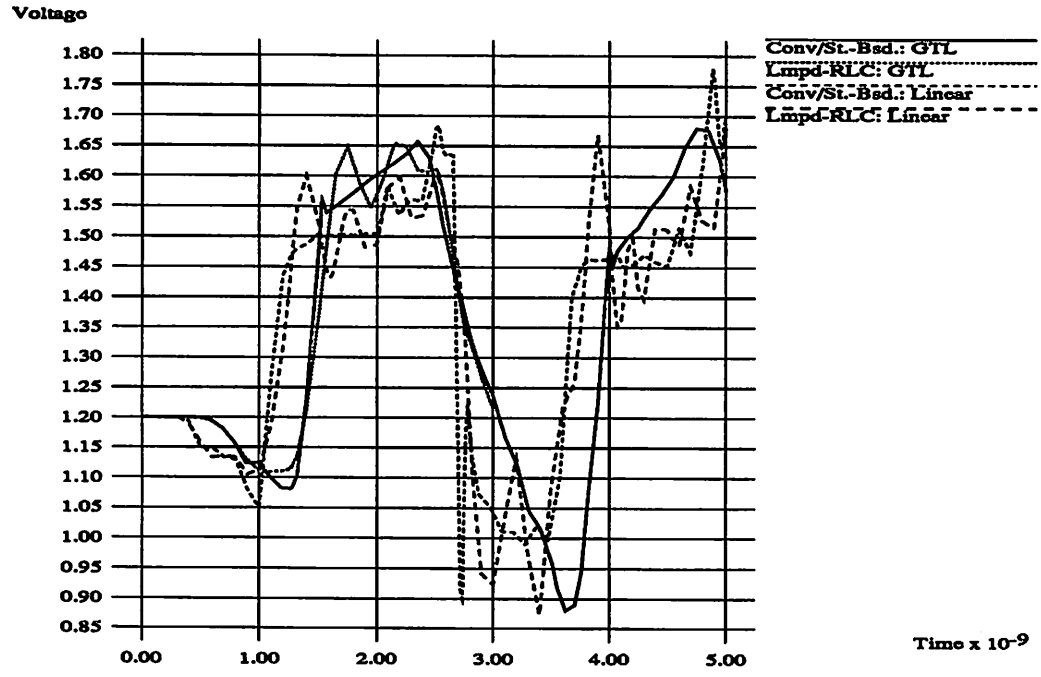

Figure 4.25: **xerox-sun-lsi** crosstalk voltage at A, Line 4

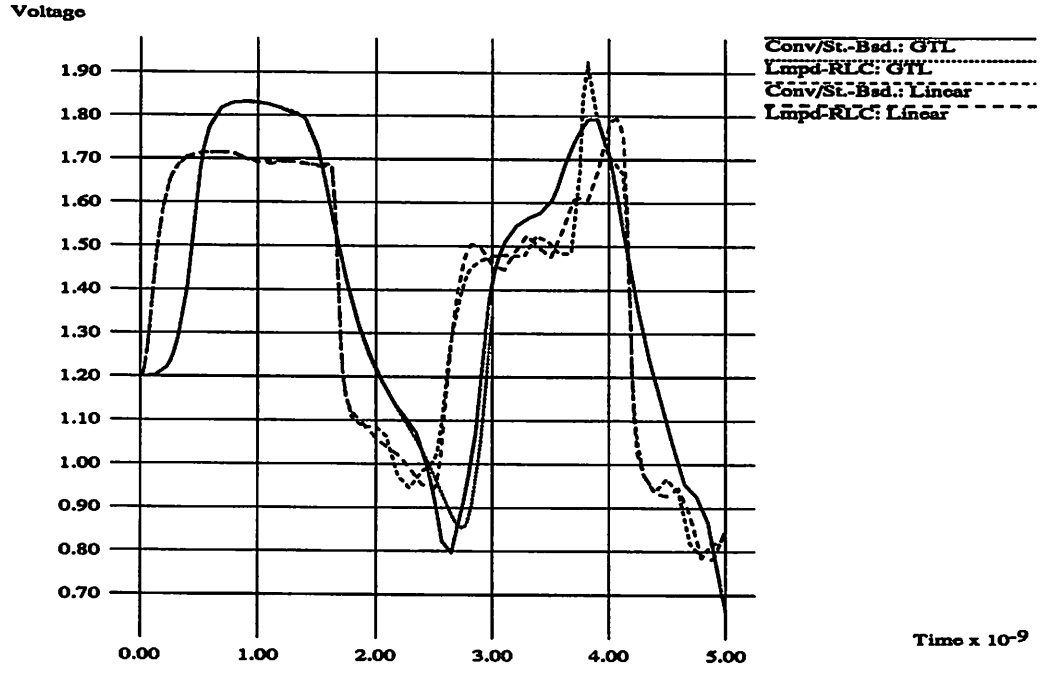

Figure 4.26: **xerox-sun-lsi** crosstalk voltage at B, Line 4

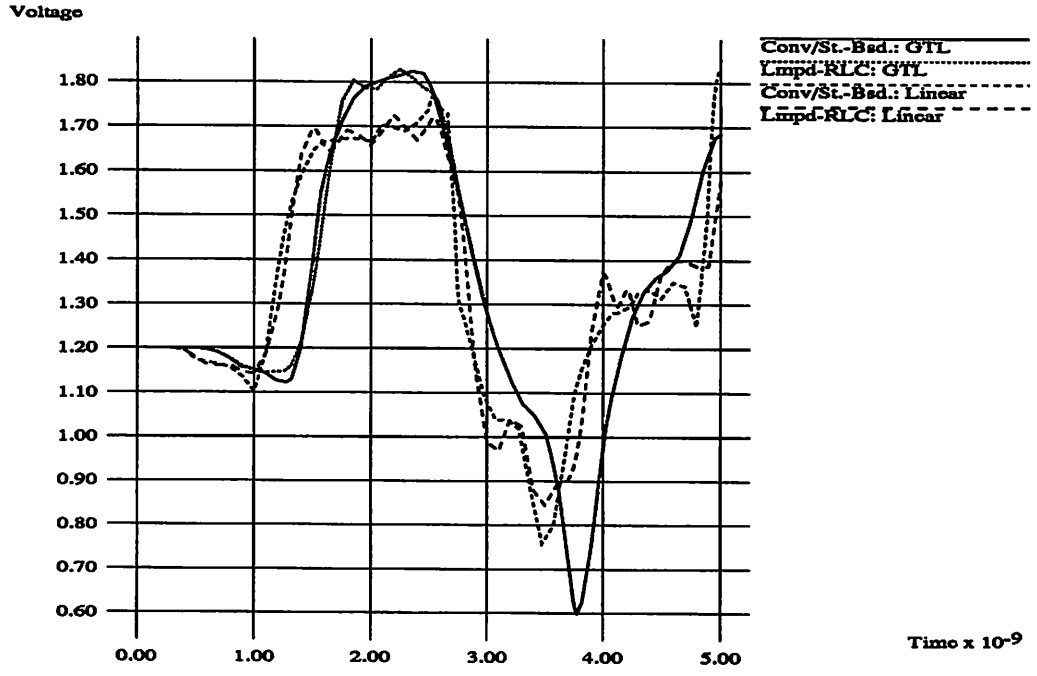

Figure 4.27: **xerox-sun-lsi** crosstalk voltage at C, Line 4

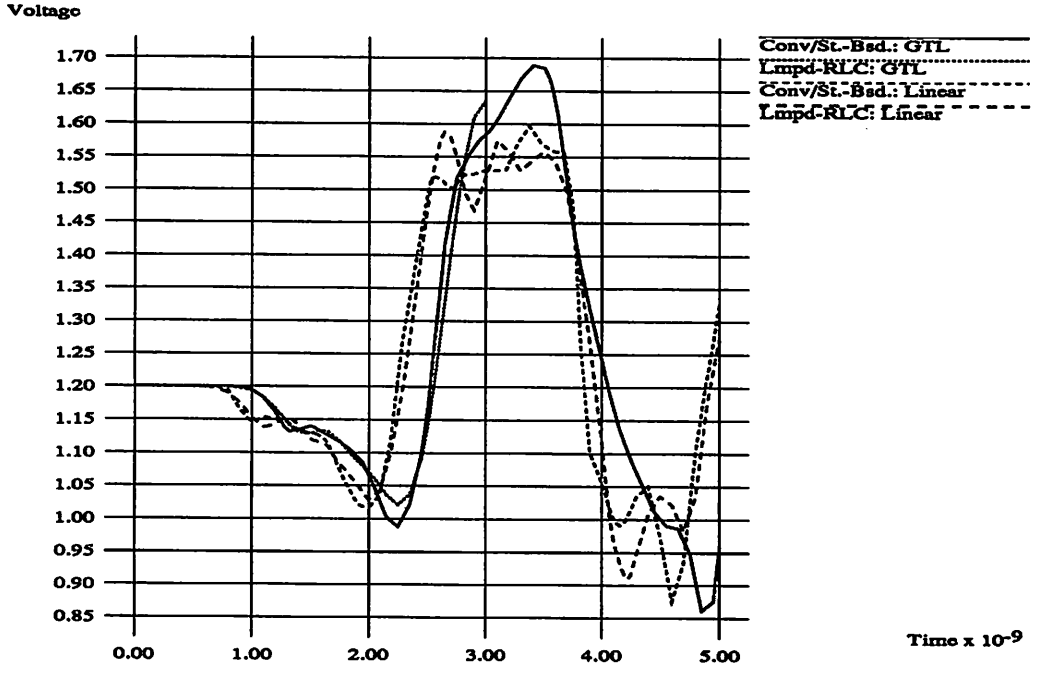

Figure 4.28: **xerox-sun-lsi** crosstalk voltage at D, Line 4

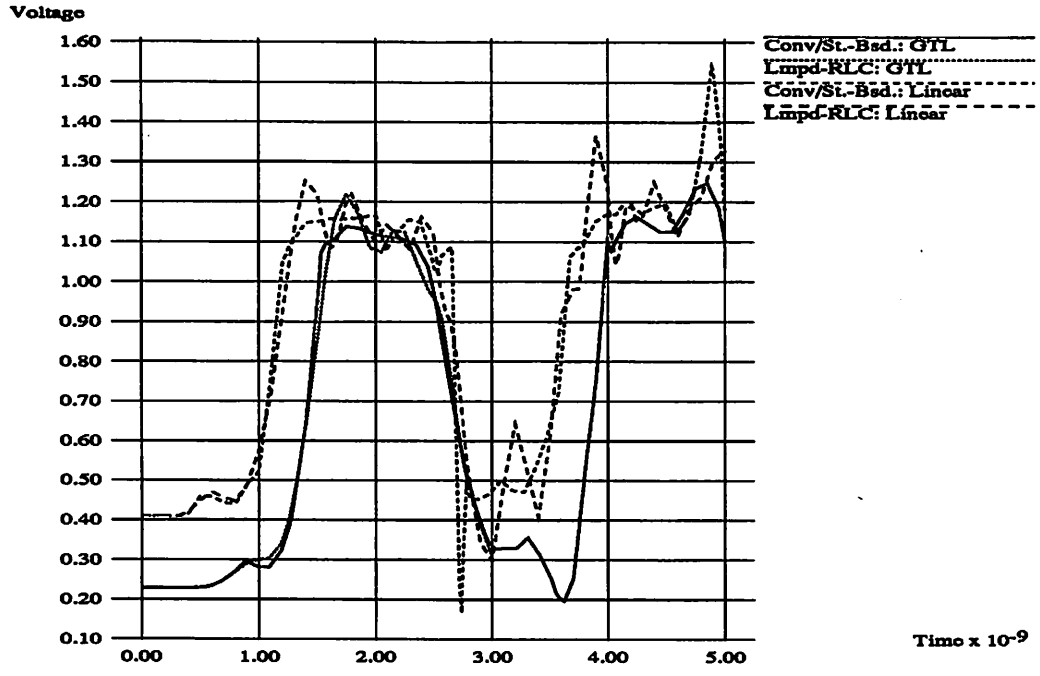

Figure 4.29: **xerox-sun-lsi** voltage at A, Line 5

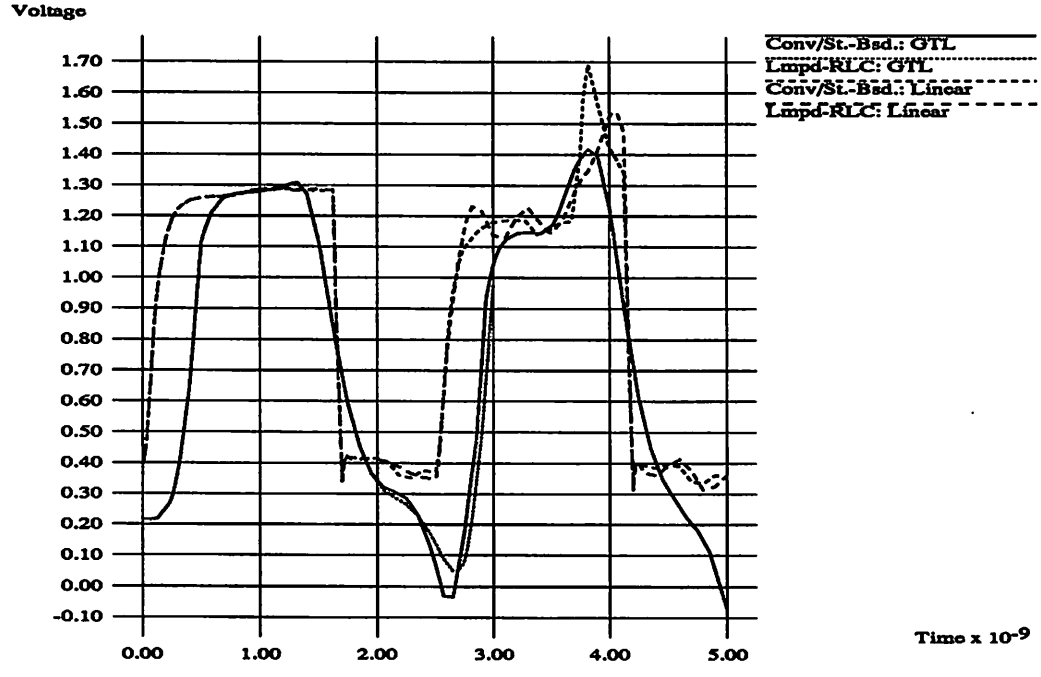

Figure 4.30: **xerox-sun-lsi** voltage at B, Line 5

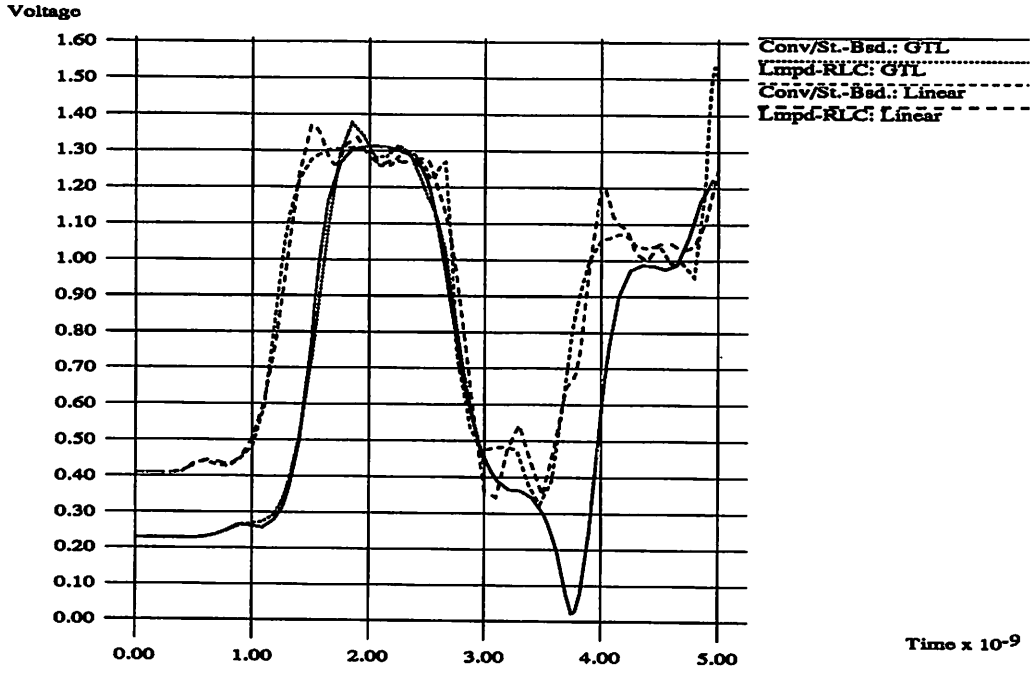

Figure 4.31: **xerox-sun-lsi** voltage at C, Line 5

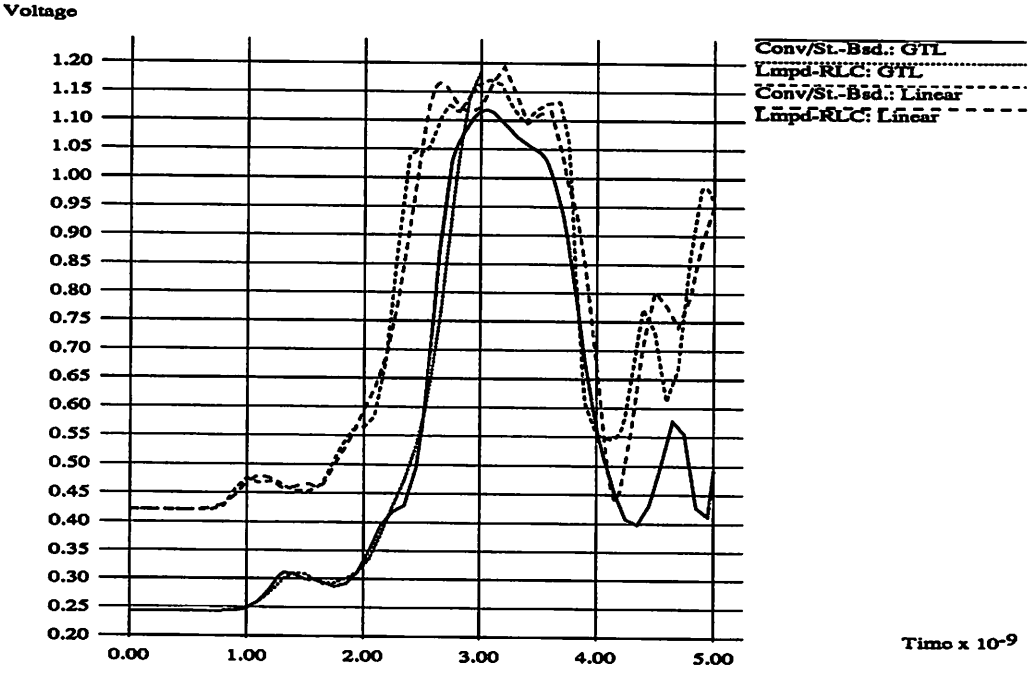

Figure 4.32: **xerox-sun-lsi** voltage at D, Line 5

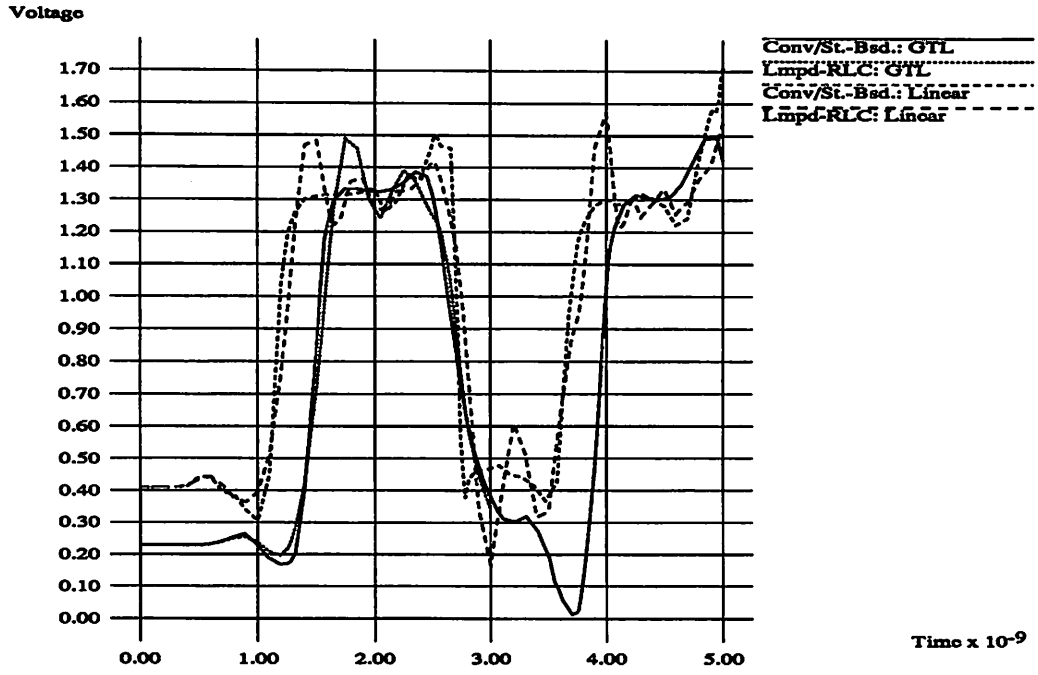

Figure 4.33: **xerox-sun-lsi** voltage at A, Line 7

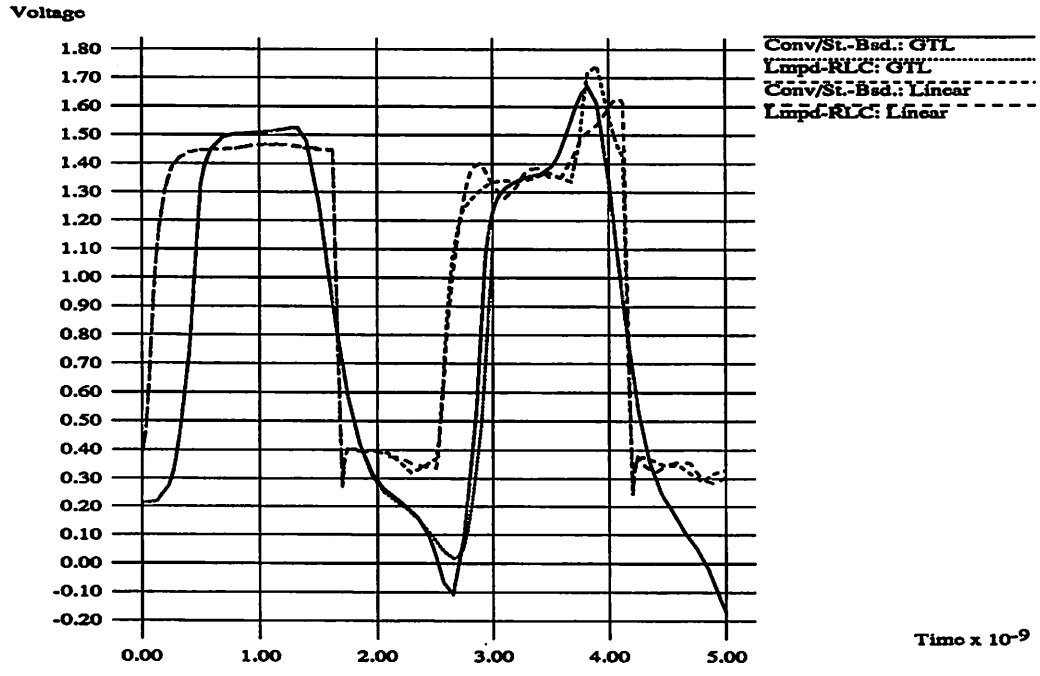

Figure 4.34: **xerox-sun-lsi** voltage at B, Line 7

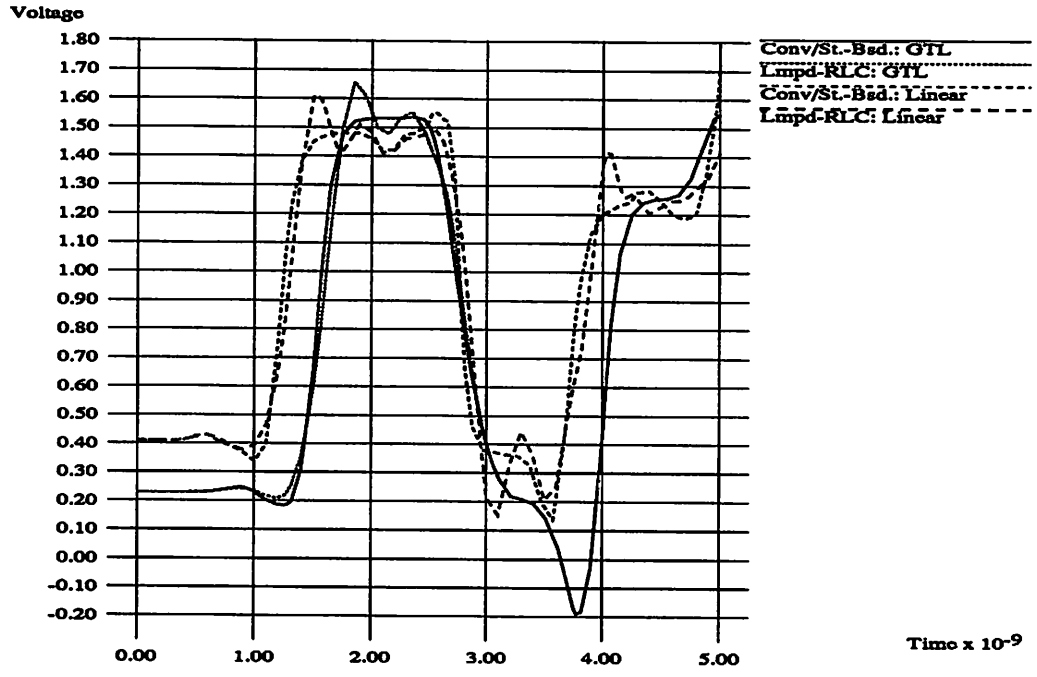

Figure 4.35: **xerox-sun-lsi** voltage at C, Line 7

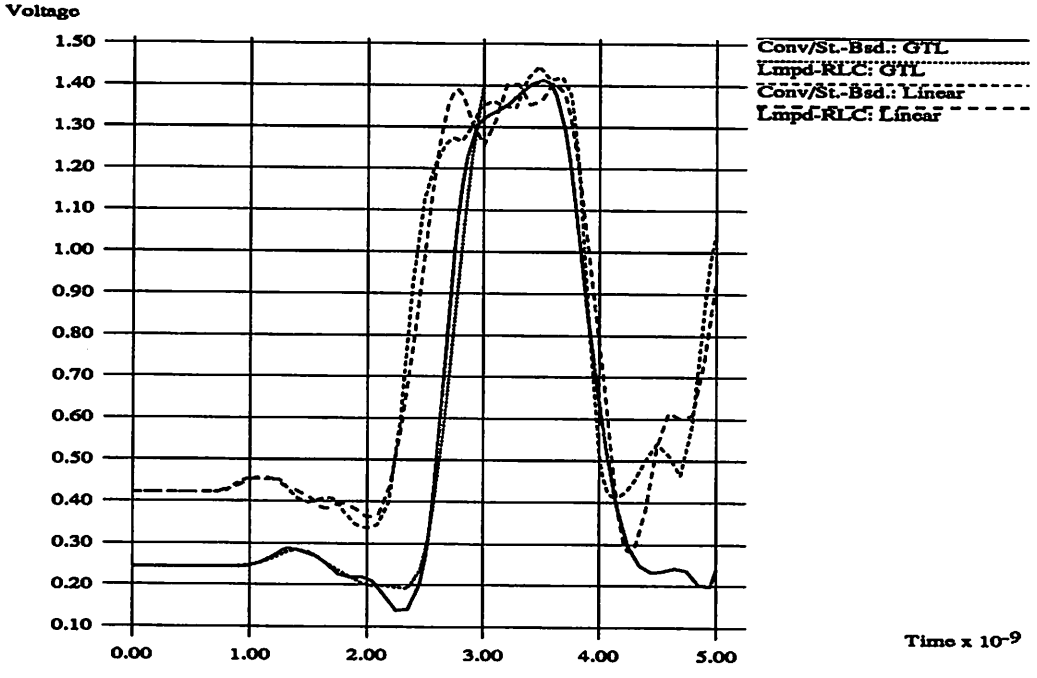

Figure 4.36: **xerox-sun-lsi** voltage at D, Line 7

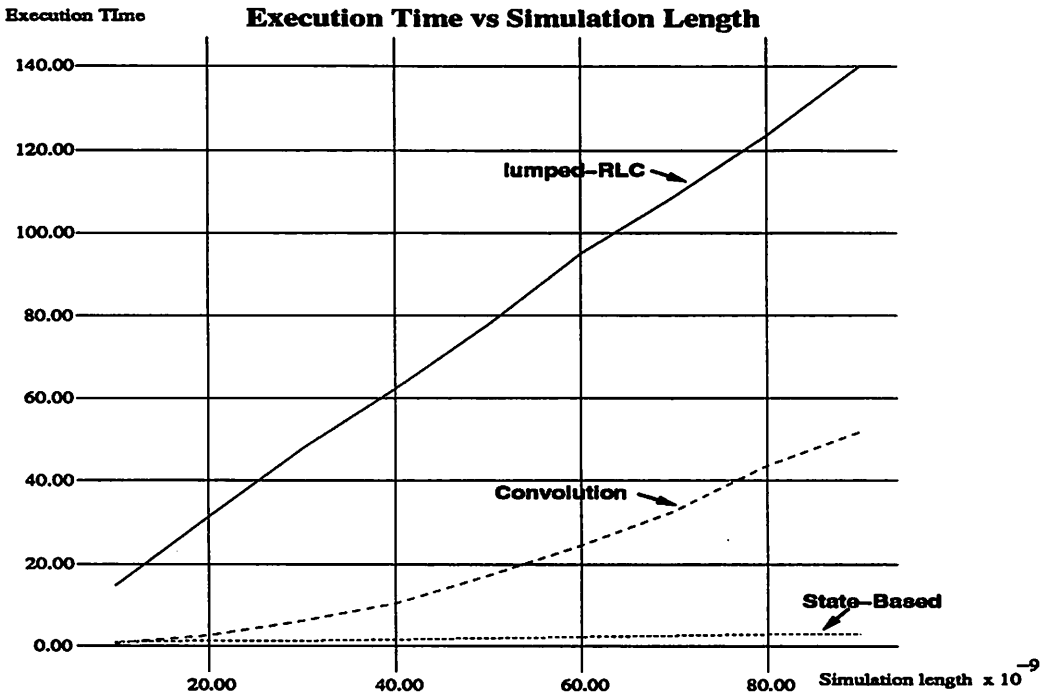

Figure 4.37: modified **mosaic**: execution time vs simulation length

Figure 4.37 is a plot of execution time vs. simulation length for the three methods. Both the state-based and lumped-RLC methods grow linearly with time, but the graph for lumped-RLC method displays a much greater slope than that for the state-based method. Convolution is seen to have quadratic time complexity, with execution times comparable to the state-based method for short simulations, but rising disproportionately as the length of the simulation is increased.

From Table 4.1 and Figure 4.37, it is observed that the state-based method can speed up simulations by factors of more than 10 and 50 over the convolution and lumped-RLC methods respectively. Note also that the convolution method can be more than 5–10 times faster than the lumped-RLC method. The state-based and convolution methods are equally accurate, equivalent or superior to the lumped-RLC method.

4.2 Lines with Skin Effect

The techniques for frequency varying lines outlined in Section 2.5 were used to simulate interconnect with skin effect, a high frequency nonideality.

The physical parameters of the aluminium interconnect (taken from [14]) are: width = 11μm, thickness = 2μm, height above ground plane = 10μm, SiO_2 dielectric, length of line = 10cm, R_{dc} = 12 ohms/cm, L_{dc} = 8.79 nH/cm, C_{dc} = 1 pF/cm. Dielectric loss (parallel conductance G) is assumed to be zero at all frequencies. Skin-effect is accounted for using two models, one with a sharp transition point between the DC and skin effect regimes (the **abrupt** model), and one with a smooth transition region (the **smooth** model, [29]).

4.2.1 Abrupt Skin Effect Model

The **abrupt** model is based on the following equations:

$$R(f) = \begin{cases} R_0\sqrt{f} & f \geq f_T \\ R_{dc} & f < f_T \end{cases} \tag{4.1}$$

$$L(f) = \begin{cases} L_{ext} + \frac{L_0}{\sqrt{f}} & f \geq f_T \\ L_{dc} & f < f_T \end{cases} \tag{4.2}$$

$C(f)$ is assumed constant at C_{dc}; f_T, the transition frequency after which skin-effect becomes significant, is taken to be 1 GHz from [11]; L_{ext}, the inductance external to the wire and less than L_{dc}, is taken to be 4 nH/cm. From these, R_0 and L_0 are calculated to be 3.7947×10^{-4} and 1.5147×10^{-4} respectively. The ideal delay $T = l\sqrt{L_{dc}\,C_{dc}}$ is 0.9375 ns.

The impulse responses of the pure nonideality Δh_Y, Δh_γ and $\Delta h_{\gamma Y}$ contain impulse (delta function) components which are first separated out. $\Delta h'_Y$, $\Delta h'_\gamma$ and $\Delta h'_{\gamma Y}$, the components without impulses, were calculated by numerical inversion of the Fourier transform, and are shown in Figs. 4.38, 4.39 and 4.40. The following relations can be shown to hold:

$$\Delta h_Y(t) = M_Y\,\delta(t) + \Delta h'_Y(t) \tag{4.3}$$

$$\Delta h_\gamma(t) = M_\gamma\,\delta(t-T) + \Delta h'_\gamma(t) \tag{4.4}$$

$$\Delta h_{\gamma Y}(t) = M_{\gamma Y}\,\delta(t-T) + \Delta h'_{\gamma Y}(t) \tag{4.5}$$

For this example, M_Y = 0.42021, M_γ = −0.53263, and $M_{\gamma Y}$ = −0.51601. In order to obtain a quantitative estimate of the error caused by truncation, the functions

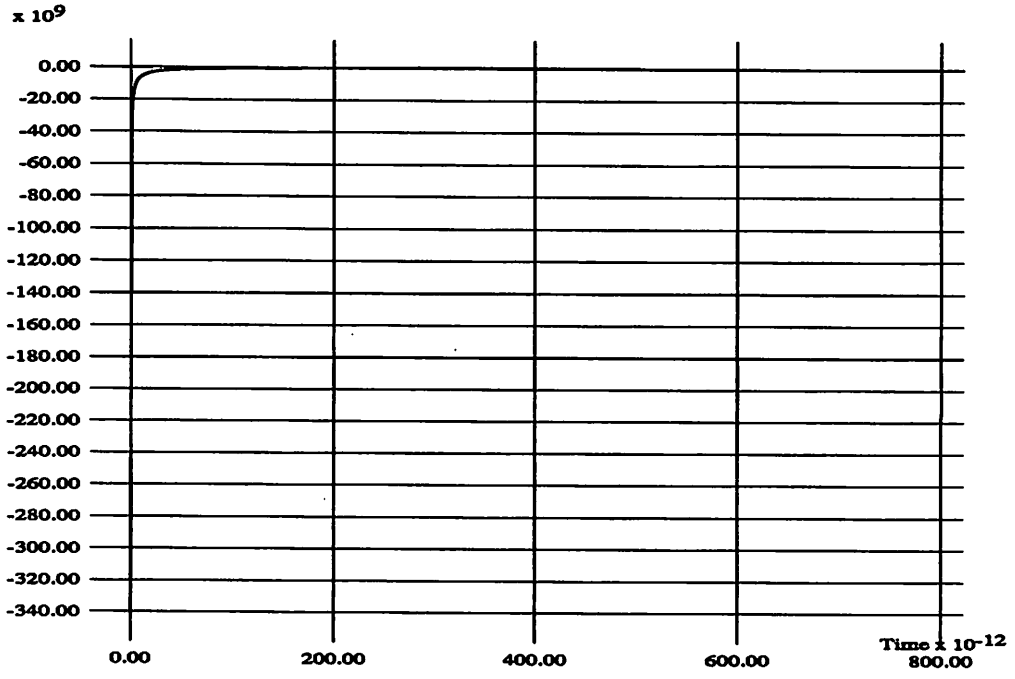

Figure 4.38: Abrupt model: $\Delta h'_Y(t)$

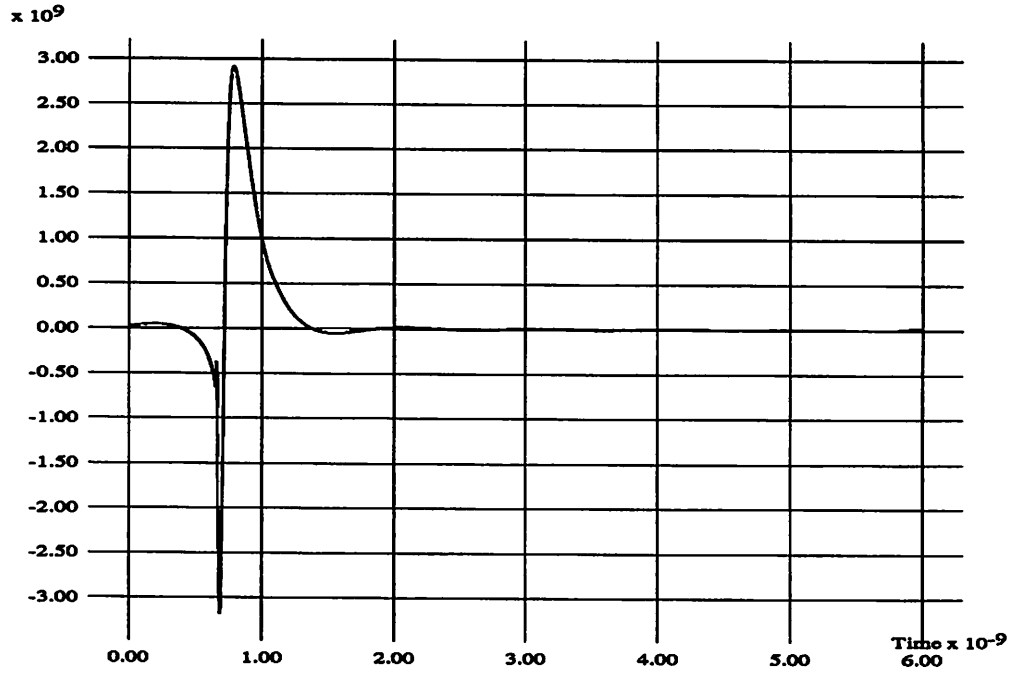

Figure 4.39: Abrupt model: $\Delta h'_\gamma(t)$

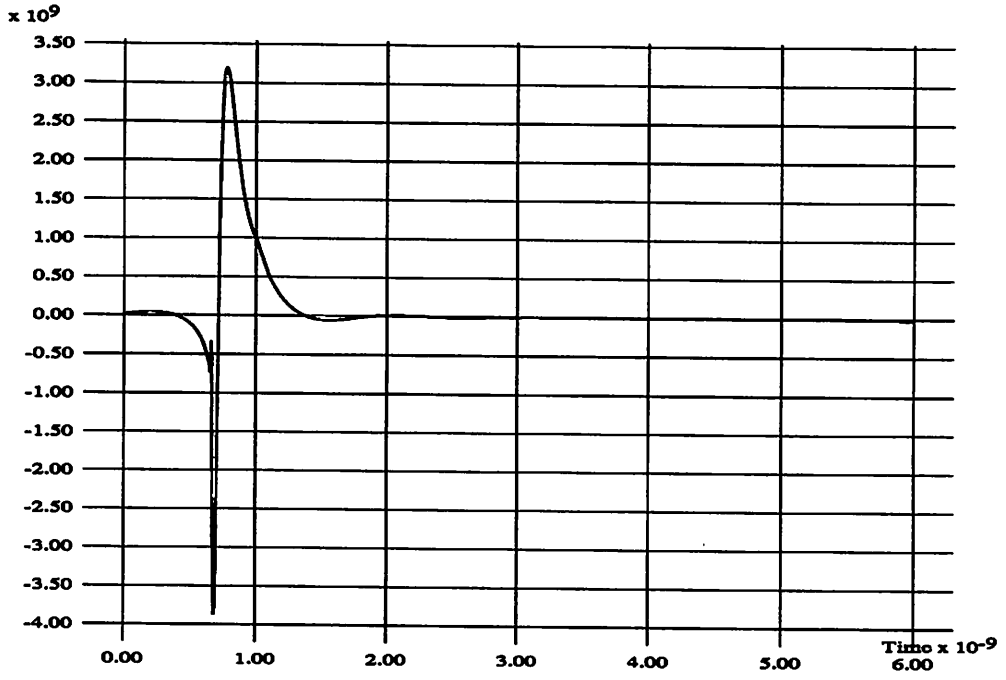

Figure 4.40: Abrupt model: $\Delta h'_{\gamma Y}(t)$

$\int_0^t \Delta h'_Y(\tau)\,d\tau$, $\int_0^t \Delta h'_\gamma(\tau)\,d\tau$, and $\int_0^t \Delta h'_{\gamma Y}(\tau)\,d\tau$ are useful. Plots of these functions for this example are shown in Figs. 4.41, 4.42 and 4.43; the point after which these functions achieve a steady value is the effective length of the response. An upper bound estimate of the relative error caused by truncation at time $t = \kappa$ of (for example) $\Delta h'_Y(t)$ under appropriate assumptions is easily seen to be given by:

$$\epsilon_r \leq \frac{|\int_0^\infty \Delta h'_Y(\tau)\,d\tau - \int_0^\kappa \Delta h'_Y(\tau)\,d\tau|}{|\int_0^\kappa h_Y(\tau)\,d\tau|}$$

That $\int_0^\infty \Delta h'_Y(\tau)\,d\tau$ is finite follows from that $\int_0^\infty \Delta h_Y(\tau)\,d\tau = \Delta H_Y(0) = 0$, a consequence of the high-frequency nature of the nonideality.

For this example, the effective durations of $\Delta h'_Y$, $\Delta h'_\gamma$ and $\Delta h'_{\gamma Y}$ were 600ps, 3ns and 3ns respectively, as seen from the plots of their integrals. Convolution was performed using the numerical formula in Chapter 3.

The circuit was the same as the fourth example of Section 4.1 (Figure 4.14). Rise times of 10ps and 1ns were used.

Figure 4.44 illustrates the voltage at the load end for the 10ps rise-time case. Simulation by pure convolution and the state-based/conv. technique of this paper are seen

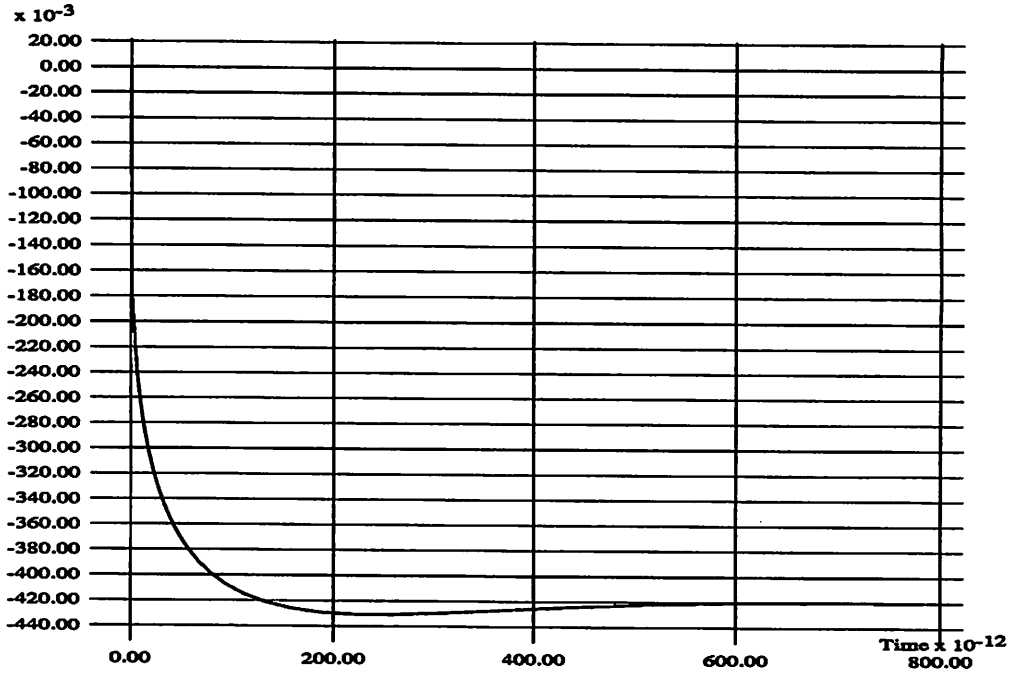

Figure 4.41: Abrupt model: $\int_0^t \Delta h'_Y(\tau)\, d\tau$

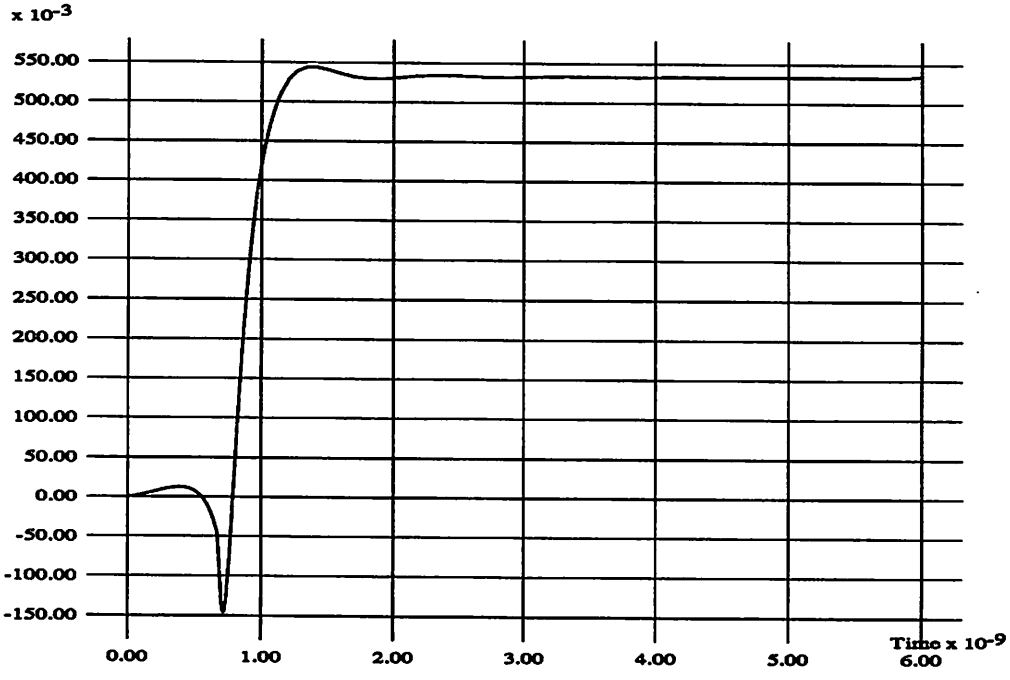

Figure 4.42: Abrupt model: $\int_0^t \Delta h'_\gamma(\tau)\, d\tau$

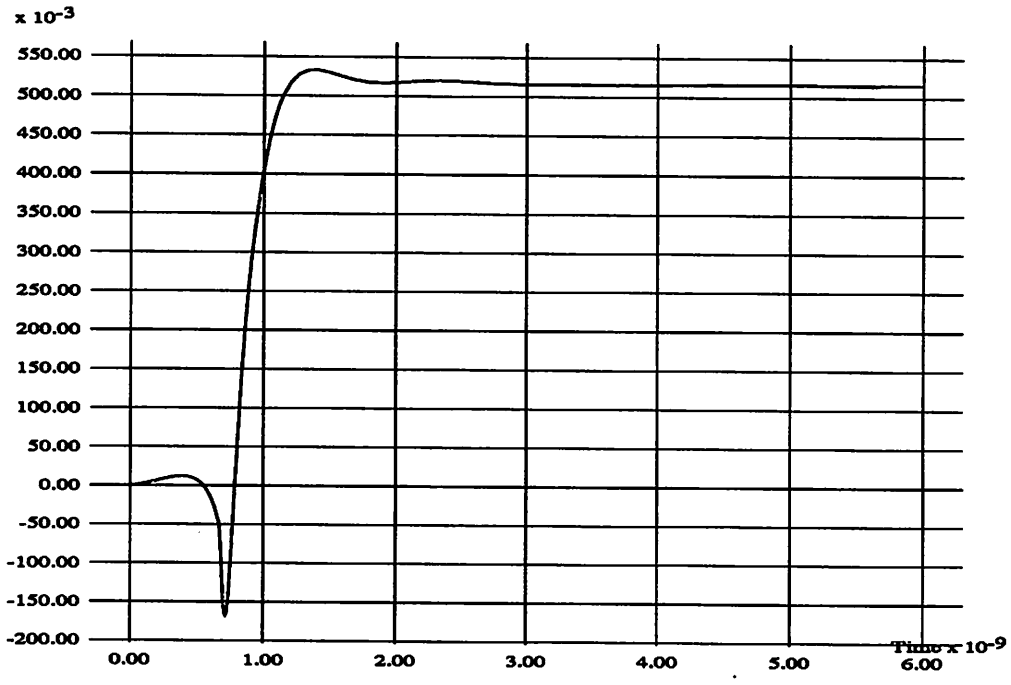

Figure 4.43: Abrupt model: $\int_0^t \triangle h'_{\gamma Y}(\tau)\, d\tau$

to yield identical results. Also shown is the results of simulation without skin-effect and only DC losses considered. The rise-time degradation caused by skin-effect, and the rounding of edges, can be seen clearly.

It is seen that the skin effect waveforms have a sharp undershoot at the delay of the line, a surprising and unexpected phenomenon. This undershoot is non-physical, caused by a modelling error, namely the abrupt transition in the frequency-domain impedance model [29, 41]. The smooth model described in the next section eliminates this undershoot.

Figure 4.45 shows the load voltage for a rise-time of 1ns. It is seen that skin-effect makes virtually no difference to the waveform in this case.

An interesting feature is that it is possible to simulate just the high-frequency non-ideality without simulating DC losses (Figure 4.46). Though such a situation is physically impossible, it offers some insight into features of the waveform caused purely by skin-effect.

Table 4.2 and Figure 4.47 show computation time as a function of total simulation length for the state-based and the pure convolution techniques. The linear and quadratic complexities of the two methods are apparent from the figure.

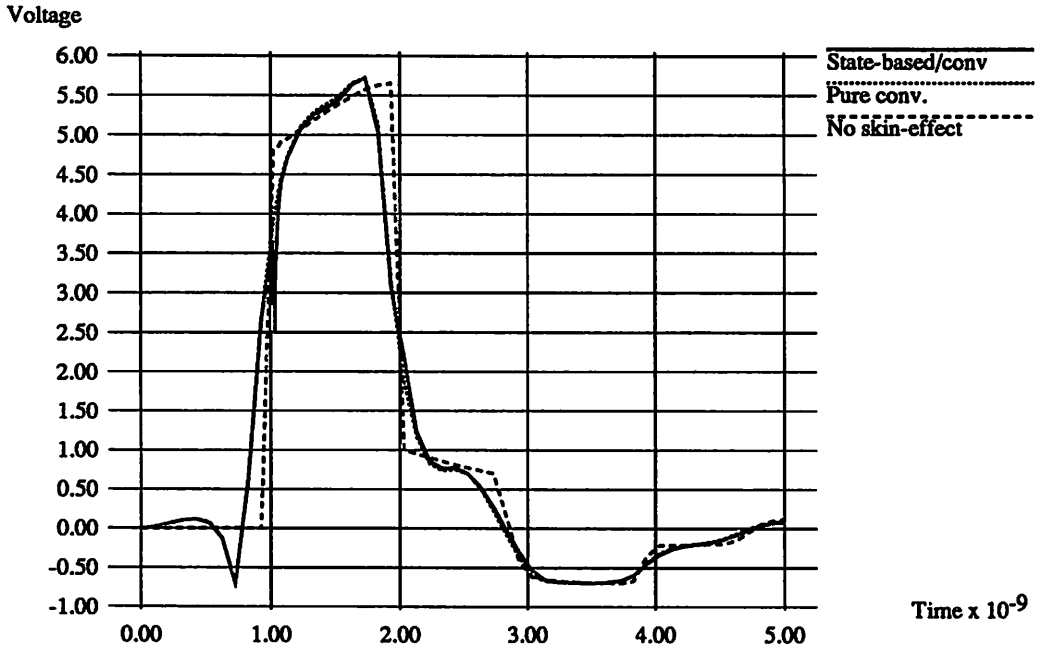

Figure 4.44: Load voltage, 10ps rise-time

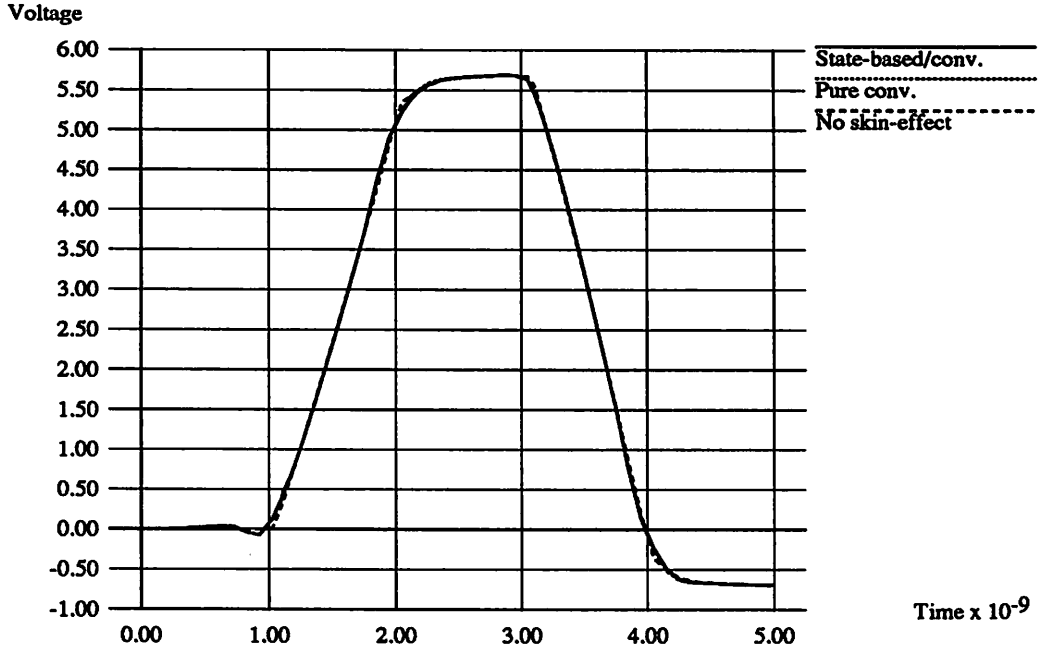

Figure 4.45: Load voltage, 1ns rise-time

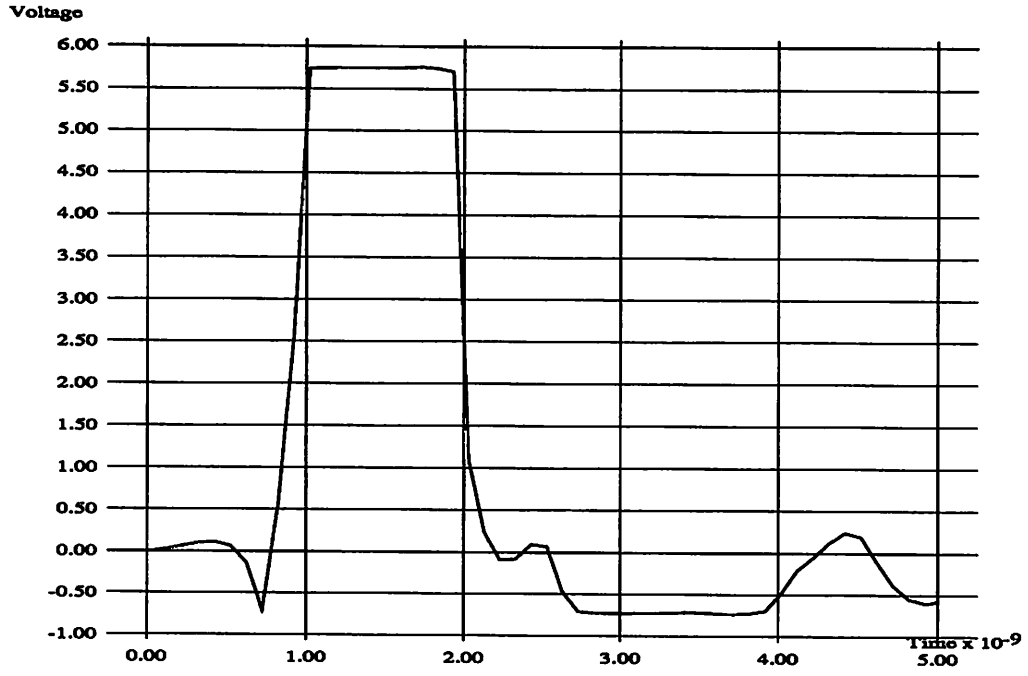

Figure 4.46: Load voltage, skin losses only (no dc loss)

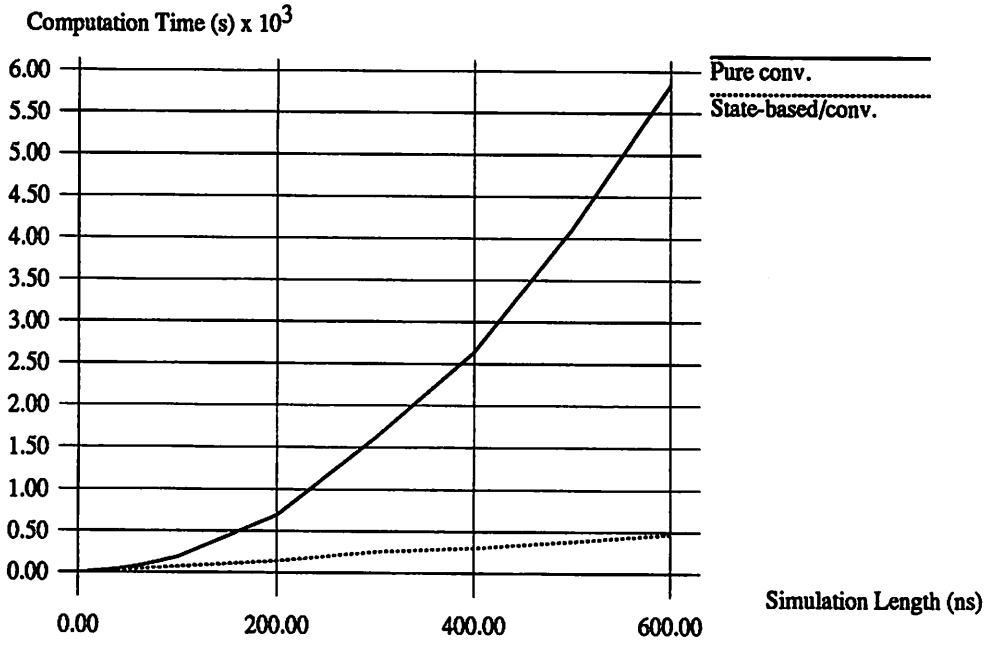

Figure 4.47: Execution time vs. simulation length

Simulation Length	Execution Time[a]	
	State-based/conv.	Convolution only
10 ns	6.82 s	4.90 s
20 ns	13.4 s	12.83 s
40 ns	26.72 s	38.26 s
60 ns	40.35 s	75.8 s
80 ns	53.59 s	126 s
100 ns	70.16 s	186.2 s
200 ns	140.78 s	695 s
300 ns	253.8 s	1619.5 s
400 ns	302.4 s	2635.1 s
500 ns	383.5 s	4110.6 s
600 ns	473.2 s	5839.9 s

[a]CPU times on a DEC 5000/200 running Ultrix 4.2

Table 4.2: Skin Effect: Comparison of Execution Times

4.2.2 Smooth Skin Effect Model

The **smooth** model is based on the classical model [38]. The parameters for the interconnect for this model were the same as for the **abrupt**, with the exception of L_{dc} being 10.27nH per cm. The corner frequency for this model was also 1GHz. The nominal characteristic impedance Z_0 for this example is 101.36Ω.

As in the abrupt model, the impulse responses $Z_0 \Delta h_Y$, Δh_γ and $Z_0 \Delta h_{\gamma Y}$ contain impulse (delta function) components which are first separated out. $Z_0 \Delta h'_Y$, $\Delta h'_\gamma$ and $Z_0 \Delta h'_{\gamma Y}$, the components without impulses, were calculated by numerical inversion of the Fourier transform, and are shown in Figs. 4.48, 4.49 and 4.50.

For this example, $Z_0 M_Y = 0.05683$, $M_\gamma = 0.5574$, and $M_{\gamma Y} = 0.55481$.

For this example, the effective durations of $Z_0 \Delta h'_Y$, $\Delta h'_\gamma$ and $Z_0 \Delta h'_{\gamma Y}$ were 1ns, 2.08ns and 2.38ns respectively, as seen from the plots of their integrals.

The circuit was the same as for the abrupt model of the previous section. Rise times of 10ps, 100ps and 1ns were used.

Figure 4.54 illustrates the voltage at the load end for the 10ps rise-time case. The rise-time degradation caused by skin-effect, and the rounding of edges, can be seen clearly. It is seen that the use of the smooth model for skin effect has eliminated the spurious undershoot that appeared in the **abrupt** model results of the previous section.

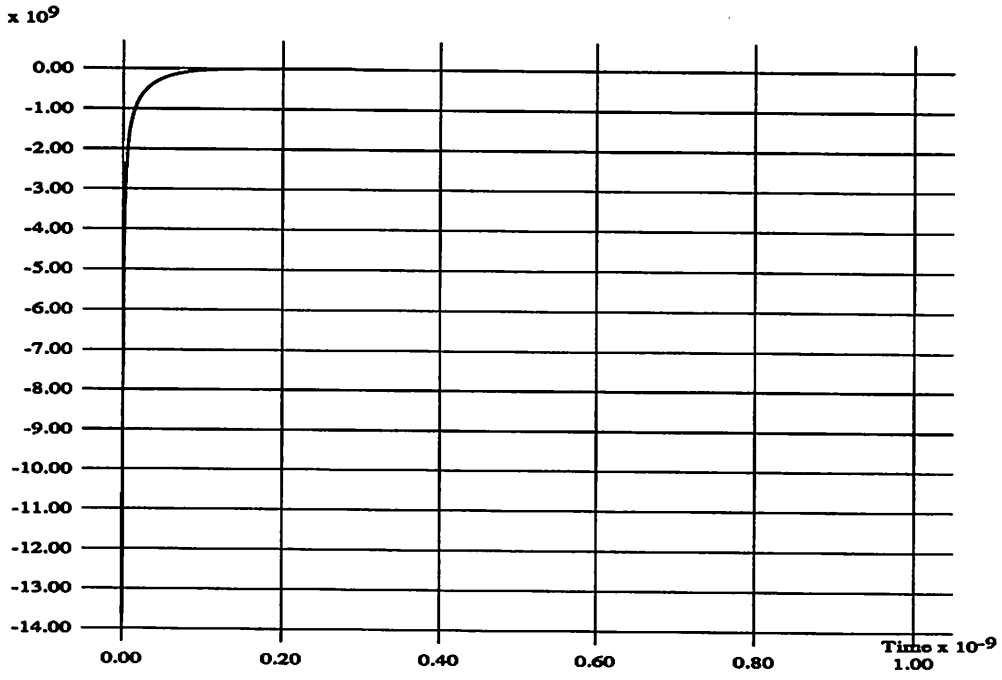

Figure 4.48: Smooth model: $Z_0 \triangle h'_Y(t)$

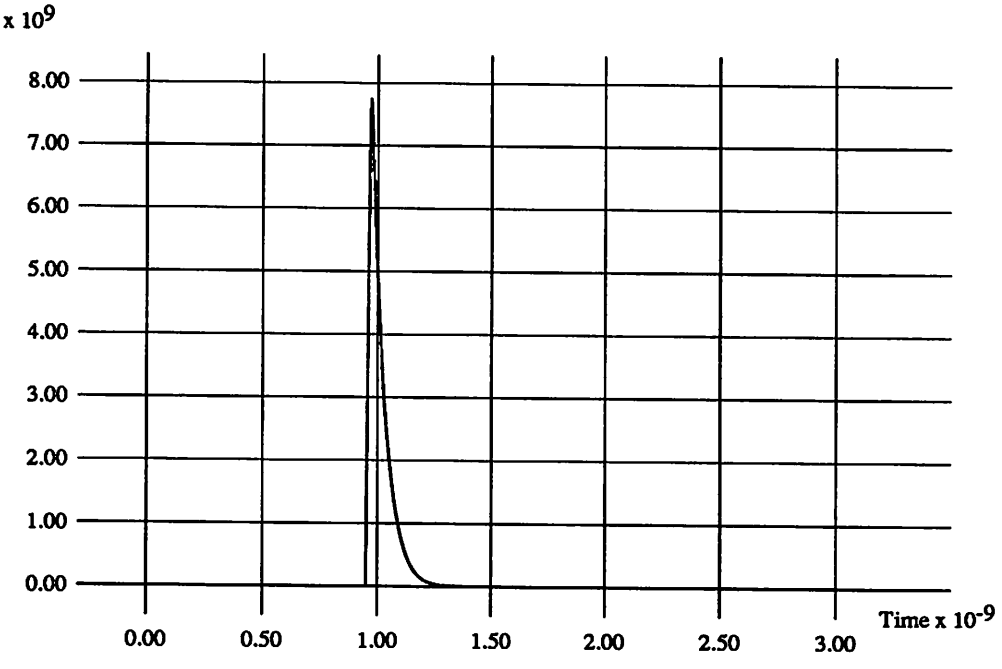

Figure 4.49: Smooth model: $\triangle h'_\gamma(t)$

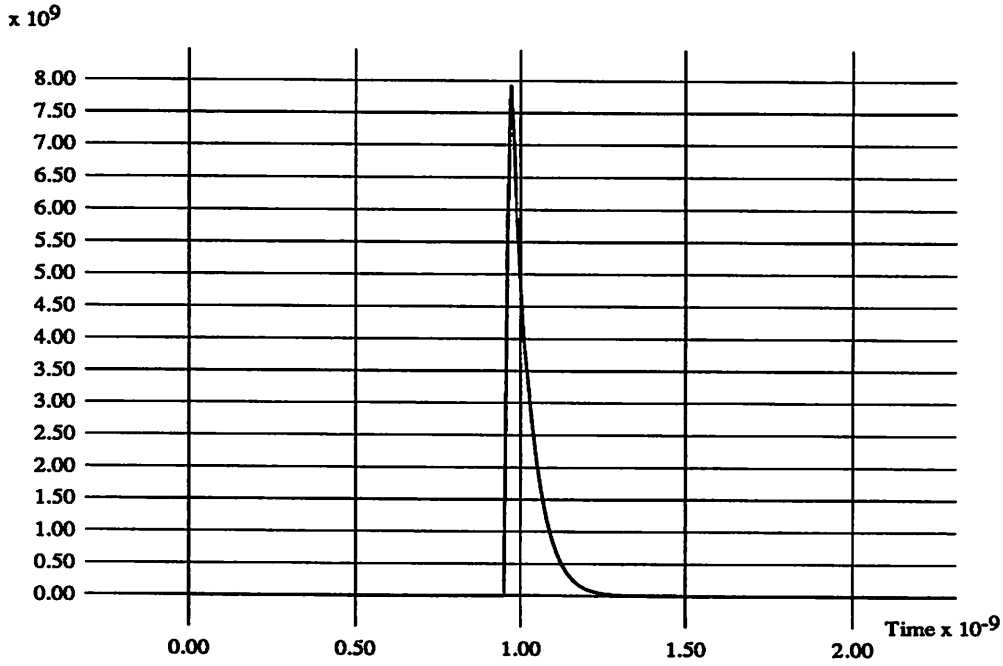

Figure 4.50: Smooth model: $Z_0 \, \Delta h'_{\gamma Y}(t)$

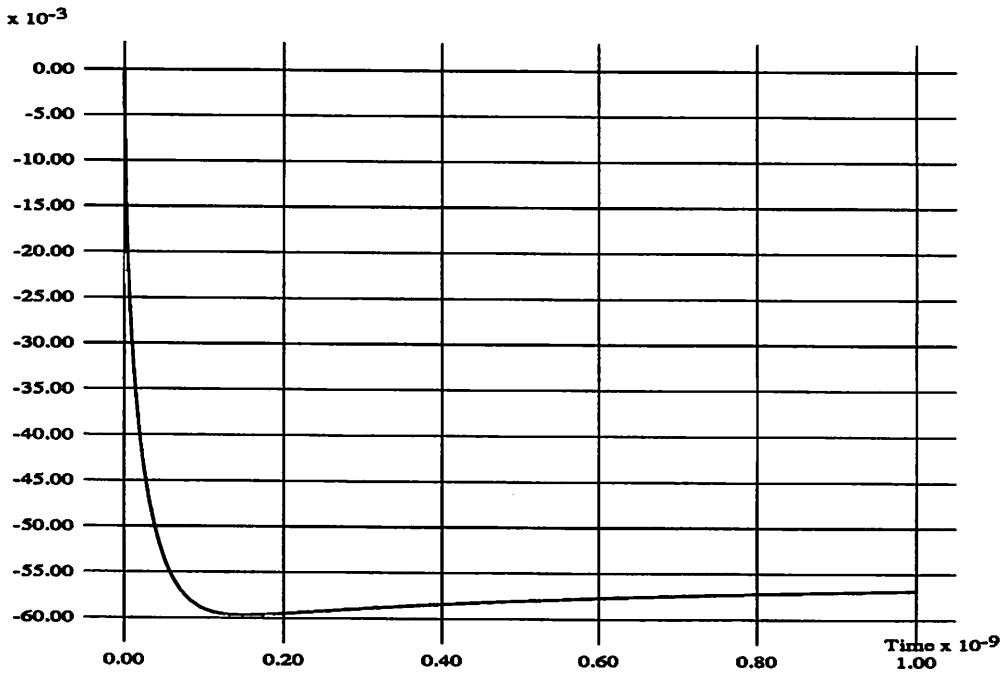

Figure 4.51: Smooth model: $Z_0 \int_0^t \Delta h'_Y(\tau) \, d\tau$

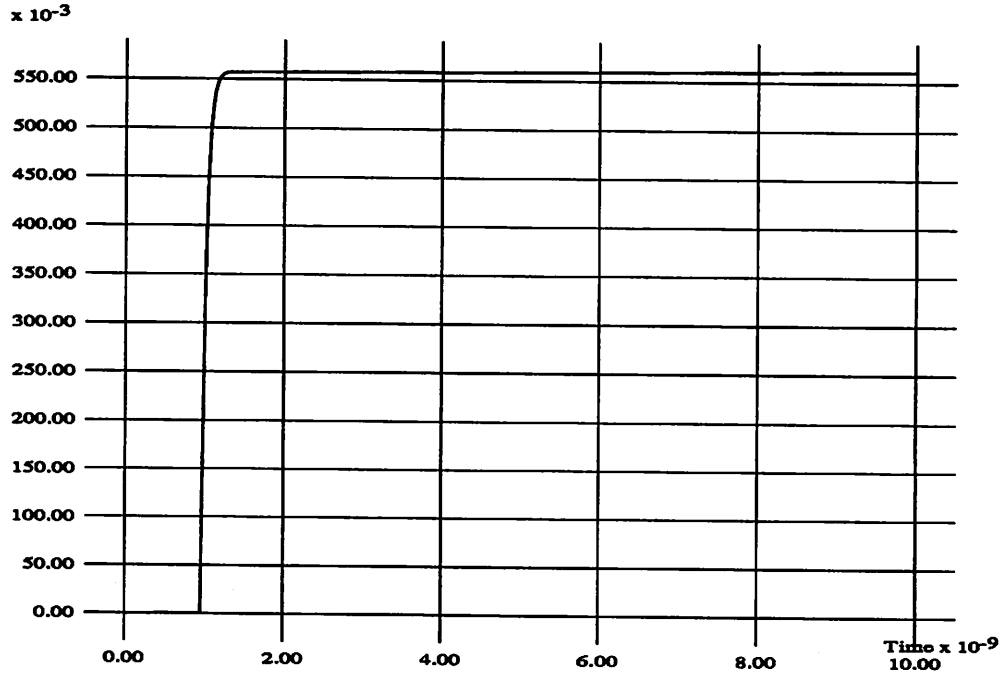

Figure 4.52: Smooth model: $\int_0^t \Delta h'_\gamma(\tau)\, d\tau$

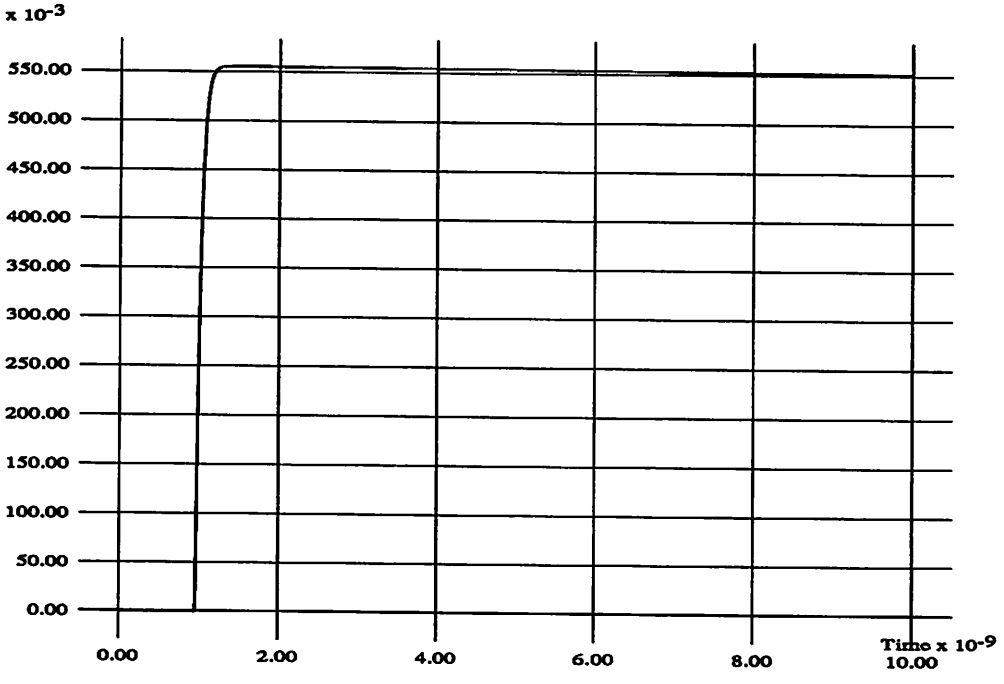

Figure 4.53: Smooth model: $Z_0 \int_0^t \Delta h'_{\gamma Y}(\tau)\, d\tau$

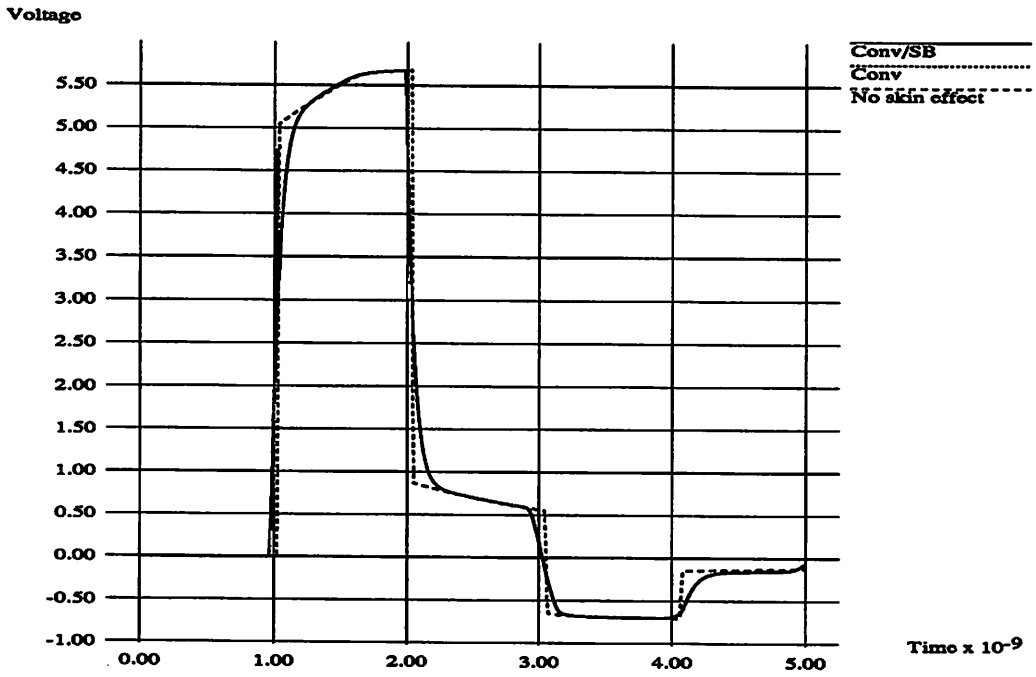

Figure 4.54: Smooth model: load voltage, 10ps rise-time

Figure 4.55 illustrates the voltage at the load end for the 100ps rise-time case. Rise-time degradation caused by skin effect can be seen in this case too.

Figure 4.56 shows the load voltage for a rise time of 1ns. It is seen that skin-effect makes virtually no difference to the waveform in this case, as expected.

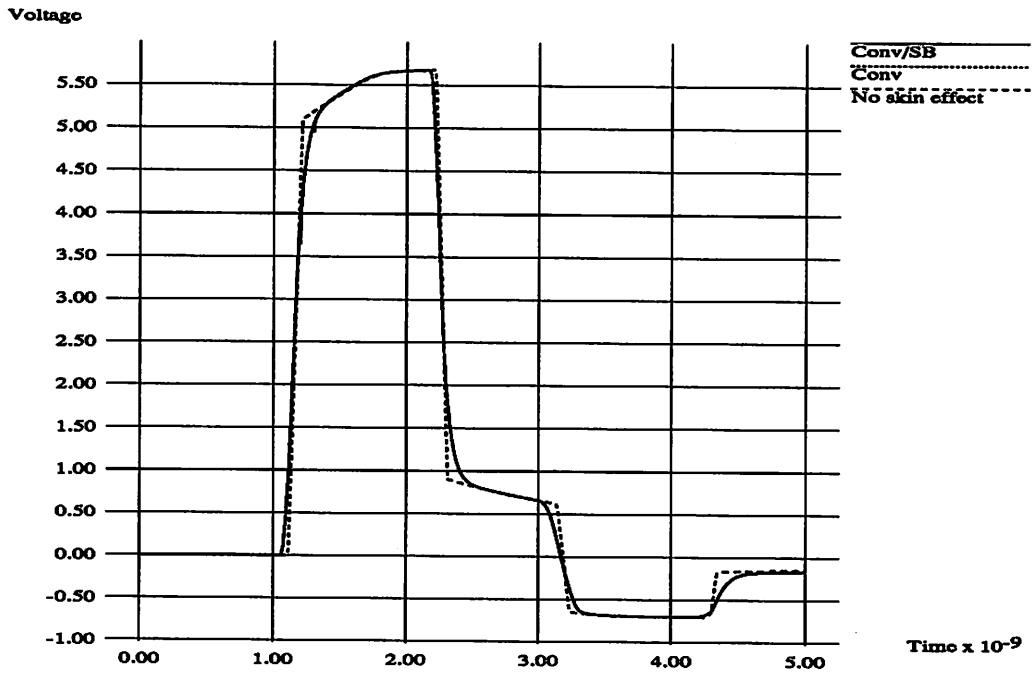

Figure 4.55: Smooth model: load voltage, 100ps rise-time

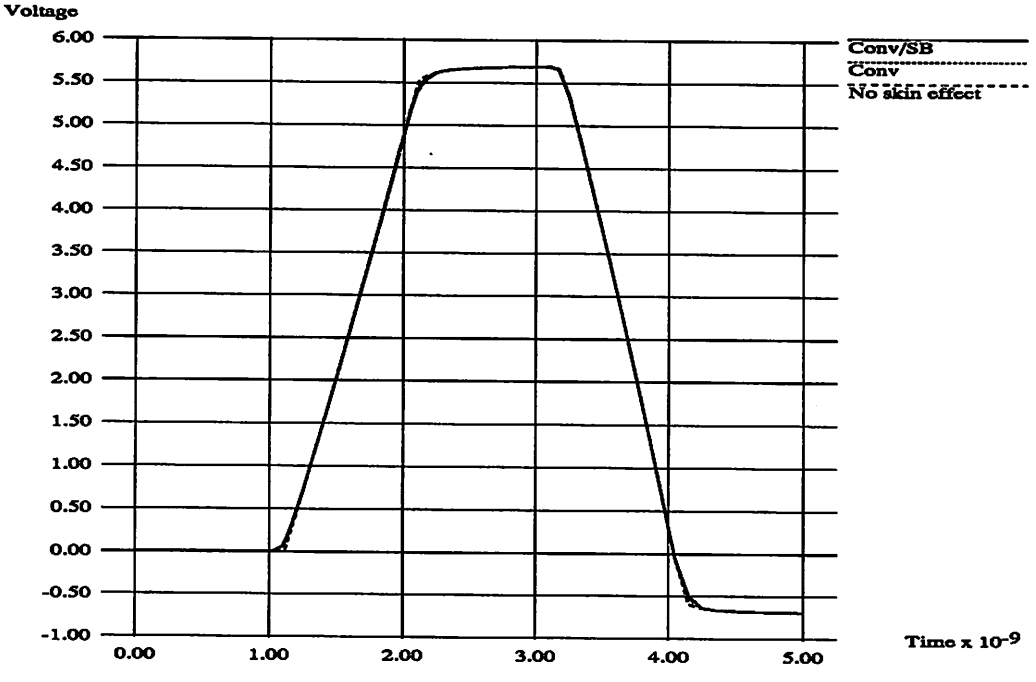

Figure 4.56: Smooth model: load voltage, 1ns rise-time

Chapter 5

Conclusion

It has been shown that uniform simple lossy lines may be accurately simulated using techniques based on analytic formulae.

The convolution technique for simulating SLLs has been extended by identifying analytic expressions for the impulse responses of the lossy line. Numerical convolution with these impulse responses is performed using a technique obtained by generalizing the trapezoidal integration method, which has higher-order accuracy than previous convolution methods and also leads to further closed-form expressions that can be applied directly. This technique suffers from the disadvantage of quadratic complexity, which leads to disproportionately high execution times for simulations of many time-points. Despite this, example simulations demonstrate that the technique can be an order of magnitude faster than the lumped-RLC method for short simulations, while being superior in accuracy.

A technique for solving the quadratic complexity problem while maintaining accuracy (the state-based method) has been developed. Unlike previous methods for linear complexity which use a reduced-order approach for linear complexity, the state-based method relies on utilising the dynamic internal state of the transmission line. The technique substitutes convolution by a fixed-length space integral, thereby eliminating the quadratic complexity problem associated with convolution. Analytic formulae are used for the impulse responses of the line. Analytic formulae are also identified for the kernels of the space integrals. The use of these analytic formulae leads to higher accuracy compared to techniques using numerical inversion. Essential to the efficiency of the technique is the dynamic sampling of the internal state during simulation, with sample locations varying both in number and position from time-point to time-point. Dynamic state sampling automatically ensures

that lines with little internal activity use little computation, resulting in the exploitation of latency in circuits with several transmission lines. Example simulations confirm the linear complexity property and demonstrate significant computational advantage over the convolution and lumped-RLC methods for long simulations.

Skin effect and other high-frequency nonideal phenomena can also be modelled by this approach. Augmenting the Telegrapher equations with additive terms can be used to incorporate nonideal phenomena into the state-based formulation if the terms are chosen appropriately. It is shown that the non-ideal line may be treated as two almost independent parts, one consisting of a simple lossy line and the other the additional nonideal part. Under the assumption that the purely nonideal part of the line has short responses that can be truncated, the overall simulation of the line can be performed in linear time. An example with thin multi-chip module interconnect demonstrates that skin effect can be simulated accurately in linear time for some real situations.

A previous result by other authors [19] makes it possible to use the techniques developed in this work to simulate the special case of identical, locally-coupled multiconductor lines. It is anticipated that the linear time property of the state-based method will carry over to general multiconductor lines, with the limitation that impulse responses and space integral kernels must be determined numerically as it is unlikely that closed-form expressions will be available. Techniques for the efficient and accurate inversion of functions with time-domain discontinuities need to be developed for the state-based simulation of general multiconductor lines to become practical. The parallel implementation of the state-based method holds promise for increased speed because of an intrinsic decoupling in the computation procedure for the internal line state.

Bibliography

[1] M. Abramowitz and I.A. Stegun, editors. *Handbook of Mathematical Functions.* Dover Books on Advanced Mathematics. Dover Publicatons, Inc., New York, 1970.

[2] F. Assadourian and E. Rimai. Simplified theory of microstrip transmission systems. *Proceedings of the Institute of Radio Engineers*, pages 1651–1657, December 1952.

[3] F.Y. Chang. The generalised method of characteristics for waveform relaxation analysis of lossy coupled transmission lines. *IEEE Transactions on Microwave Theory and Techniques*, MTT-37(12):2028–2038, December 1989.

[4] F.Y. Chang. Waveform Relaxation Analysis of RLCG Transmission Lines. *IEEE Transactions on Circuits and Systems*, 37(11):1394–1415, November 1990.

[5] F.Y. Chang. Relaxation Simulation of Transverse Electromagnetic Wave Propagation in Coupled Transmission Lines. *IEEE Transactions on Circuits and Systems*, 38(8):916–936, August 1991.

[6] L.O. Chua and P-M. Lin. *Computer-aided analysis of electronic circuits : algorithms and computational techniques.* Prentice-Hall, Englewood Cliffs, N.J., 1975.

[7] A.R. Djordjević and T.K. Sarkar. Analysis of Time Response of Lossy Multiconductor Transmission Line Networks. *IEEE Transactions on Microwave Theory and Techniques*, MTT-35(10):898, October 1987.

[8] G. Doetsch. *Guide to the Applications of the Laplace and Z Transforms.* Van Nostrand Reinhold Company, 1971.

[9] H.W. Dommel. Digital Computer Solution of Electromagnetic Transients in Single and Multiphase Networks. *IEEE Transactions on Power Apparatus and Systems*, PAS-88(4):388, April 1969.

[10] D. J. Erdman, S. W. Kenkel, G. B. Nifong, D. J. Rose, and R. Subrahmanyan. CAzM: A Numerically Robust, Table-based Circuit Simulator. *Technical Report Series, MCNC*, (TR89-23), July 1989.

[11] A. Deutsch et al. High-speed signal propagation on lossy transmission lines. *IBM Journal of Research and Development*, 34(4):601–615, July 1990.

[12] A.R. Djordjević et al. Analysis of Lossy Transmission Lines with Arbitrary Nonlinear Terminal Networks. *IEEE Transactions on Microwave Theory and Techniques*, MTT-34(6):660, June 1986.

[13] A.R. Djordjević et al. Time-Domain Response of Multiconductor Transmission Lines. *Proceedings of the IEEE*, 75(6):743, June 1987.

[14] C.A. Neugebauer et al. High Performance Interconnections between VLSI Chips. *Solid State Technology*, June 1988.

[15] C.W. Ho et al. The Thin Film Module as a High Performance Semiconductor Package. *IBM Journal of Research and Development*, 26(3), May 1982.

[16] L-T. Hwang et al. The Effects of the Skin-Depth on the Design of a Thin-Film Package. Source unknown. The authors are with MCNC, Research Triangle Park, NC.

[17] L. W. Nagel et al. ADVICE: Circuit Simulator used at AT&T Bell Laboratories.

[18] G. Fodor. *Laplace Transforms in Engineering.* Akademiai Kiado, Budapest, 1965.

[19] D. S. Gao, A. T. Yang, and S. M. Kang. Modeling and Simulation of Interconnection Delays and Crosstalks in High-Speed Integrated Circuits. *IEEE Transactions on Circuits and Systems*, 37(1):1–9, January 1990.

[20] C.W. Gear. *Numerical initial value problems in ordinary differential equations.* Prentice-Hall series in automatic computation. Prentice-Hall, Englewood Cliffs, N.J., 1971.

[21] V. Ghoshal and L.N. Smith. Finite element analysis of skin-effect in copper interconnects at 77K and 300K. In *Proceedings of the 1988 IEEE Microwave Theory and Techniques Symposium*, pages 773–776, 1988.

[22] A.J. Gruodis. Transient Analysis of Uniform Resistive Transmission Lines in a Homogeneous Medium. *IBM Journal of Research and Development*, 23(6), November 1979.

[23] A.J. Gruodis and C.S. Chang. Coupled Lossy Transmission Line Characterization and Simulation. *IBM Journal of Research and Development*, January 1981.

[24] Bill Gunning, Leo Yuan, Trung Nguyen, and Tony Wong. A CMOS Low-Voltage-Swing Transmission-Line Transceiver. In *IEEE Solid-State Circuits Conference*, San Francisco, CA, February 1992.

[25] Gerald J. Herskowitz. *Computer-aided Integrated Circuit Design.* McGraw-Hill Book Company, 1968.

[26] Claude Hilbert, David A. Gibson, and Dennis Herrell. A Comparison of Lossy and Superconducting Interconnect for Computers. *IEEE Transactions on Electron Devices*, 36(9):1830–1839, September 1989.

[27] W.C. Johnson. *Transmission Lines and Networks.* John Wiley and Sons, 1950.

[28] Erwin Kreyszig. *Advanced Engineering Mathematics.* Wiley Eastern Limited, New Delhi, 1985.

[29] Kenneth S. Kundert. Personal communication, April 1992.

[30] E. Lelarasmee, A. E. Ruehli, and A. L. Sangiovanni-Vincentelli. The waveform relaxation method for time domain analysis of large scale integrated circuits. *IEEE Transactions on Computer-Aided Design*, 1:131—145, July 1982.

[31] S. Lin and E.S. Kuh. Padé Approximation Applied to Transient Simulation of Lossy Coupled Transmission Lines. In *IEEE Multi-Chip Module Conference*, Santa Cruz, CA, March 1992. To appear.

[32] T. K. Liu and F. M. Tesche. Analysis of antennas and scatterers with nonlinear loads. *IEEE Journal of Antennas and Propagation*, AP-24:131, March 1976.

[33] K.D. Marx. Propagation Modes, Equivalent Circuits, and Characteristic Terminations for Multiconductor Transmission Lines with Inhomogeneous Dielectrics. *IEEE Transactions on Microwave Theory and Techniques*, MTT-21(7), July 1973.

[34] K.D. Marx and R.I. Eastin. A Configuration Oriented Spice Model for Multiconductor Transmission Lines with Homogeneous Dielectrics. *IEEE Transactions on Microwave Theory and Techniques.* To appear.

[35] L.W. Nagel. *SPICE2: a computer program to simulate semiconductor circuits.* PhD thesis, EECS department, University of California, Berkeley, Electronics Research Laboratory, 1975. Memorandum no. ERL-M520.

[36] Robert A. Pucel, Daniel J. Masse, and Curtis P. Hartwig. Losses in Microstrip. *IEEE Transactions on Microwave Theory and Techniques*, MTT-16(6), June 1968.

[37] T.L. Quarles. *Analysis of Performance and Convergence Issues for Circuit Simulation.* PhD thesis, EECS department, University of California, Berkeley, Electronics Research Laboratory, April 1989. Memorandum no. UCB/ERL M89/42.

[38] Simon Ramo, John R. Whinnery, and Theodore Vand Duzer. *Fields and waves in communication electronics.* John Wiley, New York, 1984.

[39] F. Romeo and M. Santomauro. Time-domain Simulation of n Coupled Transmission Lines. *IEEE Transactions on Microwave Theory and Techniques*, MTT-35, February 1987.

[40] J.S. Roychowdhury and D.O. Pederson. Efficient Transient Simulation of Lossy Interconnect. In *Proceedings of the IEEE Design Automation Conference*, pages 740–745, San Francisco, CA, June 1991.

[41] Albert E. Ruehli. Personal communication, December 1991.

[42] R.A. Sainati and T.J. Moravec. Estimating High Speed Circuit Interconnect Performance. *IEEE Transactions on Circuits and Systems*, 36(4):533–541, April 1990.

[43] J.E. Schutt-Aine and R. Mittra. Analysis of Pulse Propagation in Coupled Transmission Lines. *IEEE Transactions on Circuits and Systems*, CAS-32(12), December 1985.

[44] J.E. Schutt-Aine and R. Mittra. Scattering Parameter Transient Analysis of Transmission Lines loaded with Nonlinear Terminations. *IEEE Transactions on Microwave Theory and Techniques*, MTT-36:529–536, 1988.

[45] J.E. Schutt-Aine and R. Mittra. Nonlinear Transient Analysis of Coupled Transmission Lines. *IEEE Transactions on Circuits and Systems*, 36(7), July 1989.

[46] A. Semlyen and A. Dabuleanu. Fast and Accurate Switching Transient Calculations on Transmission Lines with Ground Return Using Recursive Convolution. *IEEE Transactions on Power Apparatus and Systems*, PAS-94:561–571, 1975.

[47] K. Singhal and J. Vlach. Computation of Time Domain Response by Numerical Inversion of the Laplace Transform. *Journal of the Franklin Institute*, 299(2):109–126, February 1975.

[48] K. Singhal, J. Vlach, and M. Nakhla. Absolutely Stable, High Order Method for Time Domain Solution of Networks. *Archiv Fur Elektronik und Ubertragungstechnik*, 30(4):157–166, 1976.

[49] Jiri Vlach. Numerical Method for Transient Responses of Linear Networks with Lumped, Distributed or Mixed Parameters. *Journal of the Franklin Institute*, 288(2):99–113, August 1969.

[50] R. Wang and O. Wing. Analysis of VLSI Multiconductor Systems by Bi-Level Waveform Relaxation. In *Proceedings of the IEEE International Conference on Computer Aided Design*, pages 166–169, 1990.

[51] A.G. Webster. *Partial Differential Equations of Mathematical Physics.* Dover Publications, 1955.

[52] W.T. Weeks, A. J. Jimenez, G.W. Malhoney, D. Mehta, H. Qassemzadeh, and T.R. Scott. Algorithms for ASTAP - A Network Analysis Program. *IEEE Transactions on Circuit Theory*, CT-20:628–634, November 1973.

[53] W.T. Weeks, L.L. Wu, M.F. McAllister, and A. Singh. Resistive and inductive skin-effect in rectangular conductors. *IBM Journal of Research and Development*, 23(6):652–660, November 1970.

[54] H.A. Wheeler. Formulas for the skin effect. *Proceedings of the Institute of Radio Engineers*, 30:412–424, 1942.

[55] Jacob K. White and Alberto Sangiovanni-Vincentelli. *Relaxation techniques for the simulation of VLSI circuits.* Kluwer Academic Publishers, Boston, 1987.

[56] W. Wlodarczyk and V. Besch. Skin-Effect Losses of Interconnect Lines in Frequency and Time-Domain. *Electronics Letters*, 26(16):1237–1238, 2nd August 1990.

[57] Chu-Sun Yen, Zvonko Fazarinc, and Richard L. Wheeler. Time-Domain Skin-Effect Model for Transient Analysis of Lossy Transmission Lines. *Proceedings of the IEEE*, 70(7):750, July 1982.

Appendix A

Dealing with an nonzero initial DC condition

Consider the Telegrapher Equations (Equations 2.1 and 2.2), reproduced here:

$$\frac{\partial v}{\partial x} = -\left(L\frac{\partial i}{\partial t} + Ri\right) \tag{A.1}$$

$$\frac{\partial i}{\partial x} = -\left(C\frac{\partial v}{\partial t} + Gv\right) \tag{A.2}$$

Assume there exist two sets of solutions $(v^a(x,t), i^a(x,t))$ and $(v^b(x,t), i^b(x,t))$ to the above equations. Since the Telegrapher Equations are *linear* PDEs, any linear combination of the above solutions (with coefficients not involving x or t) is also a solution of the Telegrapher Equations. The DC solution $(v^{DC}(x), i^{DC}(x))$ of the Telegrapher Equations is independent of time. Therefore, given any other solution $(v(x,t), i(x,t))$, the linear combination $(v^\dagger(x,t), i^\dagger(x,t))$, where $v^\dagger(x,t) = v(x,t) - v^{DC}(x)$, $i^\dagger(x,t) = i(x,t) - i^{DC}(x)$, satisfies the Telegrapher Equations.

Therefore, v and i can be replaced by $v^\dagger$ and $i^\dagger$ in all the equations in Chapter 2. This has the advantage that if the simulation is assumed to start when the circuit is in a DC steady-state, then $v^\dagger(x,0) = i^\dagger(x,0) = 0$, and some computation is saved.

Appendix B

Numerical computation of $E(\cdot,\cdot)$ and $F(\cdot,\cdot)$

Analytic expressions for $E(h_\gamma, t)$, $F(h_\gamma, t)$ and $E(h_{\gamma Y}, t)$ (refer Chapter 2) have not been found yet, hence these functions must be computed numerically. While these integrals may be computed using any standard numerical integration method, it has been found that using piecewise-linear approximations for $h(\cdot)$ leads to insignificant loss of accuracy in many cases. The following formulae find application if this assumption holds. $h(\tau)$ is assumed known at two points t_1 and t_2, and to be linear, i.e.:

$$h(\tau) = h(t_1) + \frac{h(t_2) - h(t_1)}{t_2 - t_1}(\tau - t_1) \tag{B.1}$$

It is desired to calculate the following:

$$u(t) \triangleq \int_a^t h(\tau)d\tau \tag{B.2}$$

$$v(t) \triangleq \int_b^t u(\tau)d\tau \tag{B.3}$$

$$w(t) \triangleq \int_c^t v(\tau)d\tau \tag{B.4}$$

Using Equation B.1 in Equation B.2 leads to:

$$u(t) = (t-a)\,h(t_1) + \frac{h(t_2) - h(t_1)}{2\,(t_2 - t_1)}\left\{(t-t_1)^2 - (a-t_1)^2\right\} \tag{B.5}$$

Using Equation B.5 in Equation B.3 results in an expression for $v(\cdot)$:

$$v(t) = \frac{h(t_1)}{2}\left\{(t-a)^2 - (b-a)^2\right\} + \frac{h(t_2) - h(t_1)}{2\,(t_2 - t_1)} \times$$

$$\left\{\frac{(t-t_1)^3-(b-t_1)^3}{3}-(a-t_1)^2(t-b)\right\} \quad \text{(B.6)}$$

Using Equation B.6 in Equation B.4 yields an expression for $w(\cdot)$:

$$\begin{aligned} w(t) &= \frac{h(t_1)}{2}\left[\frac{(t-a)^3-(c-a)^3}{3}-(b-a)^2(t-c)\right] \\ &\quad +\frac{h(t_2)-h(t_1)}{2(t_2-t_1)}\left[\frac{\frac{(t-t_1)^4-(c-t_1)^4}{4}-(b-t_1)^3(t-c)}{3}\right. \\ &\quad \left.-(a-t_1)^2\frac{(t-b)^2-(c-b)^2}{2}\right] \end{aligned} \quad \text{(B.7)}$$

Using the above formulae, $E(h_\gamma,t)$, $F(h_\gamma,t)$ and $E(h_{\gamma Y},t)$ may be calculated.